Spring 5-31-2014

Kinetic analysis of thiol oxidation to study the effects of fluorinated groups on metal phthalocyanine catalysts

Nellone Eze Reid
New Jersey Institute of Technology

Copyright Warning & Restrictions

The copyright law of the United States (Title 17, United States Code) governs the making of photocopies or other reproductions of copyrighted material.

Under certain conditions specified in the law, libraries and archives are authorized to furnish a photocopy or other reproduction. One of these specified conditions is that the photocopy or reproduction is not to be "used for any purpose other than private study, scholarship, or research." If a, user makes a request for, or later uses, a photocopy or reproduction for purposes in excess of "fair use" that user may be liable for copyright infringement,

This institution reserves the right to refuse to accept a copying order if, in its judgment, fulfillment of the order would involve violation of copyright law.

Please Note: The author retains the copyright while the New Jersey Institute of Technology reserves the right to distribute this thesis or dissertation

Printing note: If you do not wish to print this page, then select "Pages from: first page # to: last page #" on the print dialog screen

ABSTRACT

KINETIC ANALYSIS OF THIOL OXIDATION TO STUDY THE EFFECTS OF FLUORINATED GROUPS ON METAL PHTHALOCYANINE CATALYSTS

by
Nellone Eze Reid

The oxidation of thiol (RSH) to disulfide (RSSR) is important biologically and industrially. Corrosive and malodorous thiols exist as contaminants in wastewater discharge from mining facilities, pulp and paper mills, tanneries, and oil refineries. The elimination of thiols from petroleum products is necessary for even cleaner fuels. Thiols in gas products can also inhibit catalyst activity for some downstream processes.

Experiments and mechanistic kinetic studies were conducted for the aerobic oxidation of 2-mercaptoethanol (2-ME) and 4-fluorobenzenethiol (4-FBT) catalyzed by cobalt phthalocyanines: H_{16}PcCo, F_{16}PcCo, and F_{64}PcCo, each exhibiting a metal center subject to increasing Lewis acidity and steric hindrance. The experiments were performed in a reaction-limited, isothermal, bench-scale, semi-batch reactor, with thiol concentrations measured using GC/FID. Conversions of 2-ME to 2-hydroxyethyl disulfide and 4-FBT to 4-fluorophenyl disulfide in excess of 90% are achieved.

Kinetic analyses suggest that the substrate binding and electron transfer are directly related to the Lewis acidity and steric bulkiness of catalyst molecules. Radical expulsion seems to be related to steric bulkiness. Substrate binding was found to be the slow step for thiol oxidations catalyzed by H_{16}PcCo. The rate determining step for thiol oxidations, catalyzed by F_{16}PcCo and F_{64}PcCo, is the expulsion of the thiyl ($RS^{\bullet}$) radical from the catalyst molecule. Catalytic models show that the radical coupling to form the disulfide (RSSR) product occurs in solution, outside the catalyst cavity.

KINETIC ANALYSIS OF THIOL OXIDATION TO STUDY THE EFFECTS OF FLUORINATED GROUPS ON METAL PHTHALOCYANINE CATALYSTS

by
Nellone Eze Reid

A Dissertation
Submitted to the Faculty of
New Jersey Institute of Technology
in Partial Fulfillment of the Requirements for the Degree of
Doctor of Philosophy in Chemical Engineering

Department of Chemical, Biological and Pharmaceutical Engineering

May 2014

.

APPROVAL PAGE

KINETIC ANALYSIS OF THIOL OXIDATION TO STUDY THE EFFECTS OF FLUORINATED GROUPS ON METAL PHTHALOCYANINE CATALYSTS

Nellone Eze Reid

Dr. Robert B. Barat, Dissertation Advisor — Date
Professor of Chemical Engineering, NJIT

Dr. Basil C. Baltzis, Committee Member — Date
Professor and Interim Dean of Newark College of Engineering, NJIT

Dr. Reginald P.T. Tomkins, Committee Member — Date
Professor of Chemical Engineering, NJIT

Dr. Norman Loney, Committee Member — Date
Professor and Chair of Chemical Engineering, NJIT

Dr. Xianqin Wang, Committee Member — Date
Professor of Chemical Engineering, NJIT

Dr. Robert Farrauto, Committee Member — Date
Professor of Professional Practice, Columbia University

BIOGRAPHICAL SKETCH

Author: Nellone Eze Reid

Degree: Doctor of Philosophy

Date: May 2014

Undergraduate and Graduate Education:

- Doctor of Philosophy in Chemical Engineering,
  New Jersey Institute of Technology, Newark, NJ, 2014

- Bachelor of Science in Chemical Engineering,
  Hampton University, Hampton, Virginia, 2008

Major: Chemical Engineering

Presentations and Publications:

Reid, N.; Barat, R.; Kinetic Analysis of Hydroxide-Catalyzed, Aerobic Oxidation of 2-Mercaptoethanol, Chemical Engineering Communication, March 2014

Reid, N. Kinetic Analysis of Thiol Oxidation to Study the Effects of Perfluorinated Groups on Metal Phthalocyanine Catalysis. National Organization of Black Chemists and Chemical Engineers 40th Annual Conference, Indianapolis, IN. 2013

Reid, N.; Patel, H.; Kinetic Analysis of Thiol Oxidation to Study the Effects of Perfluorinated Groups on Metal Phthalocyanine Catalysis. The Catalysis Society of Metropolitan New York Spring Symposium, Princeton, N.J. 2013

Loas, A.; Reid, N.; Patel, H.; Badiola, C.; Biologically Inspired Fluoroalkyl-Substituted Phthalocyanines for Homogeneous and Heterogeneous Catalysis. The 3rd Annual Dana Know Student Research Showcase, Newark, N.J. 2011 (Gold Medal for Graduate Research)

Loas, A.; Reid, N.; Abbreviated Enzymes for Electronic Materials and Green Catalysts. The 6th Annual Graduate Student Research Day, Newark, N.J. 2010

If you can keep your head when all about you
Are losing theirs and blaming it on you,
If you can trust yourself when all men doubt you,
But make allowance for their doubting too;
If you can wait and not be tired by waiting,
Or being lied about, don't deal in lies,
Or being hated, don't give way to hating,
And yet don't look too good, nor talk too wise:

If you can dream—and not make dreams your master;
If you can think—and not make thoughts your aim;
If you can meet with Triumph and Disaster
And treat those two impostors just the same;
If you can bear to hear the truth you've spoken
Twisted by knaves to make a trap for fools,
Or watch the things you gave your life to, broken,
And stoop and build 'em up with worn-out tools:

If you can make one heap of all your winnings
And risk it on one turn of pitch-and-toss,
And lose, and start again at your beginnings
And never breathe a word about your loss;
If you can force your heart and nerve and sinew
To serve your turn long after they are gone,
And so hold on when there is nothing in you
Except the Will which says to them: 'Hold on!'

If you can talk with crowds and keep your virtue,
Or walk with Kings—nor lose the common touch,
If neither foes nor loving friends can hurt you,
If all men count with you, but none too much;
If you can fill the unforgiving minute
With sixty seconds' worth of distance run,
Yours is the Earth and everything that's in it,
And—which is more—you'll be a Man, my son!

(Rudyard Kipling, If)

To my loving parents, Neville and Orla Reid, for instilling within me the belief that God has blessed me with all the tools for achievement. Thank you and I love you!

ACKNOWLEDGMENT

First and foremost, I could not be more fortunate to have had Professor Robert Barat as my advisor and mentor. From day one, your dedication and passion for quality work has remained consistent throughout the classroom, lab and most certainly in the completion of this dissertation. I thank you for teaching me the value of independence and initiative in a working environment, as well as the importance of asking questions until the right answers are determined.

I commend the members of my committee, Prof. Basil Baltzis, Prof. Reginald Tomkins, Prof. Norman Loney, Prof. Xianqin Wang and Prof. Robert Farrauto for their availability and support in all matters leading towards my graduation. I have a tremendous amount of appreciation for the entire Chemical Engineering department, especially Cynthia Wos and Shawn Yetman for their hard work and continual words of encouragement. A special thanks goes to Yogesh Gandhi in the Chemistry department. Thank you to Prof. Jale Akyurtlu, Prof. Ates Akyurtlu and Prof. Morgan Morris at Hampton University. Your support has undoubtedly encouraged me through my years in both undergraduate and graduate schools. I also acknowledge Prof. Gorun for his initial establishment of the project, as well as his students, Mr. Hemant Patel and Dr. Andreis Loas, for synthesis of F_{64}PcCo catalyst and informative scientific discussions. I thank the New Jersey Institute of Technology and the National Science Foundation for funding me throughout my Ph.D. candidacy.

My Lord and Savior has certainly blessed me with an amazing support system from the day I was born. I thank God for my parents; my mother, Orla Reid – for continually pushing me to scholastically challenge myself; and my father, Neville Reid –

for allowing me to believe in myself, no matter the odds. I still remember telling my parents I wanted to quit school after kindergarten because I thought first grade would be too difficult. And now…

I thank God for my family always encouraging me and keeping me in their prayers. My grandmother – Elsie Nurse; grandfather – Leon Reid; brother – Nevoughn Reid; and all of my uncles, aunts and cousins. I particularly thank Terry Nurse, Shamena Nurse, Merissa Daniels and Curtis Lancaster for not only being supportive family members but also providing me with irreplaceable friendships.

In addition to a very large family, I have also been blessed with a circle friends, that I am honored to call my extended family. My brothers – Jevon Roberts, Jay Orr, Tivern Turnbull, Trevis Craig, Kareem McQuilkin, Clyde Chapman, Kenald Bernard, LeSean Brereton, Brandon Joseph and Alex Plass. Thank you for always supporting my efforts in and outside of school. My sisters – Cherelle Lloyd, Brittney Parkinson, Brittany Chance, Monisha Henderson, Aisha Harrison, Karisma Jones, Kamaria Braithwaite, and Mounia Asiedu. Thank you for giving me a reason to not cut school and showing me how to truly be a gentleman. I have the fortune of retaining friends from every stage of my life, from elementary to graduate school. I thank God for Kimberly Arango, Ebony Grice, Dr. Michal-Ann Newman, Antonio Blake, Henry Warner, Taurean St. John, Courtney Mitchell, Rayon Williams, Dr. Priscilla Paul, Harry Obamije, Joel Henriquez, Lisa Bergamotta, Manchit Cheng, and Douglass Purnell.

The Alpha Alpha Lambda chapter of Alpha Phi Alpha, Fraternity Inc. has played an important role in expanding my incredible support system. I thank God for my line brothers Bro. Patrick Council, Bro. Dr. Jerald Grace, Bro. Fashade Afolabi, Bro. Derricke

Dennis, as well as the entire AAL chapter! I pray to continue to move Onward and Upward!

Unfortunately, some knew of my journey but were unable to physically see the final achievement. I thank God for my grandmother Mavis Reid. I pray to embody half of your unbelievable strength. I thank God for my Uncle Clifton Reid. The memory of your smile, and true happiness when I told you that I would be pursuing my Ph.D. in Chemical Engineering served as a day to day inspiration. Ms. Laksmi Nor – we lost you a few weeks after I began at NJIT. Without you encouraging me to read great books from your vast library in order to prepare for the SAT's, who knows where I would have ended up. I thank God for my little cousin Texroy Vickerie. I remember when you were born. And too loose you at such a young age still breaks my heart, but I know you would be proud of me today and are looking down on me with that beautiful smile.

Finally, and certainly not least, I thank God for my past, present and future. Karen Patrice Joyce. Words cannot express how grateful I am to have you as the love of my life. You push me to be a better man. Your fervor to please God has challenged me spiritually and is one that I will continue to welcome all the days of our lives. We began dating at the start of my journey at NJIT and I am excited to walk confidently into the next stage of my life with you tightly on my arm.

I pray for all of my cousins, nieces, nephews, godchildren and future children. Although the words to follow may not be in your realm of interest, take note the effort, the sacrifice and commitment required to write this dissertation. Remember with God, nothing is beyond your reach.

Anytime you see a turtle up on top a fence post, you know he had some help. -Alex Haley

TABLE OF CONTENTS

TABLE OF CONTENTS
(Continued)

TABLE OF CONTENTS
(Continued)

Chapter **Page**

TABLE OF CONTENTS
(Continued)

Chapter **Page**

LIST OF TABLES

LIST OF TABLES
(Continued)

LIST OF TABLES
(Continued)

Table **Page**

LIST OF FIGURES

LIST OF FIGURES
(Continued)

Figure **Page**

LIST OF FIGURES
(Continued)

Figure **Page**

LIST OF FIGURES
(Continued)

Figure **Page**

LIST OF FIGURES
(Continued)

Figure **Page**

CHAPTER 1

INTRODUCTION

1.1 Background

Catalysis-based chemical synthesis accounts for 60% of today's chemical products and 90% of current chemical processes.[1] This has motivated the present work to investigate "green" catalytic processes. For example, catalytic oxidation using air as a "green" oxidant functioning at less severe conditions than conventional processes would save energy. Natural enzymes, such as Cytochrome P-450, inspire this goal. Cytochrome P-450 enzymes are largely responsible for drug metabolism and bio-activation.[2] These mono-oxygenase reactions insert an oxygen atom from O_2 while producing the byproduct, water. "Green" industrial oxidation catalysts should display similarly high conversion efficiencies and selectivity, be robust in the harsh environment of free radicals, ions, and oxygenated species, yet differ by not requiring reducing equivalents for oxidations that may occur via different mechanisms.

This study focuses on the electronic and steric properties of new classes of aerobic oxidation catalysts, which are organically based and chemically resistant to the activated oxygen species they produce. The reaction chosen is the biologically related radical auto-oxidation of thiols, an environmentally important reaction ultimately used to reduce the sulfur level in fuels.

Novel phthalocyanine catalysts are designed to promote this ecologically beneficial aerobic auto-oxidation of thiols (mercaptans). These catalysts are believed to exhibit high solubility in organic solutions and exceptional stability toward oxidative degradation.[3] New catalysts are free of C-H bonds, and are partly fluoroalkylated with

enzyme-like active sites. Fluorine substituents cause the metal center to not only be more Lewis acidic, but to also be protected sterically by larger substituents on the molecule scaffold.[3] Kinetic analyses of mercaptan oxidations, in the presence of catalysts with varying structures, will allow for greater understanding of electronic and steric effects.

1.2 Auto-Oxidations of Thiols

The oxidation of thiol (RSH) to disulfide (RSSR) is important biologically[4] and industrially.[5] Corrosive and malodorous thiols exist as contaminants in wastewater discharge from mining facilities, pulp and paper mills, tanneries, and oil refineries.[6] For example, refinery streams such as catalytic cracker naphtha can contain thiols at hundreds of parts-per-million (by weight). Auto-oxidation is a preferred means of thiol removal here instead of hydrotreating since the latter process can diminish desirable naphtha qualities such as octane number. The elimination of thiols from petroleum products is necessary as the pressure grows to produce cleaner fuels. Due to its corrosive nature, thiol presence in gas products may also inhibit catalyst activity for some downstream processes.[7]

The Merox (**mer**captan **ox**idation) process, developed by UOP in 1959, is used to convert mercaptans (thiols) to disulfides via aerobic and peroxide-induced coupling via,

Net Reaction: $4RSH + O_2 \rightarrow 2RSSR + 2H_2O$

for which transition homogeneous metallo-based phthalocyanine catalysts (PcM's) were found to be quite effective.[8]

The oxidation involves three reactions.[9] The process begins with the elementary reaction (Eq. 1.1), where a mercaptan is near-instantaneously transformed into mercaptan thiolate ion (RS^-) to be used in the next, non-elementary reaction (Eq. 1.2). This first

reaction occurs because the RSH is essentially a weak acid. The mechanism defining Equation 1.2 is primarily catalytic – the main focus of this study, though a minor, non-Pc parallel pathway exists. The second non-elementary reaction is also non-catalytic (Eq. 1.3), and occurs via the hydrogen peroxide produced in the first non-elementary reaction (Eq. 1.2). Both contribute to mercaptan conversion and must be considered when calculating the rate of mercaptan consumption.

$$4RSH + 4HO^- \rightarrow 4RS^- + 4H_2O \textit{ (elementary)} \quad (1.1)$$

$$2RS^- + 2H_2O + O_2 \rightarrow RSSR + H_2O_2 + 2HO^- \textit{ (non-elementary)} \quad (1.2)$$

$$H_2O_2 + 2RS^- \rightarrow RSSR + 2HO^- \textit{ (non-elementary)} \quad (1.3)$$

Thiols studied in the current work include 2-mercaptoethanol (pKa~9.64) and 4-fluorobenzenethiol (pKa~6.4). The larger, 4-fluorobenzenethiol thiol is also more acidic. These thiols were chosen for comparison purposes to further elucidate steric and electronic affects.

a. 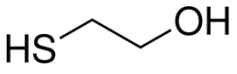

b. 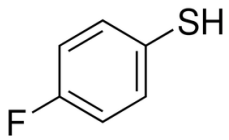

Figure 1.1 (a) 2-Mercaptoethanol (2-ME), (b) 4-Fluorobenzenethiol (4-FBT).

1.3 Phthalocyanines

Metal-centered phthalocyanines (PcM) are catalysts often used for redox reactions; e.g., sulphonated derivatives of M = Cobalt as catalysts for the Merox process.[7] This process is widely used in petroleum refineries to remove mercaptans from various distillate streams. The structure of the phthalocyanine catalyst mimics porphyrin enzymes. In porphyrin enzymes, the nitrogen atoms work to bind a metal to the center of the

molecule, while the surrounding scaffold assists in thermal and chemical stability.[2] The PcM's are good candidates as mercaptan oxidation catalysts. The metal atom is the catalytic site, while the Pc structure around the metal atom can be tailored to enhance catalytic activity while improving catalyst lifetime.

Deactivation and aggregation of phthalocyanines are other issues that must be considered in newly designed catalysts. The C-H bonds on unsubstituted cobalt(II) phthalocyanines, $H_{16}PcCo$ (Figure 1.2a)[10], are susceptible to attack from the radicals produced in the aerobic oxidation which they catalyze.[11] Electrophillic substitution, where an electrophile reacts with the benzene ring to yield a substituted molecule, is also a likely degradation mechanism.

In order to discourage free radical attack, hydrogen atoms are replaced with fluorine, resulting in the cobalt(II) hexadecafluorophthalocyanine, $F_{16}PcCo$ (Figure 1.2b).[12] The electron-withdrawing fluorine groups cause the macrocyclic molecule to become electron poor, and consequently decreases the likelihood of electrophillic attack. However, the addition of electron withdrawing fluorine groups now enhance the possibility of nucleophillic attack which might also result in undesired displacement of an aromatic fluorine.[12] In addition, $F_{16}PcCo$ molecules are shown to exhibit a large amount of aggregation (dimerization) due to their flat structure.[13] Dimerization leads to a decrease in available active sites, and subsequently a reduction in catalytic activity.

Fluorine and fluoroalkylated substituents on the phthalocyanine cause its metal center to be electron-poor, thus potentially enhancing its catalytic oxidation capability, while also serving to protect the phthalocyanine itself from oxidative destruction.[14] Novel catalysts were designed by Gorun et al.,[3] where the fluorine groups of $F_{16}PcCo$ were selectively replaced with perfluoropropyl groups, C_3F_7. For example, the bulky

cobalt(II) 1,4,8,11,15,18,22,25-octafluoro-2,3,9,10,16,17,23,24 octakis-perfluoro-phthalocyanine, $F_{64}PcCo$ (Figure 1.2c)[3] molecule is robust and has the ability to resist degradation.[14] The substitution of hydrogen with fluorine atoms and aliphatic fluorine groups results in less radical attacks, while the more electron deficient molecule also resists electrophillic attacks.

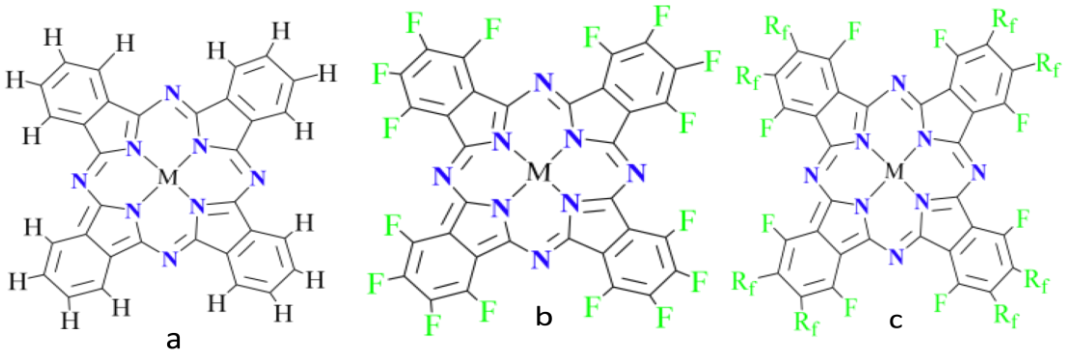

Figure 1.2 a-$H_{16}PcCo$,[10], b-$F_{16}PcCo$,[12] c-R_fPcCo, where $R_f = C_3F_7$.[3]

The bulky aliphatic fluorine groups of the C_3F_7 sterically hinder nucleophillic attack on aromatic fluorine groups, as well as preventing π-π stacking (dimerization) both in solution[15] and in the solid-state.[16,17] In addition to enhancing phthalocyanine solubility in organic solvents[14], this thesis claims that fluoroalkylated groups affect steric hindrance of the molecule and electron deficiency of its metal center, which in turn protects the molecule from degradation and has a significant effect on mercaptan reaction rates.

Although cobalt(II) phthalocyanines are the most active, stable, and cost effective catalysts for the MEROX reaction, they were known to exhibit poor solubility in organic solutions.[18-20] The kinetic effects of replacing the peripheral H atoms of $H_{16}PcCo$ with F atoms to yield $F_{16}PcCo$, are unknown. Nor are the consequences of replacing peripheral F atoms of $F_{16}PcCo$ with perfluoropropyl (C_3F_7) groups as with $F_{64}PcCo$ known.

Recent studies by Tyapochkin et al.[21] and Ganguly et al.[22] show kinetics of thiol oxidation by air in aqueous medium in the presence of 4, 4', 4", 4''' – cobalt(II)

tetrasulfophthalocyanine and cobalt(II) phthalocyanine sulfonamide, respectively. Both papers reveal that thiol oxidation follows a kinetic rate law similar to Michaelis-Menten. Neither of the derived models explicitly claims to include parallel thiol oxidation via reaction-derived H_2O_2. However, H_2O_2 has been shown to play a significant role in the oxidation of thiols.[23-28]

1.4 Goal of the Project

This project sought to further understand the advantages offered by organic chemistry in fine-tuning the steric and electronic properties of materials to be used as catalysts via kinetic analyses of mercaptan oxidation reactions.

The studied catalytic reaction is homogeneous in nature. In the reactor set-up used for the homogeneous catalytic system in this study, gas phase oxygen must be transferred to the liquid phase, where the reaction takes place. The consideration of mass transfer rate across a gas-liquid boundary is imperative for multi-phase systems. Measures were taken to minimize effects, which might be caused by mass-transfer, on quantitative kinetic data.

This dissertation reports on experimental and kinetic modeling studies of 2-mercaptoethanol and 4-fluorobenzenthiol oxidations in an organic solution, catalyzed by cobalt phthalocyanines, including those substituted with F atoms and C_3F_7 groups. Several reaction parameters were considered, including catalyst concentration, and O_2 gas phase content. The rate-determining step was identified. Kinetic analyses conducted in this study extracted parameters via catalytic modeling. This quantitative and qualitative study provided insight into the relationship between the modified phthalocyanine structures and design limitations. It was shown how the manipulation of

the structure of perfluorinated phthalocyanine catalysts impacts their oxidative reactivity toward mercaptans, while providing an understanding about reaction rates and kinetic constants.

Although this study concentrated on a specific industrial catalytic reaction, applications of peripherally substituted phthalocyanines include photosensitizers for photodynamic therapy of cancer,[29–31] materials for electrophotography, inkjet printing, semiconductors, chemical sensors and electrochromic devices,[11,32,33] nanotechnology[33] and nonlinear optics.[34] Most of these applications arise from the electronic effects. Elucidation of both electronic and steric factors involved in catalytic processes could lead to the design of new catalysts with unconventional properties.

CHAPTER 2

REACTIONS, MECHANISMS & MODELS

2.1 Overall Thiol Reaction

The oxidation of thiols involves a set of complex (parallel and consecutive) reactions (Figure 2.1). The process starts with the elementary acid/base reaction (Eq. 2.1), where the thiol (RSH) is near-instantaneously transformed into thiolate (RS^-) ions, the active reagent.[35] Next, the thiolate reacts with dissolved O_2, to produce the disulfide (RSSR) product and H_2O_2, while regenerating two hydroxide (OH^-) ions (Eq. 2.2).[36] This non-elementary reaction occurs both catalytically and non-catalytically (non-Pc). The final non-elementary reaction (Eq. 2.3) utilizes the H_2O_2 produced in Equation 2.2 to transform another pair of thiolate molecules to a second disulfide, as well as regenerating a second pair of hydroxide molecules. Non-elementary reaction Equations 2.2 and 2.3 both contribute to thiol conversion and must be considered when calculating the rate of mercaptan consumption.[23]

$$4RSH + 4OH^- \Leftrightarrow 4RS^- + 4H_2O \quad \text{(elementary)} \quad (2.1)$$

$$2RS^- + 2H_2O + O_2 \rightarrow RSSR + H_2O_2 + 2OH^- \quad \text{(non-elementary)} \quad (2.2)$$

$$H_2O_2 + 2RS^- \rightarrow RSSR + 2OH^- \quad \text{(non-elementary)} \quad (2.3)$$

The net overall reaction for the above steps is: $4RSH + O_2 \rightarrow 2RSSR + 2H_2O$

As non-Pc pathways to RSH oxidation exist, it is important to estimate their relative contribution to RSH conversion since catalytic pathways are the primary focus of this study.

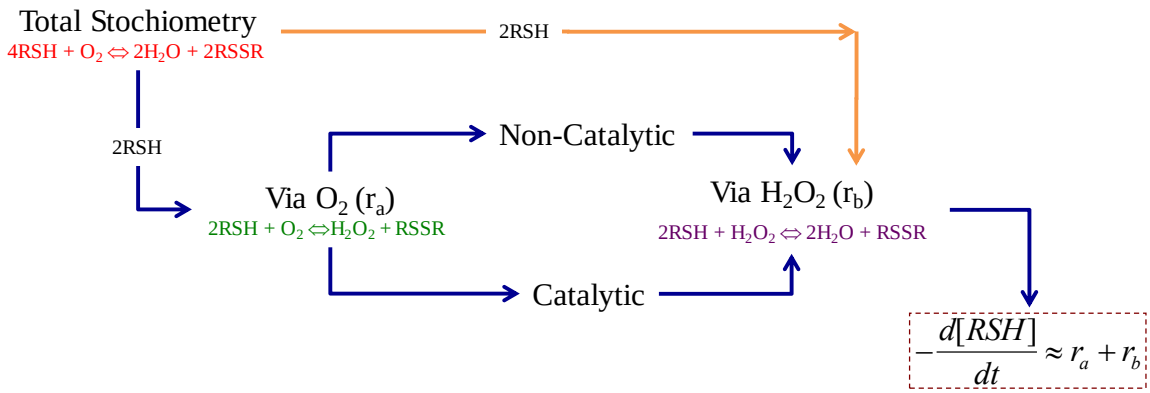

Figure 2.1 Overall mechanism for thiol oxidation. The r_a depends on choice of pathway, non-Pc vs catalytic and choice of rate-determining step. The r_b is provided by Giles et al.[23]

2.2 Oxygen-Induced Reaction

2.2.1 Hydroxide-Catalyzed Mechanism

The activation of O_2, necessary for oxidation reactions, is represented above by Equation 2.2. Loas et al.[37] observed that, in the absence of Pc catalyst, aerobic oxidation of 2-mercaptoethanol (2-ME) and 4-fluorobenzenethiol (4-FBT) still occurs, but to a significantly smaller extent. Little is published on the kinetics of the direct, non-catalyzed oxidation of these thiols by O_2 in solution.It is important consider the mechanism of action, and determine the rate model defining the non-catalyzed oxidation of the studied thiols, 2-ME and 4-FBT.

A likely mechanism, inspired by experimental results from Wallace et al.[36] is shown below:

$$RS^- + O_2 \rightarrow RSO_2^- \quad \textit{(slow)} \qquad (2.2a)$$

$$RS^- + RSO_2^- \Leftrightarrow RSSR + O_2^{2-} \qquad (2.2b)$$

$$O_2^{2-} + 2H_2O \Leftrightarrow H_2O_2 + 2OH^- \qquad (2.2c)$$

Equation 2.2a involves a thiolate reacting with dissolved oxygen to form a sulfoxide (RSO_2^-) intermediate. The sulfoxide intermediate then goes on to react with another thiolate molecule, forming a disulfide and peroxide ion in Equation 2.2b. Finally, in Equation 2c, the peroxide ion reacts with water to form hydrogen peroxide and regenerate two hydroxide molecules. Reactions 2.2b and 2.2c, which involve the sulfoxide and peroxide intermediates, respectively, are both considered to be relatively fast. Reaction 2.2a is assumed to be the rate-determining step. However, this assumption will be tested against experimental data.

The above follows a general acid/base chemistry, where there is an equilibrium involving the addition of a base to the substrate followed by a slow reaction of the complex.[38] The kinetics of thiol oxidations in the presence of hydroxide is studied as a basis for understanding the Merox process.

2.2.2 Catalytic Mechanism

The oxygen involved in catalytic thiol oxidation can also be activated catalytically. Metallo-phthalocyanine catalysts were found to be the most promising for thiol oxidations.[8] The macrocyclic structures of phthalocyanine catalysts are similar to that of porphyrins, a natural occurring group of organic compounds that help in the formation of important substances in the body such as hemoglobin.[11] Suggested potential mechanisms were based on the proposed, evidenced, and generally accepted mechanism of cytochrome P-450.[39] This well-understood mono-oxygenase enzyme mechanism (Figure 2.2) involves the insertion of one atom of oxygen into an organic substrate (RH) to form an oxygenated organic (ROH), while the other oxygen atom is reduced to water. Other borrowed concepts included its cyclic mechanism, metal center, reduction/oxidation of

the metal active site, binding substrate, and expulsion of a product. There were many different options in terms of viable mechanisms. The goal was to produce a likely mechanism that would help elucidate the effects of substituted perfluoropropyl groups by deriving models based on assumptions about each proposed mechanism and finally, determining which models were consistent with observed oxidation data.

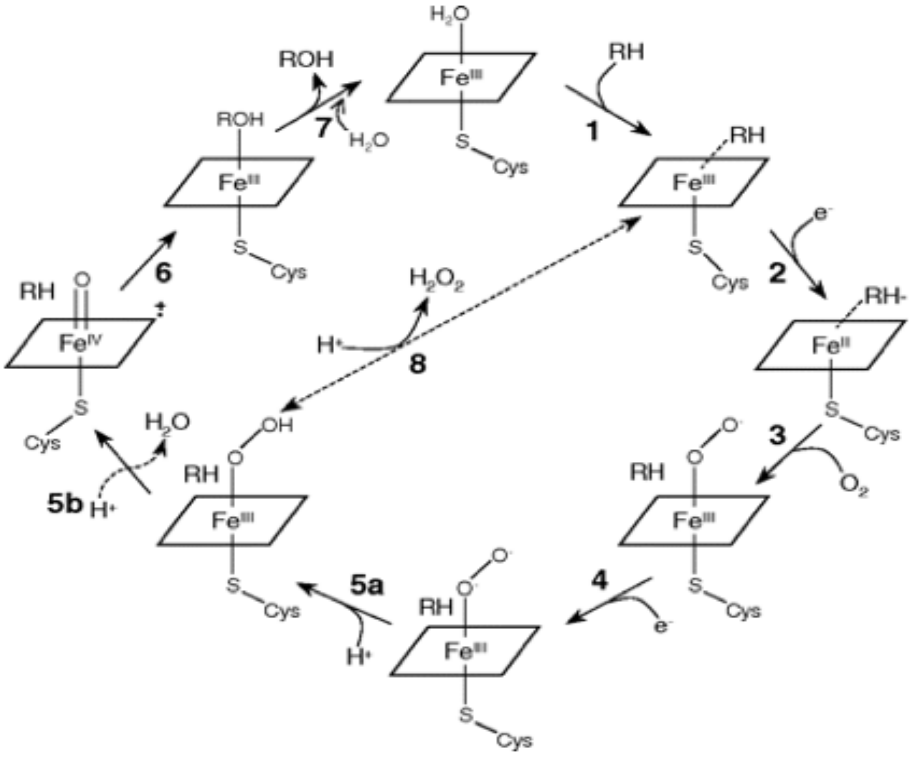

Figure 2.2 Catalytic cycle for cytochrome P-450 aerobic oxidations.[39]

Two possible mechanisms describing homogeneous metallo-phthalocyanine catalyzed oxidation of thiols were established. The mechanisms were inspired by the above cytochrome P-450 mechanism, as well as assumptions proposed by Loas.[14] Each mechanism begins with the formation of thiolate, and the subsequent insertion of the thiolate into the metal center of the catalyst. Mechanism A explored the possibility of thiyl radical ($RS^{\bullet}$) being expelled once formed in the catalyst cavity, and forming the disulfide product (RSSR) in solution (outside the cavity). Mechanism B sought to test

the likelihood of the disulfide product being formed within the catalyst cavity.

Figure 2.3 is an illustration of the proposed 10-step Mechanism A, where RSSR forms outside the catalyst molecule. After the RS^- is formed (step i, independent of the catalyst), the substrate RS^- attaches to the metal center (step ii), which is then reduced [Co(II) to Co(I) in this case, step iii]. Then, dissolved O_2 attaches to the metal center (step iv), accepting the electron from the metal "wire" (step v), with Co(I) oxidizing back to Co(II). The $RS^\bullet$ leaves the catalyst for coupling with another $RS^\bullet$ to form RSSR in solution (step vi).

After step vi, the cycle essentially repeats itself (steps vii-x) with insertion of another RS^-. One can assume, once the Co(II) is regenerated from Co(I), that the second RS^- is equally likely to coordinate to PcCo(II) as to PcCo(II)…O_2^-. The thiolate is simply looking for a metal center in the appropriate oxidation state. Therefore, the cycle in Figure 2.3 can be simplified to three summary steps (Figure 2.4). Steps ii and iii are combined, assuming that thiolate immediately transfers an electron to the metal center as it enters the catalyst cavity and attaches to the metal center. Steps iv and v are combined, assuming the O_2 withdraws an electron as it attaches to the metal center.

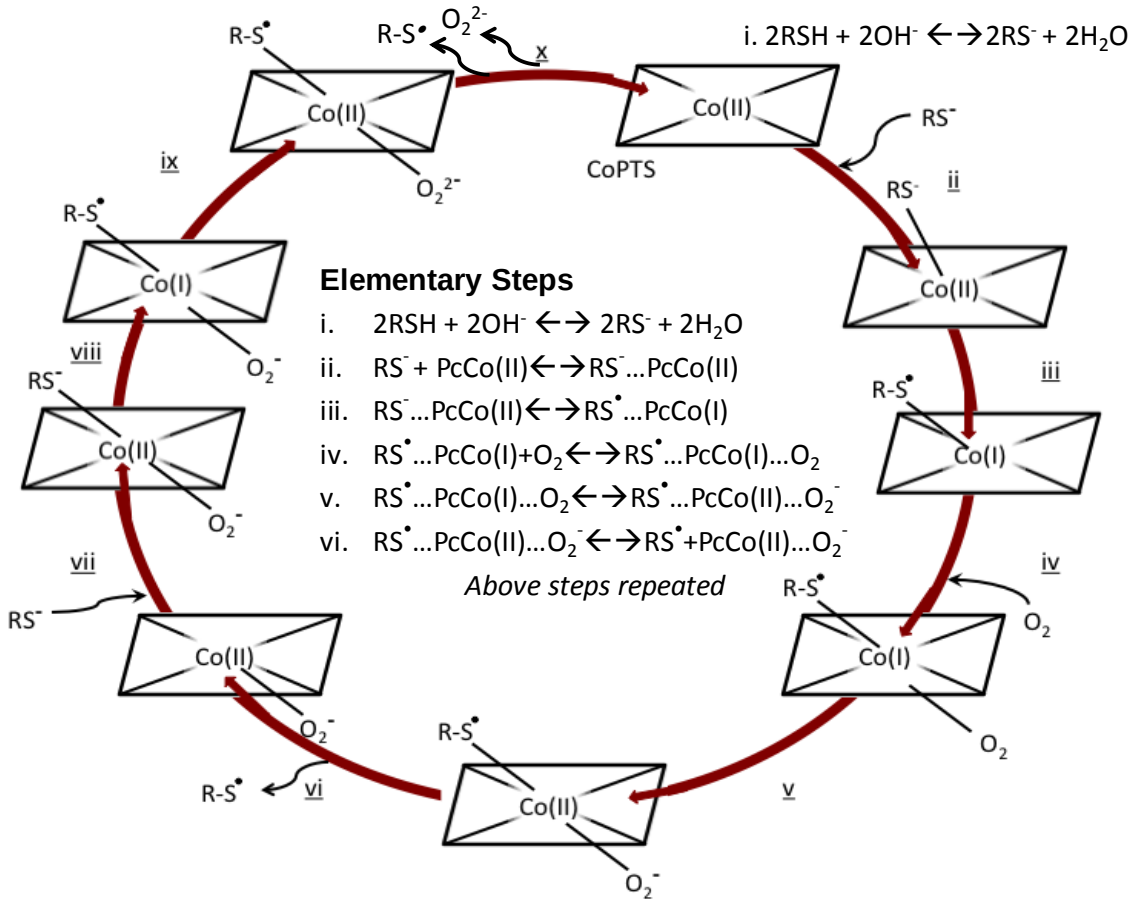

Figure 2.3 Proposed mechanism A for the aerobic oxidation of thiols catalyzed by cobalt phthalocyanines, assuming thiyl radical-radical coupling to form disulfide product in solution (outside catalyst molecule).

1. $2RSH + 2OH^- \leftrightarrow 2RS^- + 2H_2O$

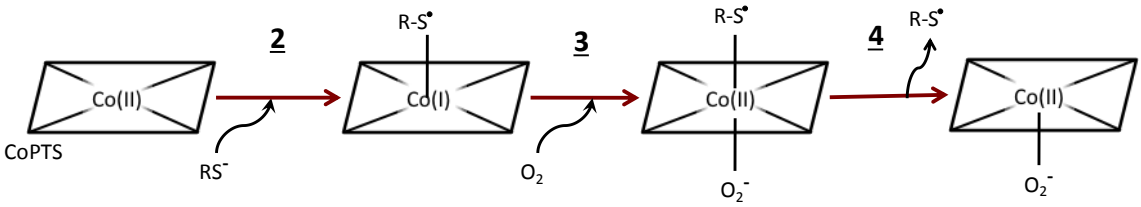

Figure 2.4 Simplified mechanism (effective steps) for the aerobic oxidation of thiols catalyzed by cobalt phthalocyanines, assuming thiyl radical-radical coupling in solution.

An alternative 9-step catalytic cycle, Mechanism B (Figure 2.5), was also considered. Here, the $RS^{\bullet}$ remains bound to the metal center as another thiolate attaches to the metal center (step vi). The thiolate transfers an electron to the metal center,

forming the second thiyl radical (step vii). As the disulfide is formed in the catalyst cavity, the reduced metal center transfers an electron to the attached superoxide (O_2^-) (step viii). Finally, the RSSR formed by thiyl radical-radical combination is expelled from the catalyst, along with the peroxide ion (O_2^{2-}) (step ix). As above, this cycle can be simplified to a sequence of essential steps, shown by Figure 2.6. Once again, electron transfer steps were assumed to occur simultaneously with its attaching/detaching counterpart.

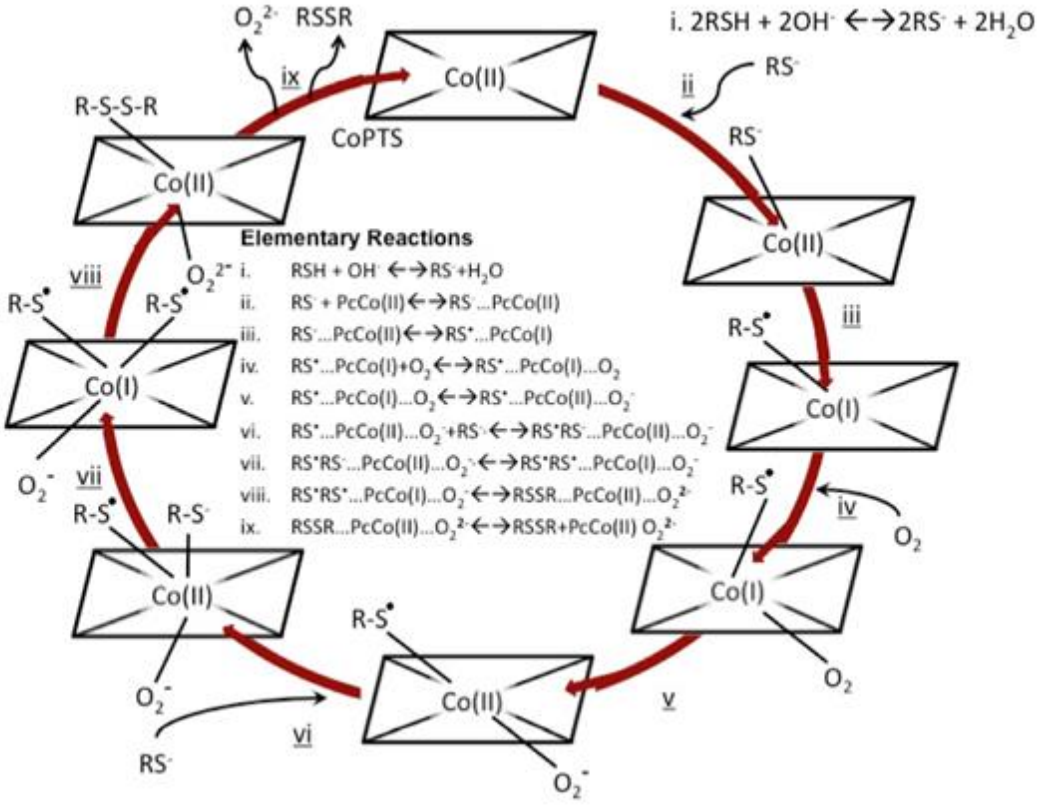

Figure 2.5 Proposed mechanism B, for the aerobic oxidation of thiols catalyzed by cobalt phthalocyanines, assuming thiyl radical-radical coupling to form disulfide product inside the catalyst cavity.

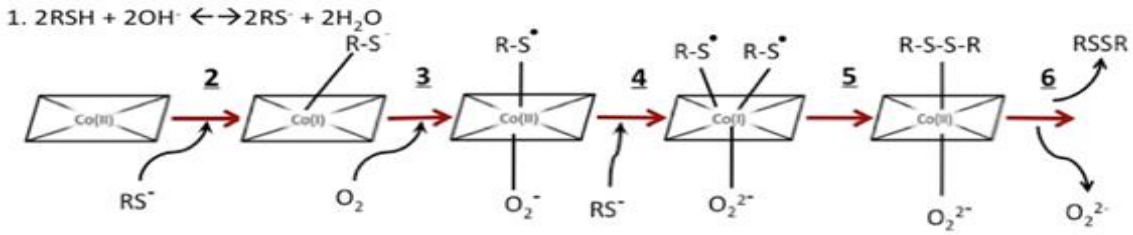

Figure 2.6 Simplified mechanism (effective steps) for the aerobic oxidation of thiols catalyzed by cobalt phthalocyanines, assuming thiyl radical-radical coupling in catalyst cavity.

2.3 Hydrogen Peroxide Induced Mechanism

Hydrogen peroxide has been shown to play a significant role in the oxidation of thiols.[23-28] Equation 2.3 shows that the above, catalytic or non-Pc mechanism, is followed by further thiol oxidation via H_2O_2, which cannot be ignored. As shown in the non-Pc mechanism, peroxide ion is formed and reacts with water (Equation 2.2c), to produce hydrogen peroxide and regenerate two hydroxide ions. Similarly, in the proposed catalytic mechanism, the activated oxygen leaves the catalyst molecule as a peroxide ion O_2^{2-}. This was then assumed to rapidly react with two H_2O to yield H_2O_2 according to $O_2^{2-} + 2H_2O \rightarrow H_2O_2 + 2OH^-$.[14]

Giles et al.[23] spectrophotometrically determined rates for the non-Pc oxidation of 2-mercaptoethanol as a function of thiol and H_2O_2 concentrations in an aqueous medium under nitrogen. Giles et al.[23] suggested that, as H_2O_2 is produced, it causes the fast consumption of the second pair of RS^-. The intermediate H_2O_2 consumes two more RS^-, thus restoring the OH^- used up to form the RS^-. Giles et al.[23] provide a mechanism for this peroxide-induced RSH consumption.

$$RS^- + H_2O_2 \rightarrow RSOH + OH^- \textit{ (slow)} \qquad (2.3a)$$

$$RS^- + RSOH \Leftrightarrow RSSR + OH^- \qquad (2.3b)$$

Within this two-step sequence, step 2.3a, production of a sulfenic acid, is the likely slow step[23], with a derived rate for RS^- consumption by H_2O_2:

$$-r_{RSH} \approx 2k_{H_2O_2}[H_2O_2][RSH] \quad (2.4)$$

Giles defined $k_{H_2O_2}$ =$k_2K_1[OH^-]/[H_2O]$.[23] Further analysis was done to determine the relevance of this hydrogen peroxide induced reaction to the conditions of interest in this study. The reaction under Giles' conditions occurs in the order of seconds. The thiol oxidation via H_2O_2 was considered relatively fast, and was very important for model development. This assumption was tested by comparing reaction rates and kinetics of hydrogen peroxide induced reaction with catalytic and non-Pc reaction pathways. Equation 2.4, proven by Giles et al.,[23] provided a functioning model included in the derivation of catalytic and non-Pc models in the present study.

Although different catalysts were used in the study, the reaction rate in solution via H_2O_2 should not change. Using the rate equation provided by Giles et al.,[23] kinetic parameters were determined under given experimental conditions. An additional mercaptan conversion experiment was also conducted, in the absence of both oxygen and catalyst. This anaerobic experiment supported the claim of the relevance of hydrogen peroxide in the consumption of mercaptan specific for the proposed system.

2.4 Model Derivation

Kinetic models for catalytic and non-Pc mercaptan oxidations were based on a set of complex reactions. The overall stoichiometry for mercaptan oxidation is shown in Equation 2.5:

$$4RSH + O_2 \rightarrow 2H_2O + 4RSSR \quad (2.5)$$

As shown in Figure 2.1, the complete reaction can be broken up into two non-elementary reactions for either oxygen-induced (catalytic or non-Pc) or hydrogen peroxide-induced cases.

a. $2RSH + O_2 \Leftrightarrow H_2O_2 + RSSR$ (via O_2)

b. $2RSH + H_2O_2 \Leftrightarrow 2H_2O + RSSR$ (via H_2O_2)

The first reaction involves two thiol species interacting with oxygen to form a disulfide and hydrogen peroxide. The peroxide then continues to react with another pair of thiol molecules to form the second disulfide and water. Equation 2.6 represents the total reaction rate and is the sum of reactions rates via activated oxygen (r_a) and hydrogen peroxide (r_b).

$$-\frac{d[RSH]}{dt} = r_a + r_b \tag{2.6}$$

where $-r_b \approx 2k_{H_2O_2}[H_2O_2][RSH]$ originates from the model derived by Giles et al.[23] (Equation 2.4). The concentration of hydrogen peroxide concentration is unknown. Because the concentration of H_2O_2 is involved in both reactions a and b, r_a must also be found.

The full derivation of the following case can be found in Appendix B. Considering the non-Pc case, Equation 2.2a was assumed as slow, while other steps were considered relatively fast. This assumption was used in derivation of the non-Pc thiol oxidation model.

$$-r_a \approx \frac{2k_2K_1[O_2][OH^-]}{[H_2O]}[RSH] \approx 2k_{app}[O_2][RSH] \tag{2.7}$$

where K_1 is the equilibrium constant representing conversion of RSH to RS^- and k_2 is the rate constant representing the binding of thiolate to O_2.

Assuming at standard conditions,the rate of hydrogen peroxide production occurs very rapidly,

$$\frac{d[H_2O_2]}{dt} \approx r_a - r_b \approx 0 \tag{2.8}$$

Plugging in Equations 2.4 and 2.7 to the above (Eq. 2.8), and making the pseudo steady-state hypothesis, the concentration of hydrogen peroxide can now be estimated for this specific case.

$$[H_2O_2] \approx k_{app}[O_2] / k_{H_2O_2} \tag{2.9}$$

The total thiol consumption can now be determined for the non-Pc case, assuming step 2 in the non-Pc mechanism is the rate-determining step and combining Equations 2.5, 2.7, and 2.9.

$$-\frac{d[RSH]}{dt} = 4k_{app}[O_2][RSH] \tag{2.10}$$

Similarly, models assuming various mechanisms and rate-determining steps were derived for both catalytic and non-Pc cases, where one step is considered slow or rate-determining, while others are considered to be in fast equilibrium. The algorithm for further derivations is as follows:

1. Determine r_a, by assuming a rate-determining step for the mechanism of interest
2. Plug r_a and r_b into Equation 2.8, and solve for estimated $[H_2O_2]$, assuming PSSH
3. Plug $[H_2O_2]$ into Equation 2.4, to solve for r_b
4. Plug values of r_a and r_b into Equation 2.6 to determine the total rate of thiol consumption.

Appendices A thru K provide detailed derivations of all models tested against observed thiol concentration versus time oxidation data.

Table 2.1 shows models for the proposed Hydroxide-catalyzed (nonPc) mechanism, and the two possible catalytic mechanisms. Parameters α, β and γ depended

on choice of rate-determining step. Mechanism A assumed radical-radical coupling to form the disulfide product occurs in solution (outside catalyst cavity), while mechanism B explored the possibility that the disulfide may be formed in the cavity of the catalyst. Mechanism A and the form of proposed models II and III are similar to that found in Ganguly et al.[40] and Tyapochkin et al.[21] Models were fitted to experimental data using a nonlinear regression computational program. Criteria for the choosing the correct model include: positive rate constants relatively large r^2 values; small 95% confidence values, relative to corresponding parameter;; models and constants which are chemically and physically logical; models and constants which are consistent with literature where available.

Table 2.1 Proposed Models and Elementary Steps of Possible Pc-catalyzed and Hydroxide-Catalyzed Mechanisms

*$2RSH + 2OH^- \longleftrightarrow 2RS^- + 2H_2O$: Initial Step: Shared by all mechanisms

Non-Catalytic Mechanism

Model	Steps	Elementary Reaction (Rate-determining step)		Rate Form
nonPcI	1	$RS^- + O_2 \longleftrightarrow RSO_2^-$	1st thiolate binding to O_2	$-r_{nonPcI} \approx 4k_{app}[O_2][RSH]$
nonPcII	2	$RS^- + RSO_2^- \longleftrightarrow RSSR + O_2^{2-}$	2nd thiolate binding to RSO_2^-	$-r_{nonPcII} \approx 4k_{app}[O_2][RSH]^2$

Mechanism A - Radical-radical combination to form disulfde occurs in solution

Model	Steps	Elementary Reaction (Rate-determining step)		Rate Form
I	1	$RS^- + PcCo(II) \longleftrightarrow RS^{\cdot} \ldots PcCo(I)$	Substrate binding, where radical-radical coupling occurs in solution	$-r_I \approx 4\alpha[RSH]$
II	2	$RS^{\cdot} \ldots PcCo(I) + O_2 \longleftrightarrow RS^{\cdot} \ldots PcCo(II)\ldots O_2^-$	Electron transfer from metal center to O_2, where radical-radical coupling occurs in	$-r_{II} \approx \frac{4\alpha[RSH]}{1+\beta[RSH]}$
III	3	$RS^{\cdot} \ldots PcCo(II)\ldots O_2^- \longleftrightarrow RS^{\cdot} + PcCo(II)\ldots O_2^-$	Radical expulsion, where radical-radical coupling occurs in solution	$-r_{III} \approx \frac{4\alpha[RSH]}{1+\beta[RSH]}$

Mechanism B - Radical-radical combination to form disulfide occurs in catalyst cavity

Model	Steps	Elementary Reaction (Rate-determining step)		Rate Form
IV	1	$RS^- + PcCo(II) \longleftrightarrow RS^{\cdot} \ldots PcCo(I)$	1st substrate binding, where radical-radical coupling occurs in catalyst cavity	$-r_{IV} \approx \frac{4\alpha[RSH]}{1+\beta/[RSH]+\gamma[RSH]}$
V	2	$RS^{\cdot} \ldots PcCo(I) + O_2 \longleftrightarrow RS^{\cdot} \ldots PcCo(II)\ldots O_2^-$	Electron transfer from metal center to O_2, where radical-radical coupling occurs in	$-r_V \approx \frac{4\alpha[RSH]}{1+\beta/[RSH]+\gamma[RSH]}$
VI	3	$RS^- + RS^{\cdot} \ldots PcCo(II)\ldots O_2^- \longleftrightarrow RS^{\cdot}\ RS^{\cdot} \ldots PcCo(I)\ldots O_2^-$	2nd substrate binding, where radical-radical coupling occurs in catalyst cavity	$-r_{VI} \approx \frac{4\alpha[RSH]^2}{1+\beta[RSH]}$
VII	4	$RS^{\cdot}\ RS^{\cdot} \ldots PcCo(I)\ldots O_2^- \longleftrightarrow RSSR \ldots PcCo(II)\ldots O_2^{2-}$	Electron transfer from metal center to O_2^-, where radical-radical coupling occurs in	$-r_{VII} \approx \frac{4\alpha[RSH]^2}{1+\beta[RSH]+\gamma[RSH]^2}$
VIII	5	$RSSR \ldots PcCo(II)\ldots O_2^{2-} \longleftrightarrow RSSR + PcCo(II) + O_2^{2-}$	Disulfide product expulsion, where radical-radical coupling occurs in catalyst cavity	$-r_{VIII} \approx \frac{4\alpha[RSH]^2}{1+\beta[RSH]+\gamma[RSH]^2}$

Hydrogen Peroxide-induced mechanism[23]

Model	Steps	Elementary Reaction (Rate-determining step)		Rate Form
	1	$RS^- + H_2O_2 \longleftrightarrow RSOH + OH^-$	Slow	$-r_{H_2O_2} \approx 2k_{H_2O_2}[H_2O_2][RSH]$
	2	$RS^- + RSOH \longleftrightarrow RSSR + OH^-$	Fast	N/A

CHAPTER 3

EXPERIMENTAL MATERIALS AND METHODS

3.1 Experimental Conditions

3.1.1 Materials

The thiols tested were 99.0% 2-mercaptoethanol (Sigma-Aldrich) and 98.0% 4-fluorobenzenethiol (Sigma-Aldrich). Other chemical compounds used in thiol oxidation experiments include NaOH (Sigma-Aldrich); H_2O_2 ~ 50 wt. % in H_2O (Sigma-Aldrich); 2-hydroxyethyl disulfide (Sigma-Aldrich); 99.9% Purified Stabilized tetrahydrofuran (THF) (Acros Organics). The 2-mercaptoethol, 2-mercaptoethanol solutions, NaOH solutions, H_2O_2 solutions and 2-hydroxyethyl disulfide were stored in a lab refrigerator. The 4-fluorobenzenethiol and 4-fluorobenzenethiol solutions were stored under an evacuated and inert gas filled storage container (Lab Conco, 5530000).

Catalysts used for thiol oxidations included H_{16}PcCo (TCI America, GCO!-MASF) and F_{16}PcCo (Sigma-Aldrich, 446645-1G), both purchased and used as received (no modification, i.e. added to silica support) from the vendors; and F_{64}PcCo, prepared and purified according to published literature procedures,[3,17] and provided under research subcontract by S. Gorun (currently at Seton Hall University, Chemistry Department, South Orange, NJ). Catalyst solutions were prepared via ultrasonic mixing in amounts specified in Section 3.1.2 in a 50ml glass Erlenmeyer flask (Pyrex USA). The 50ml solutions were then added to 200 ml of THF, shaken, and stored in a 250 ml glass bottle (Wheaton USA). Catalyst solutions were stored in the refrigerator.

Gases used in reactions and GC analysis (see Section 3.3) included zero grade compressed hydrogen (Airgas); zero grade compressed helium (Airgas); zero grade

compressed air (Airgas); zero grade compressed nitrogen (Airgas); 99.999% compressed oxygen (Airgas); 5.0002% +/- 2% compressed oxygen, balance nitrogen (Airgas). Gas flow into the reactor and GC were measured with a soap film flow meter (1-10-100 ml, Hewlett Packard, 0101-0113).

3.1.2 Aerobic Oxidation Experiments

Thiol oxidation experiments were designed to replicate prevalent mercaptan levels in industrial processes[41] and recent laboratory studies.[14] Standard initial concentrations of chemical compounds used include 140 mmol/L of thiol (0.50 ml 2-mercaptoethanol, 0.75 ml 4-fluorobenzenethiol) loaded with a 5ml gas-tight syringe (Hamilton, 1002); 0.0105 mmol/L of catalyst (H_{16}PcCo ~ 0.3 mg, F_{16}PcCo ~ 0.45 mg, F_{64}PcCo ~ 0.93 mg); 2.58 mmol/L of NaOH prepared as a 0.25 wt. % aqueous solution (~1.0 ml); and 50mL of THF in an agitated semi-batch 100 mL glass reactor. The reaction solution, including catalyst, was an entirely homogeneous, single-phase liquid. The catalysts, as purchased or delivered, were solid powders. Required amounts were weighed out with an analytical balance.

3.1.3 Reactor Set-Up

Figure 3.1 shows a schematic for the reactor experimental set-up. The reaction vessel used was a magnetically stirred (Stirrer dimensions: L: 3” x D: 0.3”, Fisher) 100 mL glass jar (Pyrex USA, 1395) with a screw top fitted with gas-tight valves. One fitting was used as an access port for liquid sample withdrawal by 25µl gas-tight syringe (25s/2”2, Hamilton, 80230), equipped with 7” needle (22s GA RN, Hamilton, 7804-02). The elongated needle was required for sample (5 µl) extraction. The same fitting was used to

purge the reactor vessel with gas concentrations specific for the experiment of interest. A Teflon©-coated thermocouple (Omega, P12C40) was inserted into the liquid. A custom-machined right-angle Teflon© baffle was fitted onto the thermocouple to break up liquid swirl and enhance gas/liquid contacting. With enhanced mixing, the reactor was operated at an agitation rate (1800 rpm) such that observed thiol consumption vs. time was independent of this rate as shown by Figure 3.2. The reactor temperature was held at 22° C in a circulated constant-temperature bath (Polyscience, 807181), while total absolute pressure of 101 kPa was actively manually maintained, and was monitored by a voltage output pressure transducer (Omega, PX309-100A5V). A Cryocool (Neslab Instruments, Inc., CC6DF) was used to cool the circulating bath for experiments held constant at temperatures lower than room temperature. A partial pressure of O_2 existed above the liquid to replenish O_2 consumed by reaction in the liquid.

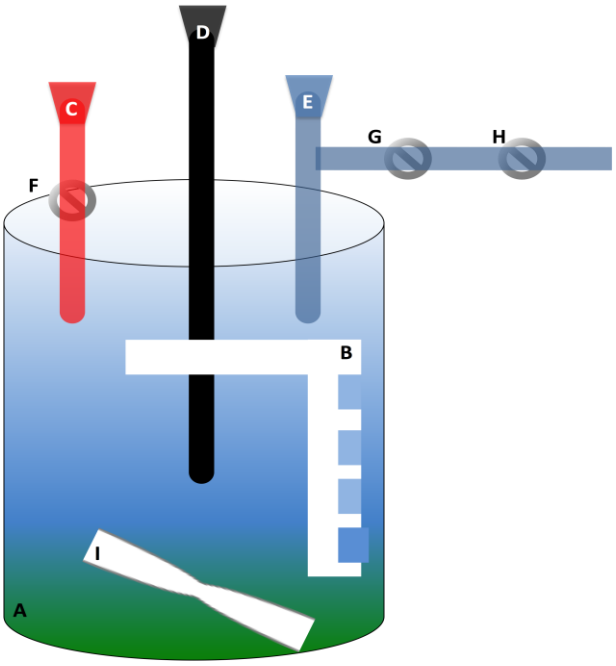

Figure 3.1 Schematic of experimental set-up. A: 100 ml glass vessel; B: Baffle; C: Port used for injection and extraction; D: Temperature Probe; E: Pressure Transducer; F: Injector/Extraction valve; G: Needle valve; H: Gas inlet valve; I: Magnetic Stirrer.

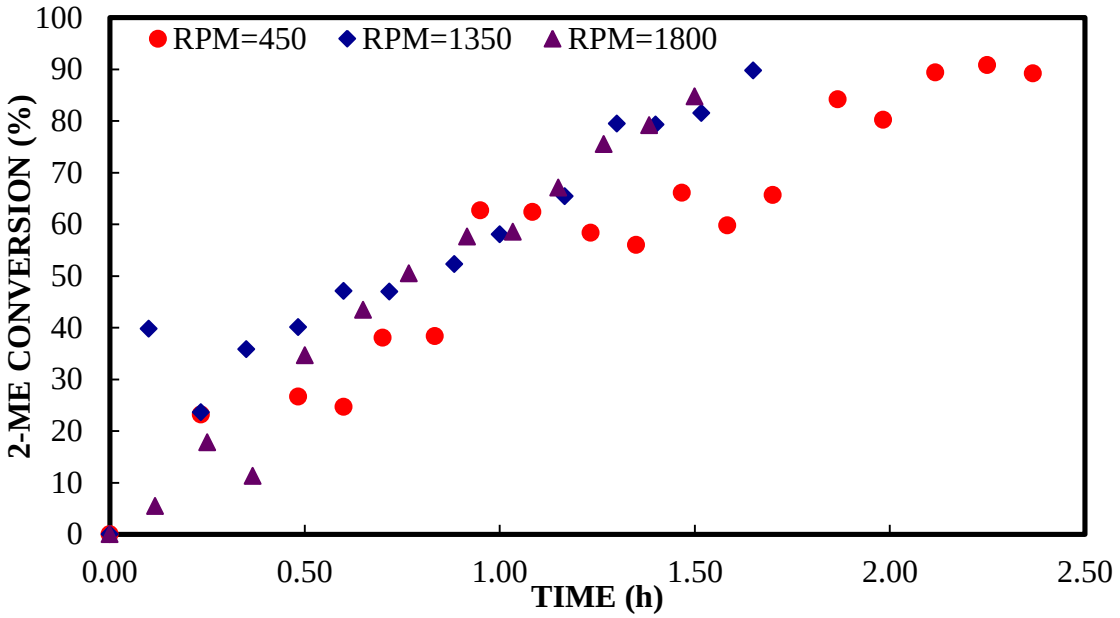

Figure 3.2 Total oxidation of 2-Mercapotethanol, catalyzed by F_{16}PcCo under air, at varying stirring speeds.

3.2 Inert Atmosphere Techniques

4-Fluorobenzenethiol was chosen as an alternate thiol to observe the effects of using a larger and more Lewis acidic molecule in terms of steric bulkiness and acidity, respectively. Unfortunately, 4-fluorobenzenethiol is found to be very reactive in air.

Due to its sensitivity in air, 4-fluorobenzenethiol solutions were prepared and handled in an Atmosbag (Sigma-Aldrich, Z530212-1EA), purged and filled with Nitrogen. Solutions were also stored in an evacuated container filled with Nitrogen.

3.3 Gas Chromatograph Analysis

Thiol concentrations were measured using a Hewlett-Packard 5890 Gas Chromatograph with flame ionization detector (FID). A number of tests were conducted in order to find the optimum column and GC conditions for thiol oxidation experiments. The most effective column for 2-mercaptoethanol and 4-fluorobenzenetihol analyses was found to

be a Zebron ZB-WaxPlus column (30m x 0.53mm x 1 mm-Phenomenex, 240261). The GC conditions were: FID air ~200 cc/min and H_2 ~25 cc/min; carrier He ~30 cc/min (all zero grade); injector/detector temperature: 250 °C; oven temperature program: starts at 65 °C (2-ME oxidations) or 85 °C (4-FBT oxidations), increases at a rate of 10 °C/min. to 150 °C. Range and attenuation were set at 5 and 0, respectively. Five microliter samples of the reaction mixture were withdrawn from the reactor, with 1 μL injected using a gastight syringe through an on-column, split-less injector. All data responses were monitored, collected and analyzed with Logger Pro 3 (Vernier Software & Technology) on a Dell Dimension 2400 2.8 GHz 512 MB RAM 200 GB Hard Drive Desktop.

Figure 3.3 shows the GC response for a 71.0 mmol/L solution of 2-mercaptoethanol. The GC response shows good separation between THF (first) and 2-mercaptoethanol (second) peaks.

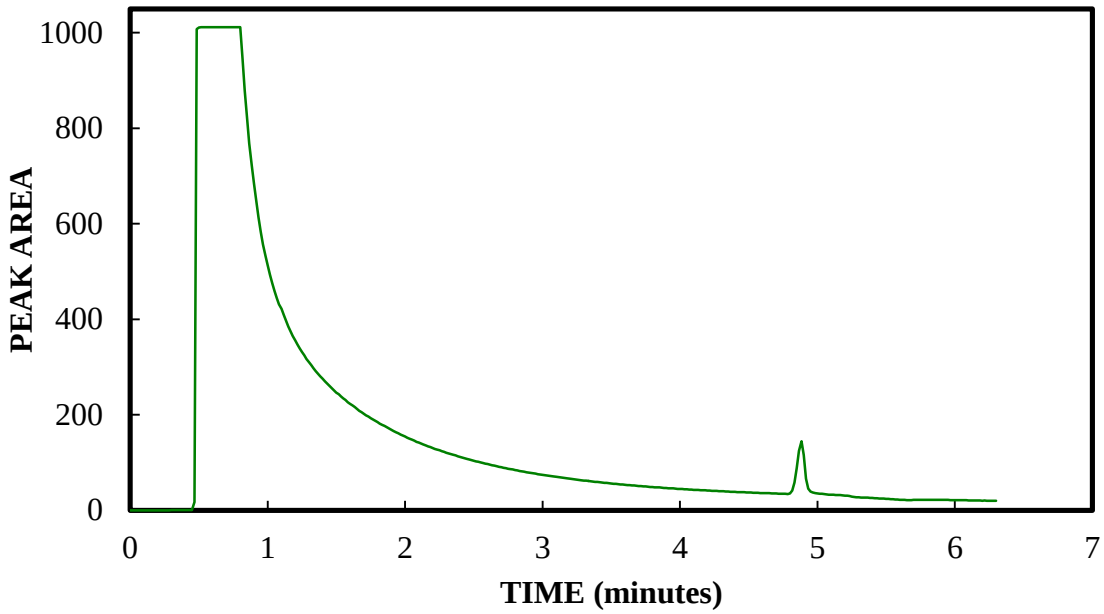

Figure 3.3 Typical GC response for 71.0 mmol/L solution of 2-mercaptoethanol under specified GC conditions.

Table 3.1 shows peak areas for repeated 71.0 mmol/L sample injections, in order to test for instrument precision. Analytical uncertainty or the relative standard deviation

(RSD) was calculated as +/- 1.84% and can be applied to all injected samples.

Table 3.1. GC Peak Areas and Statistics From Repeated GC Injections of 71.0 mmol/L Solution of 2-Mercaptoethanol Under the Specified GC Conditions

Peak 1	Peak 2	Peak 3	Average (%)	Stand Dev.	% RSD
7.08	6.92	7.23	7.06	+/- 0.13	+/- 1.84

Before each sample was injected, the syringes were rinsed with THF, and then rinsed with portions of the current sample. Known concentration standards were analyzed at the start of each experimental session.

Small amounts of catalyst necessarily existed in each of the injected reactor samples, which might have led to further reactivity within the GC column. However, repeated experiments show GC peak areas of initial (time $\approx$ 0) thoil concentration equivalent to calibration injections where no catalyst was present. This suggests that any injected catalyst at the specified range of this study did not affect GC analysis of thiol concentrations.

Standards were tested before each set of thiol oxidations in order to calibrate the GC peak response. Finding the peak area response for a set of standards with known concentrations gives a linear relationship between peak area and thiol concentration. The linear relationship was then used to calculate thiol concentration of unknown samples. Figure 3.4 shows an example of 2-mercaptoethanol standards.

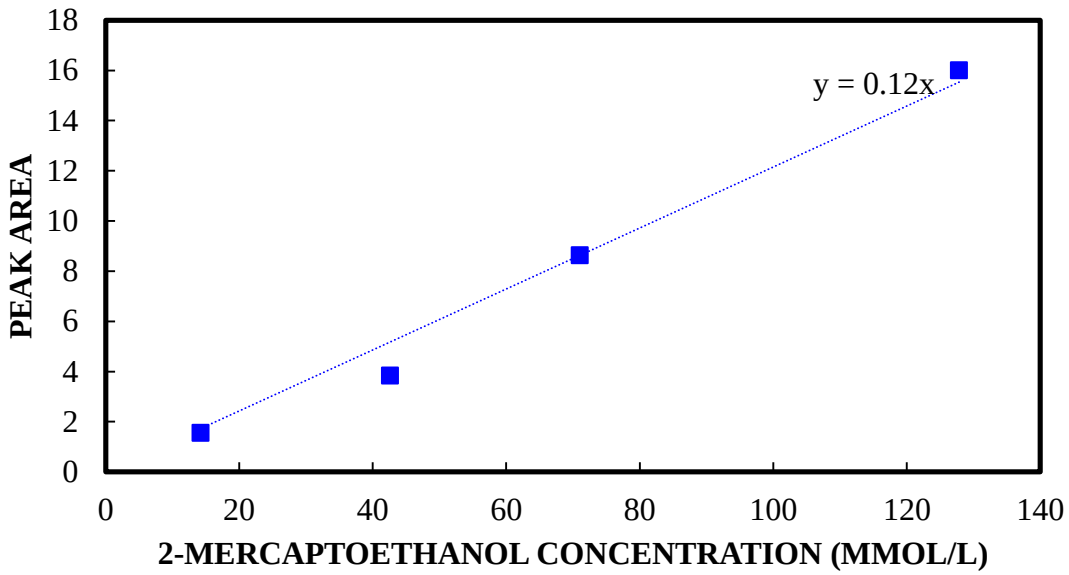

Figure 3.4 Example of GC peak response of 2-mercaptoethanol 14.2, 42.6, 72.0 and 127.8 mmol/L standards used for calibration.

In addition, an overall uncertainty was estimated. All elements of the experimental procedure were considered, including 2-ME, NaOH and THF measurements, temperature and pressure control, instrumental (GC) error and errors involved in sample extraction and injection. Figure 3.5 shows F_{16}PcCo catalyzed oxidations of 2-ME in the presence of 5% O_2 gaseous composition conducted on three days: 8/29/13, 9/9/13 and 9/17/13. Considering measurements taken at similar reaction times, an error of RSD = +/- 7% was calculated. The above calculation is considered for all experiments conducted in this study.

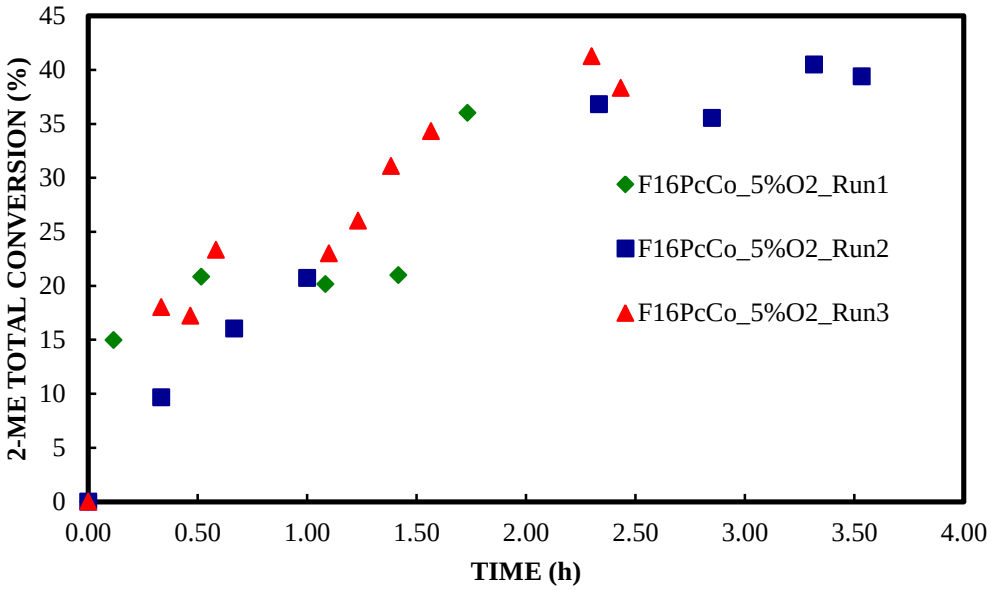

Figure 3.5 Repeated F_{16}PcCo catalyzed oxidation of 2-ME under 5% gaseous O_2.

Table 3.2 Observed Conversion of 2-ME catalyzed F_{16}PcCo for repeated Runs at ~ 1.08h

Conv. 1 (%)	Conv. 2 (%)	Conv. 3 (%)	Average (%)	Stand Dev.	% RSD
23.0	21.0	20.0	21.3	+/- 1.53	+/- 7

CHAPTER 4

BENCH SCALE OXIDATION OF 2-MERCAPTOETHANOL

4.1 Introduction

Experiments and kinetic analyses were conducted to elucidate the mechanism of action for the fluorinated, metal-centered, phthalocyanine (Pc)-catalyzed oxidation of thiols. Fluorine and fluoro-alkylated substituents on the phthalocyanine molecules cause its metal center to be electron-poor, thus potentially enhancing its catalytic oxidation capability, while also serving to protect the phthalocyanine itself from oxidative destruction.[14] The oxidations of 2-mercaptoethanol (2-ME) in the presence of commercial phthalocyanines (H_{16}PcCo, F_{16}PcCo), as well as a non-commercial phthalocyanine (F_{64}PcCo), were conducted in a small, bench-scale reactor.

In this study, 2-ME oxidation is seen to involve parallel and consecutive reactions. Thiol oxidation begins with the conversion of thiol to thiolate by OH^-.[35] The thiolate is then oxidized in a catalytic sequence inspired by cytochrome P-450.[39] This yields hydrogen peroxide, which then converts more thiolate in a simple, non-Pc pathway. Direct consumption of thiolate via dissolved O_2 was also studied, with no Pc catalyst present. In all thiolate conversion pathways, OH^- was regenerated. The OH^- can be considered a catalyst, as per Moore and Pearson[38] since any thiol oxidation cannot begin without RS^- produced from RSH by OH^-. But the emphasis of this study was Pc-catalysis. The overall oxidation stoichiometry for the thiol aerobic oxidation is:

$4\ RSH + O_2 \rightarrow 2\ RSSR + 2\ H_2O$.

Loas et al.[37] observed that, in the absence of Pc catalyst, aerobic oxidation of RSH still occurs, but to a significantly smaller extent. Little is published on the kinetics of the

direct, solely "hydroxide-catalyzed" thiol oxidation by O_2 in solution. This study also reports on recent experimental and kinetic modeling studies of the hydroxide-catalyzed oxidation of 2-mercaptoethanol (2-ME) at 22 ^{o}C and one atmosphere absolute pressure.

4.2 Hydroxide-Catalyzed Oxidation of 2-Mercaptoethanol

A likely elementary mechanism for non-Pc oxidation of 2-ME, inspired by Wallace and Schriesheim[36] is presented in Appendix A. Appendices B and C provide detailed derivations of proposed non-Pc models, Equations 4.1 and 4.2, respectively.

$$-\frac{d[RSH]}{dt} = 4k_{app}[O_2][RSH] \qquad \text{First Order} \qquad (4.1)$$

where $k_{app} = \frac{k_2 K_1 [OH^-]}{[H_2O]}$

$$-\frac{d[RSH]}{dt} = 4k_{app}[O_2][RSH]^2 \qquad \text{Second Order} \qquad (4.2)$$

where $k_{app} = \frac{k_3 K_2 K_1^2 [OH^-]^2}{[H_2O]^2}$

The hydroxide-catalyzed RSH oxidation pathway begins with the fast acid-base equilibrium to produce thiolate ion (RS^-), which is the active reagent.[35] The rate-determining step was assumed to be the coupling of RS^- to O_2, while the other steps were in a fast equilibria.

Figure 4.1 presents 2-ME (in THF) conversion data vs time for oxidation under pure O_2 in the presence of NaOH at 22 °C and 1 atm, while Table 4.1 provides numerical values for regressed parameters of assumed 1st and 2nd order models. Conversion (%) is calculated as: $([RSH]_o - [RSH])100/[RSH]_o$. The preferred fit, based on the relatively larger r^2 value, is first order in 2-ME. Leitao et al.[42] conducted similar non-catalytic

experiments, where the kinetics of N-butyl mercaptan (in n-heptane) oxidation with air in the presence of NaOH solution was studied, at 25 °C and 6 atm, stirred at 6000 rpm. Their results were also fitted to a first order model relative to thiolate ion RS^-.

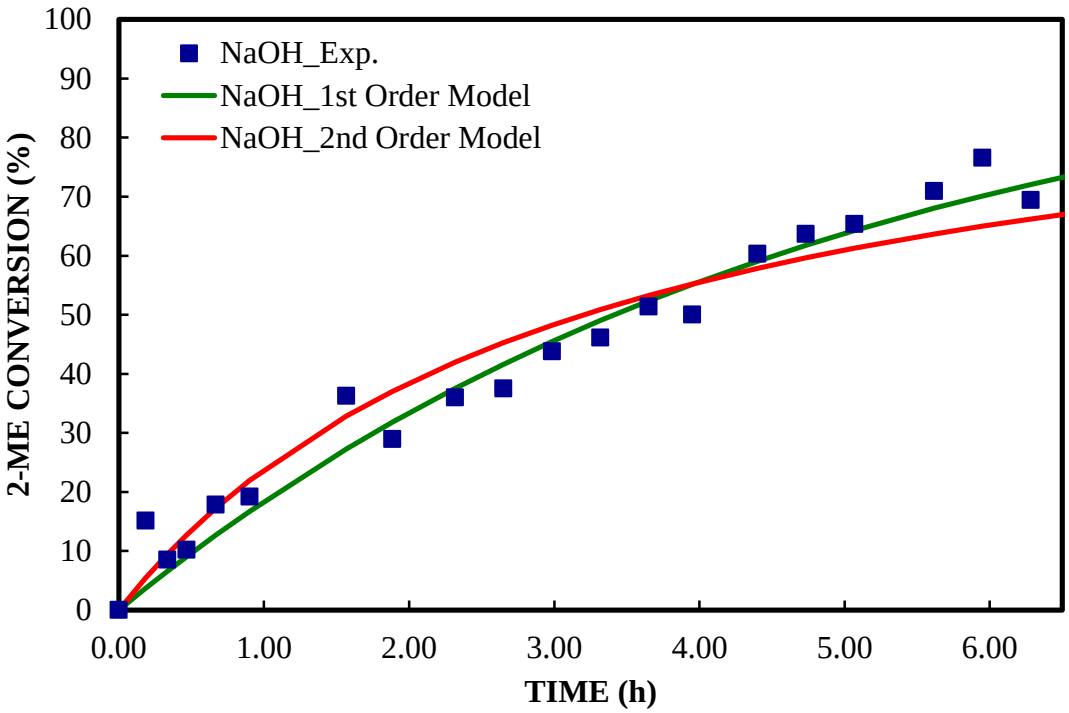

Figure 4.1 1st order and 2nd order fits of hydroxide-catalyzed oxidation of 2-ME under pure O_2 at 1 atm and 22 °C in the presence of 2.58 mmol/L of NaOH.

Table 4.1 Numerical Value and Statistics of Rate Parameter, k_{app}, for 1st and 2nd Order in [RSH], Hydroxide-Catalyzed Rate Models at Varying Concentration of NaOH in Initial Reaction Solution

NaOH (mmol/L)	Model	k_{app}(liter/mmole-hr)	r^2
1.65	1st Order	4.70E-03	0.956
	2nd Order	4.90E-05	0.930
2.58	1st Order	6.50E-05	0.966
	2nd Order	7.00E-05	0.942
5.17	1st Order	1.20E-02	0.986
	2nd Order	1.45E-04	0.947

Based on the first order kinetics, the kinetic parameter, k_{app}, suggests that the hydroxide-catalyzed oxidation of thiols is directly proportional to NaOH concentration. Experiments were conducted at additional concentrations of NaOH. Solutions of 0.16%

wt./wt. and 0.5% wt./wt. aq. of NaOH were prepared and used in the initial reaction solution. Table 4.1 also gives regressed values for 1st and 2nd order fits of these additional experiments. The preferred rate for supplemental experiments is also first order in 2-ME, as shown by Figure 4.2. Figure 4.3 shows k_{app} has a linear dependency on NaOH concentration, as predicted by the 1st order model.

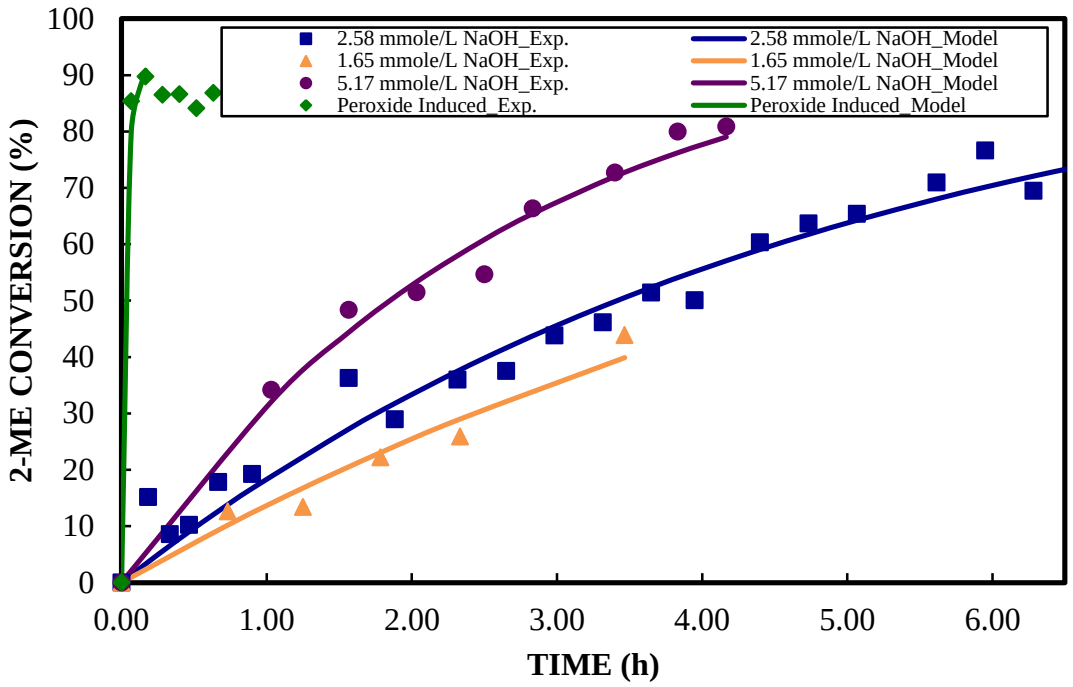

Figure 4.2 Experimental and fitted models of oxidation of 2-ME in 1.65, 2.58 and 5.17 mmol/L NaOH under pure O_2 at 1 atm and 22 °C. Experimental and fitted model of oxidation of 2-ME with H_2O_2 (stoichiometric mixture with 2-ME) under pure N_2 at 1 atm,22 °C, and NaOH = 2.58 mmol/L. Initial 2-ME concentration = 140 mmole/L in all cases.

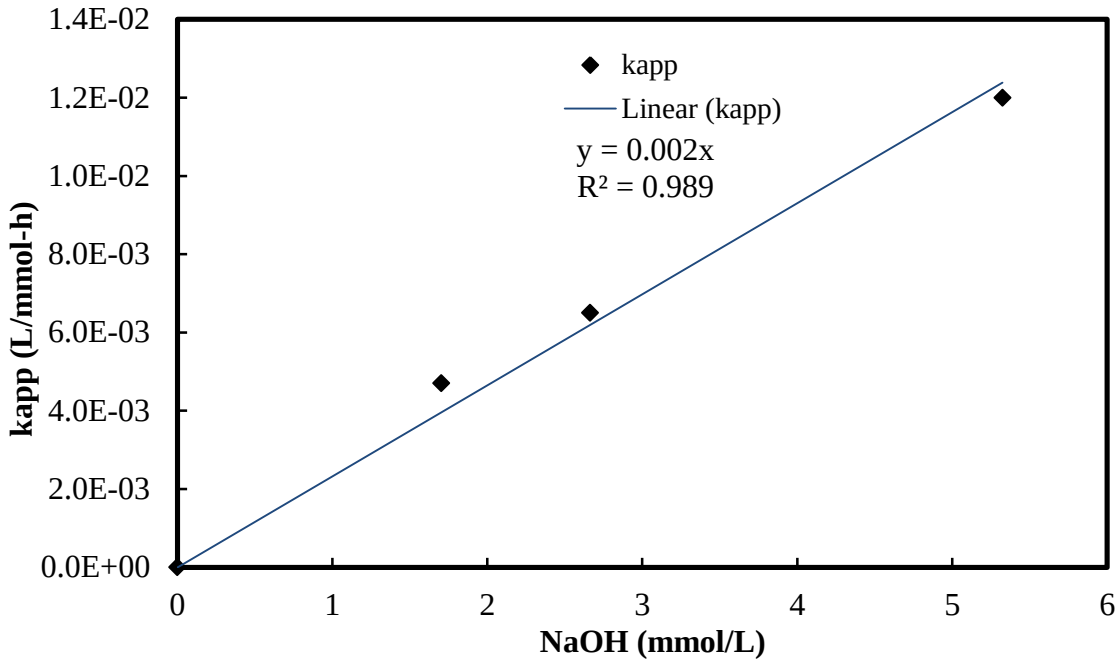

Figure 4.3 Regressed value of kinetic parameter, k_{app}, as it relates to NaOH concentration.

Giles et al.[23] suggest that, as reaction intermediate H_2O_2 is produced, it causes the fast consumption of the second pair of RS^- -- even faster than oxidation by O_2. As a test, the current experiment was repeated with a N_2 blanket (no O_2), and H_2O_2 as the oxidizing agent (initial concentration 76 mmol/L) with an approximately stoichiometric amount of 2-ME at 140 mmole/liter, the baseline 2-ME initial concentration in this study.

Under these stoichiometric conditions, and based on the rate determining step that is first order in each of RSH and H_2O_2, as shown in Equation 2.4:

$$-r_{RSH} \approx 2k_{H_2O_2}[H_2O_2][RSH] \qquad (2.4)$$

the RSH conversion data were fitted to a second order form for thiol conversion vs time, according to the integrated form of Equation 2.4, $[RSH] = \frac{[RSH]_o}{1+k_{H2O2}t[RSH]_o}$, as shown in Figure 4.2. The resulting regression yields $k_{H_2O_2}$ = 0.52 liter/mmole-hr. By direct comparison, $k_{H_2O_2}$ >> k_{app}=6.58x10^{-3} liter/mmol-hr. This suggests that, during oxidation

of 2-ME under O_2, the intermediate H_2O_2 is created and consumed as the overall reaction progresses, implying that the rate of the overall process is controlled by the original O_2 coupling. The above was applied in the derivation of non-Pc models, presented in Appendices B and C.

The slope from the regression in Figure 4.3 was used to estimate the k_2 from the H_2O_2 mechanism. Knowing the pK_a of 2-ME (pKa = 9.64) and H_2O (pKa = 15.7) for the initial acid/base reaction involving 2-ME and OH^-, K_1 was estimated as $K_1=10^{-9.643}/10^{-15.7}=1.14x10^6$. The $[H_2O]$=1100 mmol/L. The dissolved $[O_2]$=8.02 mmol/L, based on the constant O_2 gas pressure and Henry's Law constant=99.5 atm-L/mol at 22 ^oC.[43,44] The slope of Figure 4.3 provided a means of solving for k_2. The rate constant for the slow step of RS^- coupling with dissolved O_2 is $k_2=1.93x10^{-6}$ liter/mmole-hr at 22 ^oC. The above follows a general acid/base chemistry, where there is an equilibrium involving the addition of a base to the substrate followed by a slow reaction of the complex.[38]

4.3 Pc-Catalyzed Oxidation of 2-Mercaptoethanol

4.3.1 Experimental Data

Oxidations of 2-ME under pure O_2 were observed for the studied Pc catalysts, as shown in Figure 4.4. Conversion due to the non-Pc (i.e. hydroxide, but no Pc) mechanism was considered in all catalytic oxidations. While GC analysis provided the means to calculate total 2-ME conversion with time, analysis from Section 4.2 allows one to solve for 2-ME conversion via the non-Pc pathway at time, t. The total observed conversion minus conversion due to the non-Pc pathway gives conversion due to the Pc-catalytic mechanism. The above calculation was done for all catalytic data.

Among the three catalysts, F_{64}PcCo shows the fastest conversion, followed by

H_{16}PcCo, then F_{16}PcCo. Loas[14] claimed these catalysts under very similar reaction conditions exhibited structural stability exceeding 90% for 2-ME oxidations in the range of reaction times.

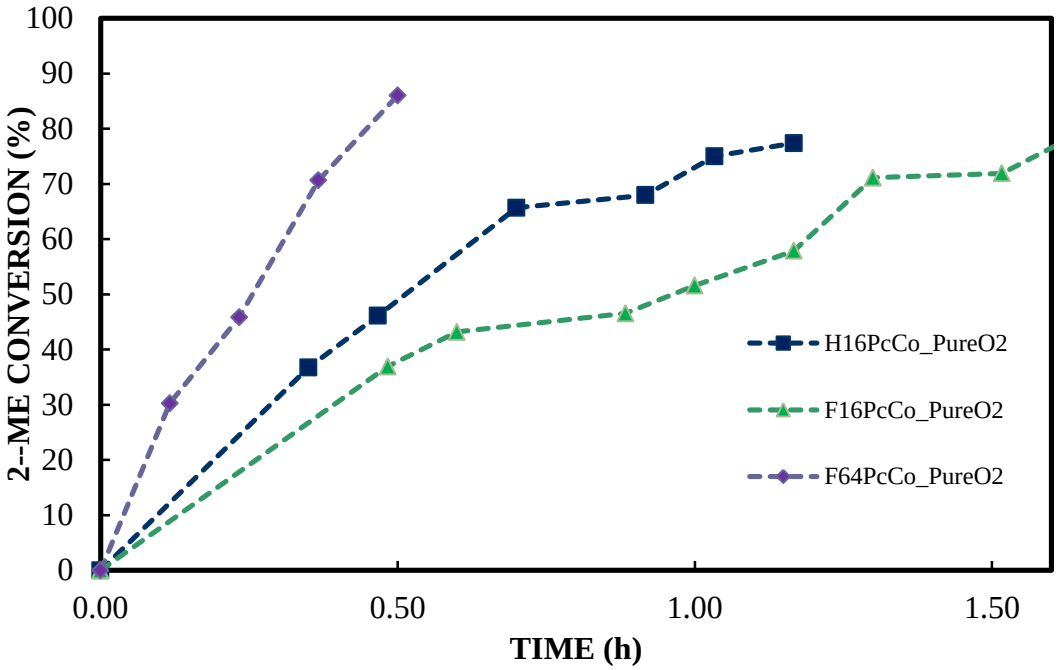

Figure 4.4 Observed thiol conversion for the catalytic oxidation of 2-ME under pure O_2, in the presence of 2.58 mmol/L NaOH at 22 °C and 1 atm. Dashed lines added for clarity.

Because of their unique extended, often flat or near-flat structure, phthalocyanines are subject to dimerization caused by π- π bonding, which is an equilibrium process. The dimerization leads to a decrease in available active sites, thus a reduction in effective catalyst concentration. Loas studied the effects of dimerization on a variety of fluorinated zinc(II) phthalocyanines.[14] Assuming dimerization is independent of the active metal center, the fraction of monomer, f_m, within solutions containing H_{16}PcCo, F_{16}PcCo, and F_{64}PcCo actually available for catalytic activity is taken as 0.85, 0.33 and 0.80, respectively, based on the Loas[14] data. As will be seen later, the reaction rate is directly proportional to the effective catalyst concentration, which can be taken as $f_m[Cat]_T$, where $[Cat]_T$ is the total initial catalyst concentration. Therefore, the observed

reaction times were adjusted for the estimated active monomer catalyst concentrations by multiplying these times by f_m to show a corrected time (TIME'). All kinetic data will thus be presented as functions of TIME' in order to better represent the true kinetic effects of fluorine groups on phthalocyanines.

Figure 4.5 shows the corrected data from the baseline catalytic runs first shown in Figure 4.4. Among the three catalysts, F_{64}PcCo shows the fastest conversion, followed by F_{16}PcCo, then H_{16}PcCo – potentially a more natural progression. The switch in perceived reaction velocity between F_{16}PcCo and H_{16}PcCo suggests that the dimerization effect is significant. The relative order shown in Figure 4.5 suggests that steric hindrance might play an important role. The F_{64}PcCo has the most steric hindrance due to its bulky substituents, followed by F_{16}PcCo due to its fluorine atoms, as opposed to the hydrogen atoms surrounding the H_{16}PcCo. Based on Figure 4.5, the mechanistic step most closely related to steric hindrance might be rate-determining.

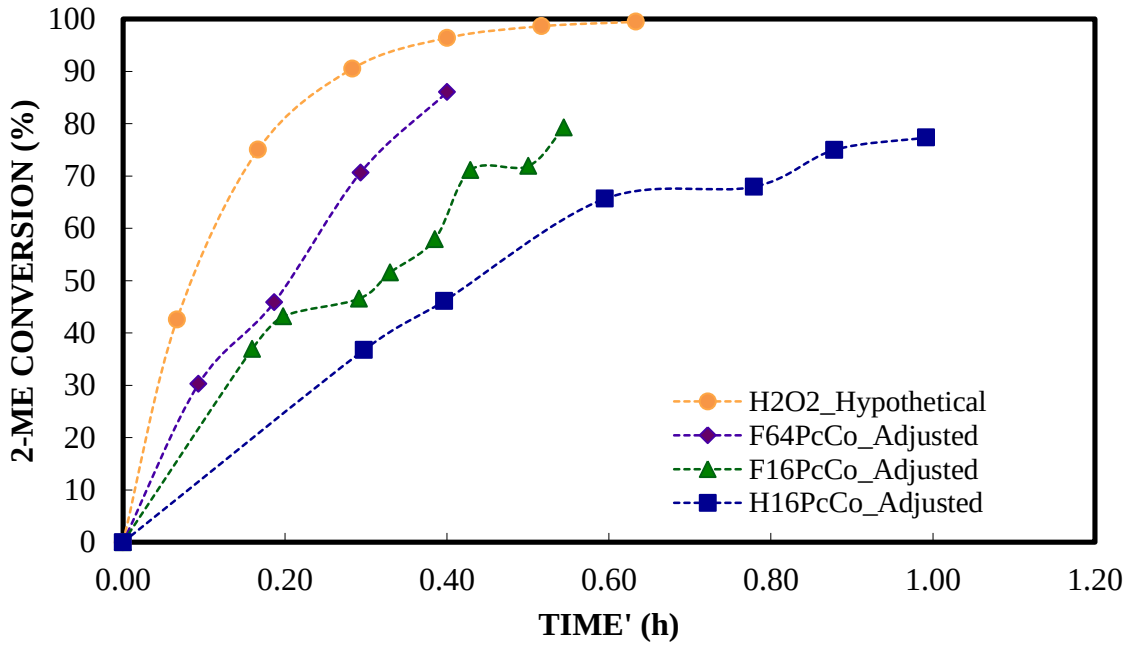

Figure 4.5 Catalytic oxidation of 2-ME under pure O_2, in the presence of 2.58 mmol/L NaOH at 22° C, 1 atm. corrected for dimerization effects. Hypothetical H_2O_2 induced oxidation of 2-ME done under pure N_2 at 22 °C and 1 atm. Dashed lines added for clarity.

Hydrogen peroxide has been shown to play a significant role in the oxidation of thiols.[23-28] Therefore, in order to focus on the impact of Pc catalyst structure, account was taken of the contribution of H_2O_2, formed as an intermediate in the thiol oxidation, to the total RSH consumption. Figure 4.5 also shows the hypothetical oxidation of 2-ME in the absence of O_2 (nitrogen blanket) in the presence of H_2O_2. The conversion of 2-ME via to H_2O_2, was calculated from Equation 2.4.

$$-r_{RSH} \approx 2k_{H_2O_2}[H_2O_2][RSH] \tag{2.4}$$

with hypothetical amounts of H_2O_2 equal to that of what would be the O_2 concentration, calculated by Henry's law (8.02 mmol/L) and $k_{H_2O_2}$ =0.52 liter/mmol-hr as calculated in Section 4.2. Like the O_2 experiments, where the O_2 partial pressure was held constant, the dissolved H_2O_2 concentration in this calculation was also taken as constant. The result was that the observed oxidation of 2-ME occurs faster via H_2O_2 when compared to any of the studied catalysts. Also, if oxidation of 2-ME via H_2O_2 contained the rate-determining step, there would be no change in rates between H_{16}PcCo, F_{16}PcCo and F_{64}PcCo catalysts. These observations are essential when deriving models for catalytic consumption of thiols, as total thiol consumption is equal to the sum of consumption via catalytic and non-Pc mechanisms, as well as consumption via H_2O_2.

Figures 4.6 thru 4.8 show oxidation of 2-mercaptoethanol under various O_2 gas phase partial pressures, as catalyzed by H_{16}PcCo, F_{16}PcCo and F_{64}PcCo, respectively – all with times corrected for the estimated dimerization. The H_{16}PcCo case shows little, if any, dependence on O_2, while F_{16}PcCo and F_{64}PcCo have greater dependencies on O_2. These O_2 dependencies were reflected in the variation of the kinetic parameters of derived models (Table 2.1) associated with each catalyst. Recognizing the correct rate-determining step and subsequent reaction model for each catalyst provided insight to the

behavior of these catalytic reactions.

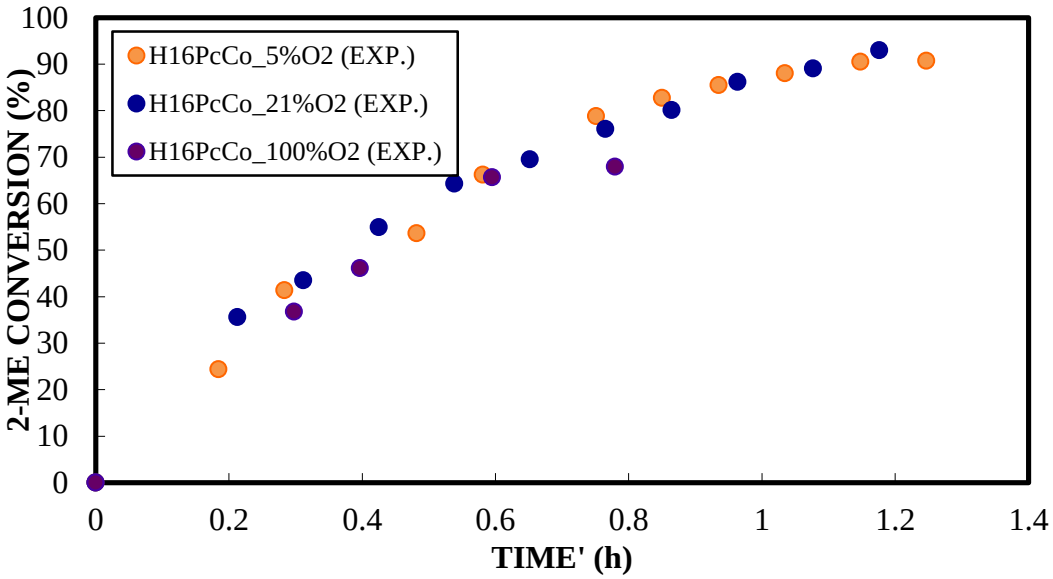

Figure 4.6 Experimental data for $H_{16}PcCo$ catalyzed oxidation of 2-ME under pure O_2, air, and diluted O_2 (5% O_2, balance N_2), in the presence of 2.58 mmol/L NaOH at 22 °C, 1 atm.

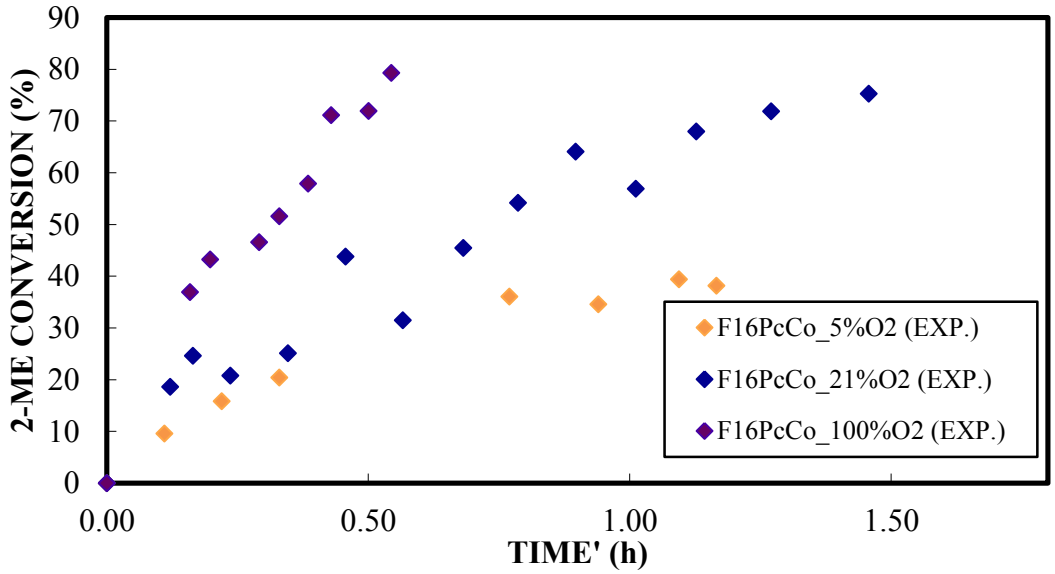

Figure 4.7 Experimental data for $F_{16}PcCo$ catalyzed oxidation of 2-ME under pure O_2, air and diluted O_2 (5% O_2, balance N_2), in the presence of 2.58 mmol/L NaOH at 22 °C and 1 atm.

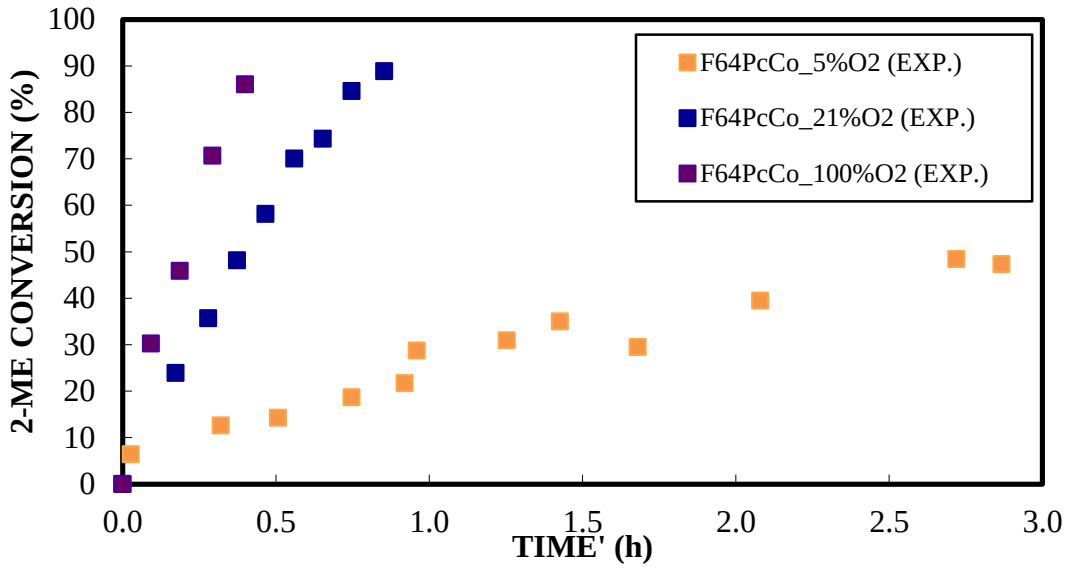

Figure 4.8 Experimental data for F_{64}PcCo catalyzed oxidation of 2-ME under pure O_2, air and diluted O_2 (5% O_2, balance N_2), in the presence of 2.58 mmol/L NaOH at 22 °C and 1 atm.

4.3.2 Identification of Preferred Rate Model

Based on the mechanisms and models fully derived in Appendices D thru K, H_{16}PcCo (Figure 4.6), F_{16}PcCo (Figure 4.7) and F_{64}PcCo (Figure 4.8) oxidation data were fitted to rate expressions. Table 4.2 thru 4.4 show the numerical values of α, β and γ for all developed catalytic models as seen in Table 2.1. Criteria for the choosing the correct (best) model include: positive rate constants; relatively large r^2 values; small 95% confidence values, relative to corresponding parameter; models and constants which are chemically and physically logical; and models and constants which are consistent with available literature. Kinetic parameters should converge on positive unique numerical values. Models which do not converge are rejected. Red values indicate cause of model rejection. As will be discussed shortly, rate forms II and III best fit F_{16}PcCo and F_{64}PcCo catalyzed oxidations of 2-ME, while form I fits the H_{16}PcCo data better.

Table 4.2 Numerical Values for Lumped Kinetic Parameters (Models I-VIII of Table 2.1) for Catalytic (H_{16}PcCo, F_{16}PcCo, F_{64}PcCo) Oxidations of 2-ME Under 5% Gas Phase O_2 Composition, in the Presence of 2.58 mmol/L NaOH at 22 °C and 1 atm.
*Represents Relatively Large 95% Confidence Values

H_{16}PcCO Oxidation of 2-ME at 5% O_2 Concentration					
Model	I	II/III	IV/V	VI	VII/VIII
α	0.22	0.26			0.03
β	-	0.001	**DOES NOT CONVERGE**	**DOES NOT CONVERGE**	.005*
γ	-	-			.0006*
r^2	0.987	0.99			0.994
F_{16}PcCO Oxidation of 2-ME at 5% O_2 Concentration					
Model	I	II/III	IV/V	VI	VII/VIII
α	0.052	0.010	0.12	0.0004	0.0001
β	-	-0.003	202	-0.01	-0.03
γ	-	-	-0.01	-	5.12E-05
r^2	0.926	0.970	0.969	0.97	0.971
F_{64}PcCO Oxidation of 2-ME at 5% O_2 Concentration					
Model	I	II/III	IV/V	VI	VII/VIII
α	0.03	0.01	0.009	0.0005	0.252
β	-	-0.002	-4.57	-0.003	21.2
γ	-	-	-0.002	-	-0.05
r^2	0.947	0.967	0.959	0.959	0.959

Table 4.3 Numerical Values for Lumped Kinetic Parameters (Models I-VIII of Table 2.1) for Catalytic (H_{16}PcCo, F_{16}PcCo, F_{64}PcCo) Oxidations of 2-ME Under 21% Gas Phase O_2 Composition, in the Presence of 2.58 mmol/L NaOH at 22 °C and 1 atm.

* Represents Relatively Large 95% Confidence Values

H_{16}PcCO Oxidation of 2-ME at 21% O_2 Concentration					
Model	I	II/III	IV/V	VI	VII/VIII
α	0.22	0.31	0.16		
β	-	0.003	-3.56	**DOES NOT CONVERGE**	**DOES NOT CONVERGE**
γ	-	-	-0.0005		
r^2	0.975	0.992	0.997		
F_{16}PcCO Oxidation of 2-ME at 21% O_2 Concentration					
Model	I	II/III	IV/V	VI	VII/VIII
α	0.12	0.11	0.4*		0.01*
β	-	0.0002	41.6*	**DOES NOT CONVERGE**	0.02*
γ	-	-	0.01*		0.0002*
r^2	0.951	0.951	0.951		0.951
F_{64}PcCO Oxidation of 2-ME at 21% O_2 Concentration					
Model	I	II/III	IV/V	VI	VII/VIII
α	0.252	0.731	1.12*		0.22*
β	-	0.012	4.99*	**DOES NOT CONVERGE**	0.20*
γ	-	-	0.02*		0.004*
r^2	0.921	0.997	0.997		0.998

Table 4.4 Numerical Values for Lumped Kinetic Parameters (Models I-VIII of Table 2.1) for Catalytic (H_{16}PcCo, F_{16}PcCo, F_{64}PcCo) Oxidations of 2-ME Under 100% Gas Phase O_2 Composition, in the Presence of 2.58 mmol/L NaOH at 22 °C and 1 atm.
* Represents Relatively Large 95% Confidence Values

H_{16}PcCO Oxidation of 2-ME at 100% O_2 Concentration					
Model	I	II/III	IV/V	VI	VII/VIII
α	0.168	0.146		0.04*	0.006
β	-	-0.0006	**DOES NOT CONVERGE**	0.19*	-0.03
γ	-	-		-	0.0002
r^2	0.982	0.983		0.984	0.986
F_{16}PcCO Oxidation of 2-ME at 100% O_2 Concentration					
Model	I	II/III	IV/V	VI	VII/VIII
α	0.29	0.55	0.38		
β	-	0.005	-3.96	**DOES NOT CONVERGE**	**DOES NOT CONVERGE**
γ	-	-	0.002		
r^2	0.943	0.965	0.965		
F_{64}PcCO Oxidation of 2-ME at 100% O_2 Concentration					
Model	I	II/III	IV/V	VI	VII/VIII
α	0.49	1.15	0.96		
β	-	0.008	-1.76	**DOES NOT CONVERGE**	**DOES NOT CONVERGE**
γ	-	-	0.006		
r^2	0.955	0.993	0.993		

Studying Tables 4.2-4.4, there were some cases where multiple models might adequately fit the same data set. For example, rate forms I, II and III provide good fits for H_{16}PcCo oxidations at 100% O_2 compositions.

A further look into models I, II and III was required for discernment between the models. Equations 4.3, 4.4 and 4.5 represent expanded forms of models I, II and III, respectively, based on Figure 2.3. These models are derived in Appendices D, E and F.

$$-r_I \approx 4(k_2 K_1 [OH^-]/[Cat]_T /[H_2O])[RSH] \tag{4.3}$$

Where $k_2 K_1 [OH^-]/[Cat]_T /[H_2O] \equiv \alpha_I$

$$-r_{II} \approx \frac{4k_3 K_2 K_1 ([OH^-]/[H_2O])[O_2][Cat]_T [RSH]}{1+K_2 K_1 ([OH^-]/[H_2O])[RSH]} \tag{4.4}$$

Where $k_3 K_2 K_1 ([OH^-]/[H_2O])[O_2][Cat]_T \equiv \alpha_{II}$, $K_2 K_1 ([OH^-]/[H_2O]) \equiv \beta_{II}$

$$-r_{III} \approx \frac{4k_4 K_3 K_2 K_1 ([OH^-]/[H_2O])[O_2][Cat]_T [RSH]}{1+K_2 K_1 ([OH^-]/[H_2O])(1+K_3[O_2])[RSH]} \tag{4.5}$$

Where $k_4 K_3 K_2 K_1([OH^-]/[H_2O])[O_2][Cat]_T \equiv \alpha_{III}$,

$K_2 K_1([OH^-]/[H_2O])(1+K_3[O_2]) \equiv \beta_{III}$

Conversion from RSH to RS^- is represented by the equilibrium constant K_1. Substrate RS^- binding to Co(II), and reduction of Co(II) to Co(I), is represented by either K_2 (an equilibrium constant) or k_2 (a rate constant) and should be related to Lewis acidity. The attachment of dissolved O_2, and electron transfer from the metal center to coordinated O_2, is represented by either K_3 (an equilibrium constant) or k_3 (a rate constant) and should also be related to the Lewis acidity of the metal center. The rate constant k_4 expulsion of $RS^{\bullet}$ from the metal center and should be related to steric hindrance. Quantitative analysis was then performed to better choose the correct rate-model and understand the dependence of kinetic parameters on phthalocyanine structure.

4.3.3 Quantitative Estimation of Kinetic Rate and Equilibrium Constants for Phthalocyanines (H_{16}PcCo)

Figure 4.6 shows little to no dependence on oxygen concentration by oxidations catalyzed by H_{16}PcCo. Unlike Equations 4.4 and 4.5, O_2 concentration does not appear in Equation 4.3. Substrate binding and reduction of the Co(II) to Co(I) should be relatively slow for the less Lewis acidic H_{16}PcCo molecule. Model I, which assumes substrate binding is the rate-determining step, best fits data from H_{16}PcCo catalyzed oxidations of 2-ME for all oxygen compositions as shown by Figures 4.9. Table 4.5 shows values of α_I at various gaseous O_2 compositions.

The slight drop in α_I might be due to degradation of H_{16}PcCo at higher dissolved O_2 concentrations. Loas[14] discussed possible degradation pathways, one of which is via electrophilic substitution. In presence of pure O_2, RSH may begin to prematurely convert

to RS^-. The insufficiently Lewis acidic $H_{16}PcCo$ might not rapidly oxidize the surplus RS^- substrate, which may then turn to attack the $H_{16}PcCo$, decreasing the effective catalyst concentration. Only considering low O_2 compositions, where $H_{16}PcCo$ is less susceptible to degradation, kinetic parameters can be estimated $\alpha_I = 0.22\ h^{-1}$. Where K_1, $[OH^-]$, $[H_2O]$ and $[Cat]_T$ are known, one can solve for the rate constant k_2 = 7.2E-3 liter/mmol-hr.

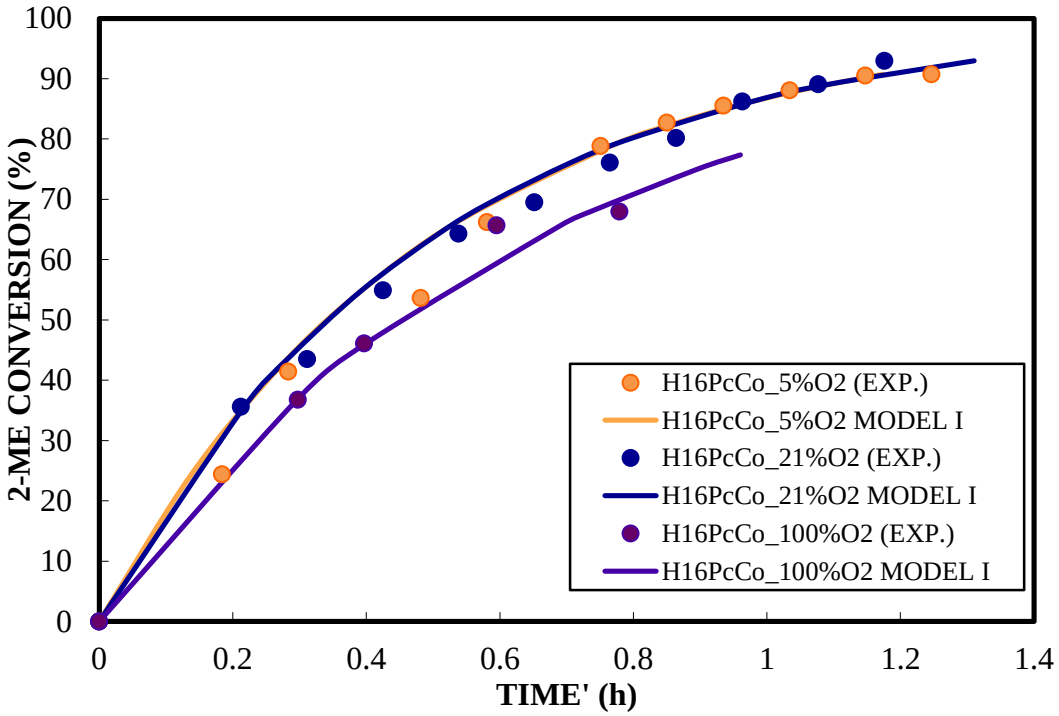

Figure 4.9 Experimental data and model fit, based on model I, for $H_{16}PcCo$ catalyzed oxidation of 2-ME under pure O_2, air, and diluted O_2 (5% O_2, balance N_2), in the presence of 2.58 mmol/L NaOH at 22 °C, 1 atm.

Table 4.5 Rate Constant α_I for $H_{16}PcCo$ Catalyzed Oxidation of 2-ME Under Pure O_2, Air, and Diluted O_2 (5% O_2, balance N_2), in the Presence of 2.58 mmol/L NaOH at 22 °C, 1 atm.

$H_{16}PcCo$	5% O_2	21% O_2	100% O_2
α_I	0.22	0.22	0.17

4.3.4 Qualitative Observations of Fluorinated Cobalt(II) Phthalocyanines (F_{16}PcCo & F_{64}PcCo)

The structural modifications from H_{16}PcCo to F_{16}PcCo and F_{64}PcCo were so significant, that it provided 2-ME oxidations via F_{16}PcCo and F_{64}PcCo catalysts an alternate rate-determining step. Figures 4.10 thru 4.11 graphically represent data, and model II/III fits for F_{16}PcCo and F_{64}PcCo catalyzed oxidations of 2-ME under pure O_2, air, and diluted O_2 (5% O_2, balance N_2) at 22 °C, 1 atm.

Tables 4.2-4.4 suggest rate form II/III best fit F_{16}PcCo and F_{64}PcCo catalyzed oxidations of 2-ME. Figures 4.7 and 4.8 show a clear dependence of O_2 concentration for oxidations catalyzed by F_{16}PcCo and F_{64}PcCo, respectively. A more thorough analysis was necessary to confirm whether either rate model II or III is correct.

Parameters K_1 and K_2 are found in rate forms II (Equation 4.4) and III (Equation 4.5). The additional F atoms increase the Lewis acidity, thereby likely making F_{16}PcCo and F_{64}PcCo better "oxidizers" than H_{16}PcCo. Due to the increasing large number of F atoms, F_{16}PcCo and F_{64}PcCo oxidations might exhibit fast substrate binding and reduction of the metal center, relative to H_{16}PcCo. The effect is significant enough that substrate binding is no longer the slow or rate-determining step for oxidations involving F_{16}PcCo and F_{64}PcCo.

As a closer inspection was done on models II (Equation 4.4) and III (Equation 4.5), the attachment of dissolved O_2, and electron transfer from the metal center to coordinated O_2, is represented by either K_3 (an equilibrium constant) or k_3 (a rate constant). Equilibrium constant K_3 was assumed to be small for F_{16}PcCo thiol oxidations due to the electronegativity of the F atoms. The F_{64}PcCo, with a largely electron deficient metal center due to all the F atoms, will likely have an even lower K_3 or k_3

because of its relatively high Lewis acidity.

Finally, k_4 represents the rate constant for the expulsion of $RS^{\bullet}$ from the metal center. Bulky fluorinated groups surrounding F_{64}PcCo might cause this value to be large. By contrast, there is much less bulkiness to accelerate expulsion of the radical from the flat, open F_{16}PcCo molecule.

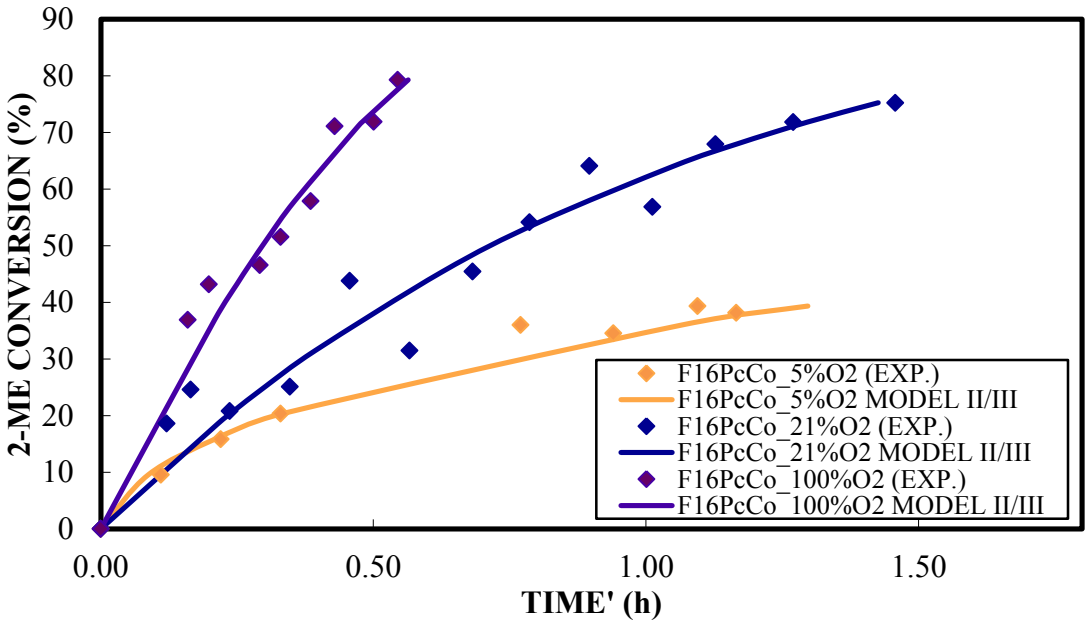

Figure 4.10 Experimental data and model fit, based on model II/II for F_{16}PcCo catalyzed oxidation of 2-ME under O_2, air and diluted O_2 (5% O_2, balance N_2), in the presence of 2.58 mmol/L NaOH at 22 °C, 1 atm.

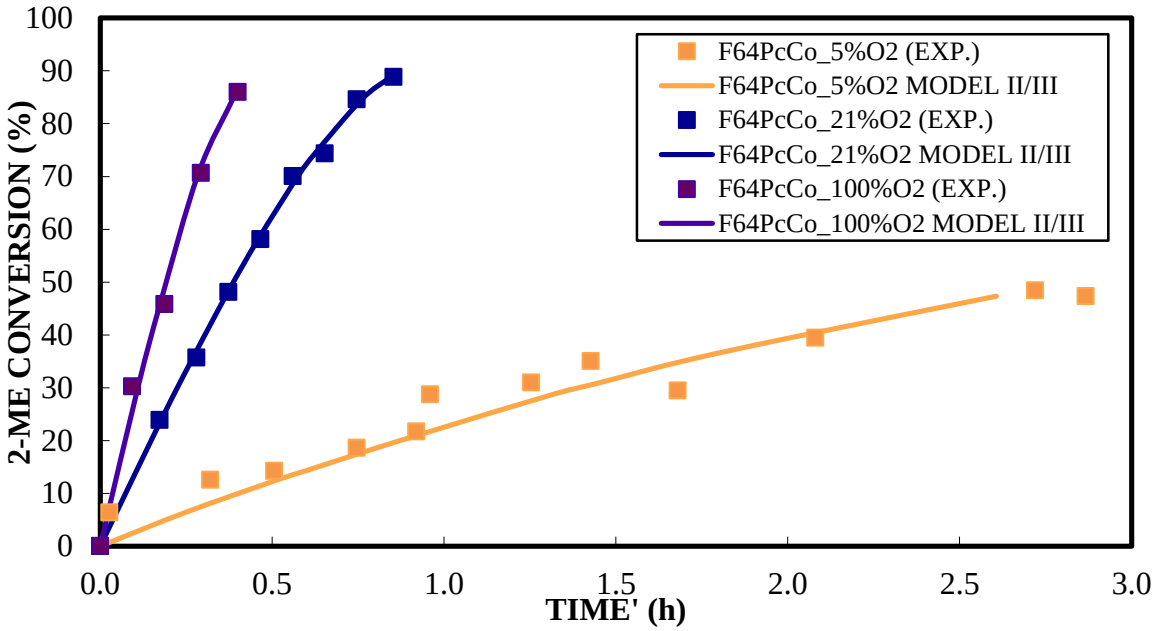

Figure 4.11 Experimental data and model fit, based on models II/III. for F_{64}PcCo catalyzed oxidation of 2-ME under O_2, air and diluted O_2 (5% O_2, balance N_2), in the presence of 2.58 mmol/L NaOH at 22 °C, 1 atm.

4.3.5 Quantitative Estimation of Kinetic Rate and Equilibrium Constants for Fluorinated Cobalt(II) Phthalocyanines (F_{16}PcCo & F_{64}PcCo)

The studied thiol oxidation required the diffusion of gaseous O_2 into the liquid phase where the reaction proceeds. In order to acquire accurate chemical kinetic data, it was necessary to minimize mass transfer effects via effective reactor design. A baffle was added to the reactor vessel used in these kinetic studies in order to break up the reaction solution bulk swirl. However, an interphase (gas-to-liquid) mass transfer resistance might still occur for sufficiently fast catalytic reaction cases. Mass transfer effects were likely not significant for H_{16}PcCo oxidations of 2-ME because there was little to no dependence on O_2.

This issue for faster, fluorinated phthalocyanine catalysts can be more easily examined using initial rates because the chemical kinetic rate expression can often be simplified. At time ≈ 0, when [RSH] was relatively large, Equation 4.4 reduces to:

$$-r_{II_0} \approx 4k_3[O_2]_o[Cat]_T \tag{4.6}$$

Similarly, Equation 4.5 reduces to:

$$-r_{I\,I_0} \approx \frac{4k_4K_3[O_2]_o[Cat]_T}{1+K_3[O_2]_o} \tag{4.7}$$

Figure 4.12 shows the observed initial rates for thiol consumption using F_{16}PcCo and F_{64}PcCo catalysts as a function of dissolved oxygen concentration. The dissolved oxygen concentrations were estimated using Henry's constant[43,44] at 22 ^{o}C and 1 atm, and the experimental O_2 partial pressure, which considers that the solvent THF exerts a considerable vapor pressure.[48]

Equation 4.6 suggests linearity with oxygen concentration related to initial rates with a y-intercept of 0. Neither of the relationships in Figure 4.12 exhibits this linear trend, suggesting model II (Equations 4.4 and 4.6) does not accurately represent 2-mercaptoethanol oxidations catalyzed by F_{16}PcCo and F_{64}PcCo.

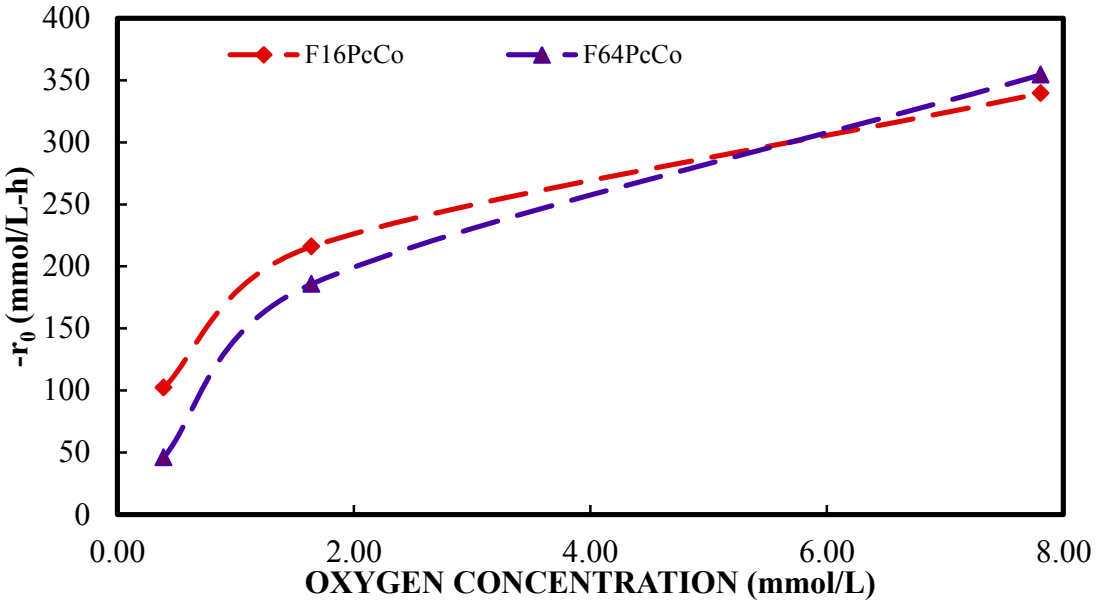

Figure 4.12 Initial rate of F_{16}PcCo and F_{64}PcCo catalyzed oxidations in various dissolved oxygen concentrations, in the presence of 2.58 mmol/L NaOH at 22^{o} C, 1 atm.

With a likely form of the initial rate now in hand (Equation 4.7), consideration was

then given to the mass transfer of O_2 from gas to liquid phase. The mass transfer driving force is equal to the difference between the partial pressure of gaseous O_2 above the liquid (p_{O_2}) and dissolved O_2 concentration in the liquid [O_2], written in partial pressure units:

$$-r_{MT} \approx k_m(p_{O_2} - [O_2]H) \tag{4.8}$$

where k_m is a mass transfer coefficient, and H is the Henry's law constant.[43,44] Equating the mass transfer rates and initial chemical rates, initial O_2 concentrations in the liquid can be estimated.

Equilibrium constant K_3 was assumed to be small for F_{16}PcCo thiol oxidations due to the electronegativity of the F atoms; hence, in Equation 4.7, $1 >> K_3[O_2]_0$. In these cases, equating Equations 4.7 (simplified) and 4.8 resulted in an estimated initial $[O_2]_0$ for the F_{16}PcCo cases:

$$[O_2]_{0.F_{16}PcCo} \approx \frac{k_m p_{O_2}}{k_m H + 4k_4 K_3 [Cat]_T} \tag{4.9}$$

Substituting Equation 4.9 into Equation 4.7 to eliminate $[O_2]_o$ provided an alternate equation for the initial rate of reaction, in terms of catalyst concentration.

$$-r_{III_0} \approx \frac{4k_4 K_3 [Cat]_T k_m p_{O_2}}{k_m H + 4k_4 K_3 [Cat]_T} \tag{4.10}$$

Equation 4.10 suggested an experiment to test initial rates vs catalyst concentration at constant oxygen partial pressure. The reciprocal of Equation 4.10 provides a linearized form, in which the y-intercept yields an estimate of the mass transfer coefficient, k_m.

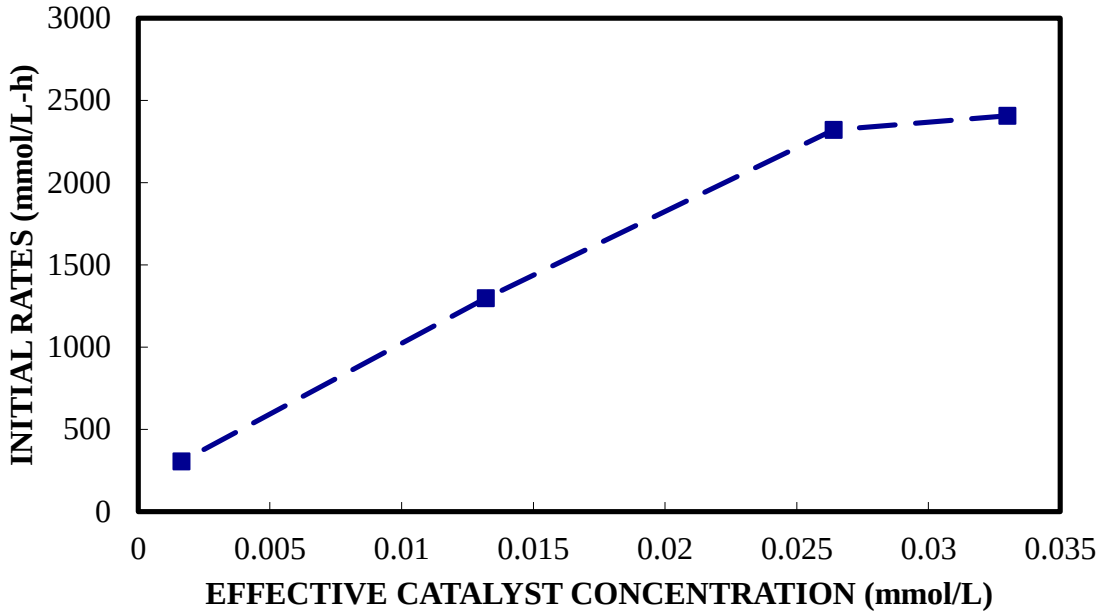

Figure 4.13 Initial rate of F_{16}PcCo catalyzed oxidation in pure oxygen as a function of catalyst amount, in the presence of 2.58 mmol/L NaOH at 22 ^{o}C and 1 atm.

$$\frac{pO_2}{-r_{I\,I_0 I}} \approx \frac{H}{4k_4K_3[Cat]_T} + \frac{1}{k_m} \tag{4.11}$$

Initial rate versus catalyst concentration data were obtained for F_{16}PcCo-catalyzed oxidations of 2-ME. A series of experiments was performed under pure O_2 at 1 atm in which the amount of F_{16}PcCo catalyst was varied. Initial rates vs effective catalyst concentration data are shown in Figure 4.13. The initial rates remain fairly linear with catalyst concentration up to approximately 0.025 mmol/L, after which a fall-off occurs. The initial rate is effectively independent of catalyst concentration above 0.025 mmole/liter.

Bartholomew and Farrauto[45] describe that a catalytic reaction is kinetically controlled when limited by the amount of catalyst, as evidenced by the initial rate linear with catalyst concentration up to a point. At larger catalyst concentrations, the reaction becomes sufficiently fast, that the bulk mass transfer of O_2 into the liquid becomes rate-

limiting. This results in a leveling off of the initial rate, as shown in Figure 4.13.

These data were regressed according to Equation 4.11, with the result shown in Figure 4.14. From the y-intercept, the mass transfer coefficient was estimated: k_m=5000 mmol/liter-h-atm. This mass transfer coefficient is assumed to system dependent, and therefore applicable to all the catalytic cases in this study at the constant agitation rate that was used.

For the reactor set-up used in this study, mass transfer resistance appears to have a significant effect at initial rate of approximately 2300 mmol/L-hr. Figure 4.12 shows initial reaction rates for F_{16}PcCo and F_{64}PcCo catalyzed oxidations of 2-ME fall well below this mass transfer resistance threshold. Recalling Figure 4.5, oxidations involving H_{16}PcCo are slower than those catalyzed by fluorinated phthalocyanines. These observations confirm that 2-ME oxidations, catalyzed by H_{16}PcCo, F_{16}PcCo and F_{64}PcCo are purely reaction limited.

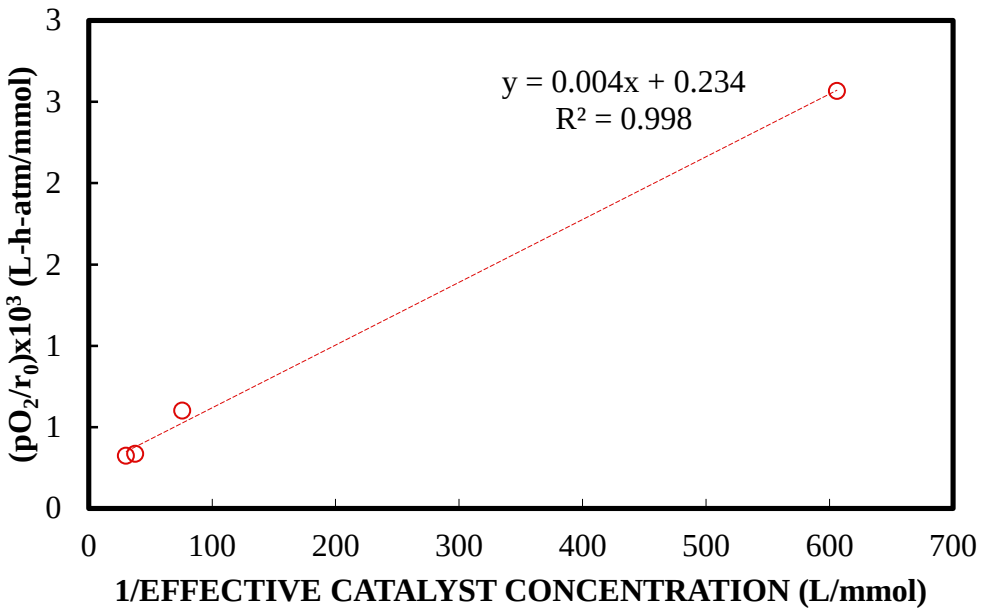

Figure 4.14 Inverse initial rate of F_{16}PcCo catalyzed oxidation in pure oxygen as a function of inverse catalyst amount, in the presence of 2.58 mmol/L NaOH at 22 ^{o}C and 1 atm.

With a mass transfer coefficient available, the values of parameters K_3 and k_4 for F_{16}PcCo and F_{64}PcCo catalysts can be estimated by applying Equation 4.12, the reciprocal of Equation 4.7, to initial rate versus $[O_2]$ data, collected at 5%, 21%, and 100% gas-phase O_2:

$$\frac{4[Cat]_T}{-r_{II_0}} \approx \frac{1}{k_4 K_3 [O]_0} + \frac{1}{k_4} \qquad (4.12)$$

A trial-and-error procedure is used since the $[O_2]_0$ might possibly be lower than Henry's Law would predict due to the potential mass transfer resistance issues. For a given O_2 partial pressure, Henry's law[43,44] provides an estimate of $[O_2]$ at initial time. Then, a plot of the data according to Equation 4.12 provides estimates for k_4 and K_3. Figure 4.15 provides inverse initial rates as a function of dissolved oxygen, as calculated from the above trial and error procedure. The Matlab™ program used for this calculation can be found in Appendices L and M for F_{16}PcCo and F_{64}PcCo, respectively.

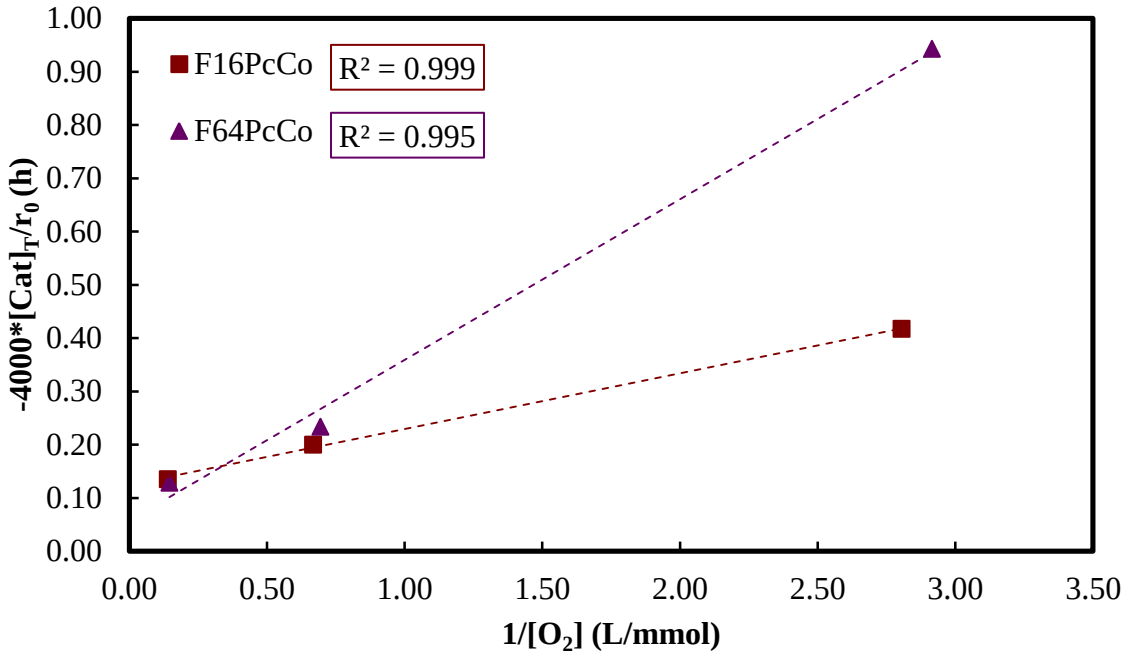

Figure 4.15 Inverse initial rate of F_{16}PcCo and F_{64}PcCo catalyzed oxidations as a function. of inverse dissolved oxygen concentration, considering mass transfer effects, in the presence of 2.58 mmol/L NaOH at 22 ^{o}C and O_2 partial pressure = 1 atm.

Table 4.6 shows values for K_3 and k_4, and estimated concentrations of dissolved O_2 for F_{16}PcCo and F_{64}PcCo catalyzed 2-ME oxidations. Knowing the pK_a of 2-ME (pKa = 9.643) and H_2O (pKa = 15.7) for the initial acid/base reaction involving 2-ME and OH^-, K_1 was estimated as $K_1=10^{-9.643}/10^{-15.7}=1.14x10^6$. The kinetic parameter describing substrate binding, K_2, is determined by fitting known values of K_1, K_3, and k_4 to complete data sets of F_{16}PcCo and F_{64}PcCo 2-ME oxidations, which will be discussed very shortly.

Table 4.6 Kinetic Parameters and Dissolved [O_2] for F_{16}PcCo and F_{64}PcCo Catalyzed Oxidations of 2-Mercaptoethanol, Derived from Model III Initial Rates of F_{16}PcCo, F_{64}PcCo, Oxidations of 2-ME Under Various Gas Phase O_2 Initial Concentrations, in the Presence of 2.58 mmol/L NaOH at 22 °C, 1 atm.,Where $y=-4000*[Cat]_T/r_0$ (h)

Cat_T (mmol/L)	km (mmol/L-h-atm)	H (L-atm/mmol)	H_2O (mmol/L)	OH^- (mmol/L)	K_1	
0.01	5000	0.10	1.10E+03	2.58	1.14E+06	
F_{16}PcCo	fm	0.33				
$-r_0$ (mmol/L-h)	y (h)	[O_2] (mmol/L)	[1/O_2] (L/mmol)	k_4 (1/h)	K_3 (L/mmol)	K_2 (L/mmol)
100	0.42	0.40	2.50	8.0E+03	1.19	8.00E-07
210	0.20	1.70	0.58			
310	0.14	8.02	0.12			
F_{64}PcCo	fm	0.80				
$-r_0$ (mmol/L-h)	y (h)	[O_2] (mmol/L)	[1/O_2] (L/mmol)	k_4 (1/h)	K_3 (L/mmol)	K_2 (L/mmol)
100	0.42	0.40	2.50	1.73E+04	0.19	3.46E-06
210	0.20	1.70	0.58			
310	0.14	8.02	0.12			

4.3.6 Quantification of Mass Transfer Effects via Liquid Oxygen Concentration Analysis

Potential mass transfer resistance (Equation 4.8) is also considered when estimating [O_2], the oxygen content in the reaction liquid. Concentration of oxygen in the reaction liquid is calculated by setting Equations 4.5 and 4.8 equal. The accepted solution provided an estimated concentration of oxygen in the reaction liquid as a function of time. Alpha and beta values as functions of time and estimated K_2, K_3 and k_4 values were also observed.

Equation 4.13 represents model III (derived in Appendix F) in terms of thiol conversion, X. Table 4.7 represents model III, where t_m is the model-calculated reaction time with estimated values of K_2, K_3 and k_4 for 2-ME conversion vs experimental TIME' data. Equation 4.14 is the integrated form of Equation 4.13 used to fit 2-ME conversion vs TIME' data.

$$\frac{dX}{dt} \approx \frac{4\alpha[RSH]_0(1-X)}{1+\beta[RSH]_0(1-X)} \tag{4.13}$$

$$t_m \approx \frac{\beta[RSH]_0 X - \log_{10}(1-X)}{4\alpha} \qquad (4.14)$$

Table 4.7 shows little to no change in concentration of oxygen in the reaction liquid, as well as calculated α and β values based on Equation 4.5. Figure 4.16 is a graphical representation of the fits provided by Table 4.7. The dissolved oxygen concentration at 22 °C and 1 atm for 100% O_2 composition is 8.02 mmol/L.[43,44] Table 4.7 shows no more than a 2% drop from predicted liquid concentration to that calculated when considering mass transfer issues. This suggested that the dissolved O_2 is effectively constant, and provided more support that mass transfer limitations for 100% gaseous O_2 oxidant is insignificant.

It is worthwhile to note that the experimental catalyst concentration was 0.01 mmole/L. For F_{16}PcCo, the effective concentration is $0.01f_m$ = 0.0033 mmole/L. This value is at the low range of Figure 4.15, suggesting that a mass transfer resistance for F_{16}PcCo with pure O_2 as the oxidant is trivial.

Table 4.7 Rate Model III Parameters as a Function of Time and Fit of F_{16}PcCo and F_{64}PcCo Catalyzed Oxidations of 2-ME Under 100% O_2 (dissolved [O_2] Concentration as Predicted by Henry's Law[43,44] = 8.02 mmol/L), in the Presence of 2.58 mmol/L NaOH at 22 °C, 1 atm. See Figure 4.16

F_{16}PcCO Oxidation of 2-ME at 100% O_2 Concentration						
t' (h)	[RSH] (mmol/L)	[O_2] (mmol/L)	α (1/h)	β (L/mmol)	t_m (h)	X(%)
0.00	140.4	8.06	1.73	0.02	0.00	0.00
0.16	84.1	8.07	1.73	0.02	0.22	36.9
0.20	74.2	8.07	1.73	0.02	0.26	43.2
0.29	66.9	8.08	1.73	0.02	0.29	46.6
0.33	58.9	8.08	1.73	0.02	0.32	51.6
0.39	48.6	8.08	1.73	0.02	0.37	57.9
0.43	28.8	8.10	1.74	0.02	0.46	71.1
0.50	25.9	8.10	1.74	0.02	0.48	71.9
0.54	14.4	8.11	1.74	0.02	0.55	79.3
F_{64}PcCO Oxidation of 2-ME at 100% O_2 Concentration						
t' (h)	[RSH] (mmol/L)	[O_2] (mmol/L)	α (1/h)	β(L/mmol)	t_m (h)	X(%)
0.00	140.0	8.02	2.56	0.02	0.00	0.00
0.09	95.0	8.03	2.57	0.02	0.12	30.3
0.19	70.6	8.04	2.57	0.02	0.19	45.9
0.29	33.0	8.07	2.58	0.02	0.30	70.7
0.40	8.65	8.11	2.59	0.02	0.41	86.0

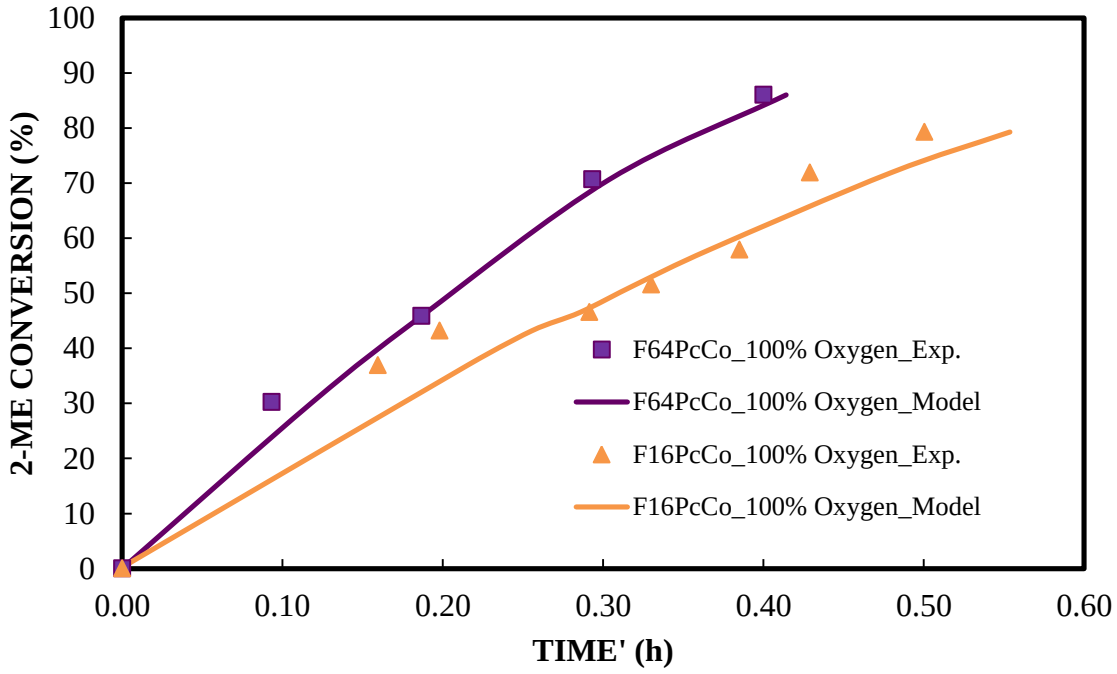

Figure 4.16 Experimental data and model fits for F_{16}PcCo and F_{64}PcCo catalyzed oxidation of 2-ME under pure O_2, in the presence of 2.58 mmol/L NaOH at 22 °C, 1 atm.

The rate model III and the rate and equilibrium constants found in Table 4.7 adequately described F_{16}PcCo and F_{64}PcCo catalyzed oxidations of 2-ME under pure O_2 at 1 atm total pressure and 22 °C. Of course, the effective partial pressure of O_2 is subject to the total pressure in which the reaction vessel is held, the purity of O_2 mixture used, as well as the vapor pressure of THF at 22 °C (~0.19 atm).[48] When pure O_2 was used as the oxidant, its partial pressure of oxygen is 0.8 atm at 22 ^{o}C.

For less than pure O_2 cases, when N_2 was present in the oxidant gas, the impact of the THF vapor pressure was more important. The THF vapor pressure is sensitive to temperature and the method of calculation.[48] When air was the oxidant, at 22 °C, the partial pressure of gaseous O_2 is 0.17 atm. When the 5% O_2 oxidant was used, the O_2 partial pressure in the reactor above the liquid was a very small 0.04 atm! The catalytic oxidations were very sensitive to partial pressure of O_2 above the liquid. These values suggested that small errors in temperature control might significantly impact the available O_2 partial pressure.

Tables 4.8 and 4.9 provide model III parameters, fitted to 2-ME conversion vs TIME' data, at 21% O_2 and 5% O_2, respectively. Figures 4.17 and 4.18 are graphical representations of Tables 4.7 and 4.8, respectively. Tables 4.7 and 4.8 also present estimated dissolved [O_2] for F_{16}PcCo and F_{64}PcCo catalyzed 2-ME oxidations with time. The calculated [O_2] values were generally comparable to that predicted by Henry's law in some cases, which suggests mass transfer resistance had minimal effect in this system. In some cases, the estimated dissolved [O_2] deviated from the Henry's law-based value in a somewhat random way. This was insufficient cause to claim any mass transfer resistance and supports the observation that catalytic initial rates were below the threshold of mass transfer resistance.

Table 4.8 Rate Model III Parameters as a Function of Time and Fit of F_{16}PcCo and F_{64}PcCo Catalyzed Oxidations of 2-ME Under 21% O_2 (dissolved $[O_2]$ Concentration as Predicted by Henry's Law[43,44] = 1.70 mmol/L), in the Presence of 2.58 mmol/L NaOH at 22 °C, 1 atm

F_{16}PcCO Oxidation of 2-ME at 21% O_2 Concentration						
t' (h)	[RSH] (mmol/L)	$[O_2]$ (mmol/L)	α (1/h)	β(L/mmol)	t_m (h)	X(%)
0.00	140.4	1.08	0.23	0.005	0.00	0.00
0.12	113.3	1.08	0.23	0.005	0.24	18.6
0.17	104.6	1.08	0.23	0.005	0.32	24.6
0.24	109.5	1.08	0.23	0.005	0.28	20.8
0.35	102.8	1.08	0.23	0.005	0.34	25.1
0.46	76.0	1.09	0.23	0.005	0.62	43.8
0.57	92.4	1.08	0.23	0.005	0.44	31.5
0.68	72.5	1.09	0.23	0.005	0.66	45.4
0.79	59.7	1.09	0.23	0.005	0.82	54.1
0.90	45.1	1.09	0.23	0.005	1.02	64.0
1.01	54.6	1.09	0.23	0.005	0.89	56.9
1.13	38.4	1.09	0.23	0.005	1.13	68.0
1.27	32.2	1.10	0.23	0.005	1.24	71.8
1.46	26.4	1.10	0.24	0.005	1.37	75.3
F_{64}PcCO Oxidation of 2-ME at 21% O_2 Concentration						
t' (h)	[RSH] (mmol/L)	$[O_2]$ (mmol/L)	α (1/h)	β (L/mmol)	t_m (h)	X(%)
0.00	140.4	2.36	0.75	0.01	0.00	0.00
0.17	105.5	2.37	0.76	0.01	0.19	23.9
0.28	88.4	2.37	0.76	0.01	0.29	35.7
0.37	70.4	2.37	0.76	0.01	0.41	48.2
0.47	55.9	2.38	0.76	0.01	0.50	58.1
0.56	38.9	2.38	0.76	0.01	0.63	70.0
0.65	32.1	2.39	0.76	0.01	0.68	74.3
0.75	17.3	2.40	0.77	0.01	0.84	84.6
0.85	10.7	2.40	0.77	0.01	0.93	88.8

Table 4.9 Rate Model III Parameters as a Function of Time and Fit of F_{16}PcCo and F_{64}PcCo Catalyzed Oxidations of 2-ME Under 5% O_2 (dissolved $[O_2]$ Concentration as Predicted by Henry's Law[43,44] = 0.40 mmol/L), in the Presence of 2.58 mmol/L NaOH at 22 °C, 1 atm

F_{16}PcCO Oxidation of 2-ME at 5% O_2 Concentration						
t' (h)	[RSH] (mmol/L)	$[O_2]$ (mmol/L)	α(1/h)	β(L/mmol)	t_m (h)	X(%)
0.00	140.4	0.44	0.09	0.003	0.00	0.00
0.11	126.5	0.44	0.09	0.003	0.23	9.54
0.22	117.5	0.44	0.09	0.003	0.39	15.8
0.33	111.0	0.44	0.09	0.003	0.52	20.4
0.77	88.5	0.44	0.09	0.003	0.97	36.0
0.94	90.3	0.44	0.09	0.003	0.93	34.5
1.09	83.3	0.44	0.10	0.003	1.08	39.3
1.17	84.9	0.44	0.10	0.003	1.05	38.2
F_{64}PcCO Oxidation of 2-ME at 5% O_2 Concentration						
t' (h)	[RSH] (mmol/L)	$[O_2]$ (mmol/L)	α(1/h)	β(L/mmol)	t_m (h)	X(%)
0.00	140.4	0.29	0.09	0.01	0.00	0.00
0.03	131.0	0.29	0.09	0.01	0.31	6.39
0.32	121.9	0.29	0.09	0.01	0.63	12.6
0.51	119.3	0.29	0.09	0.01	0.72	14.3
0.75	112.8	0.29	0.09	0.01	0.95	18.7
0.92	108.3	0.29	0.09	0.01	1.12	21.7
0.96	98.4	0.29	0.09	0.01	1.48	28.7
1.25	94.8	0.29	0.09	0.01	1.62	31.0
1.43	88.9	0.30	0.09	0.01	1.84	35.0

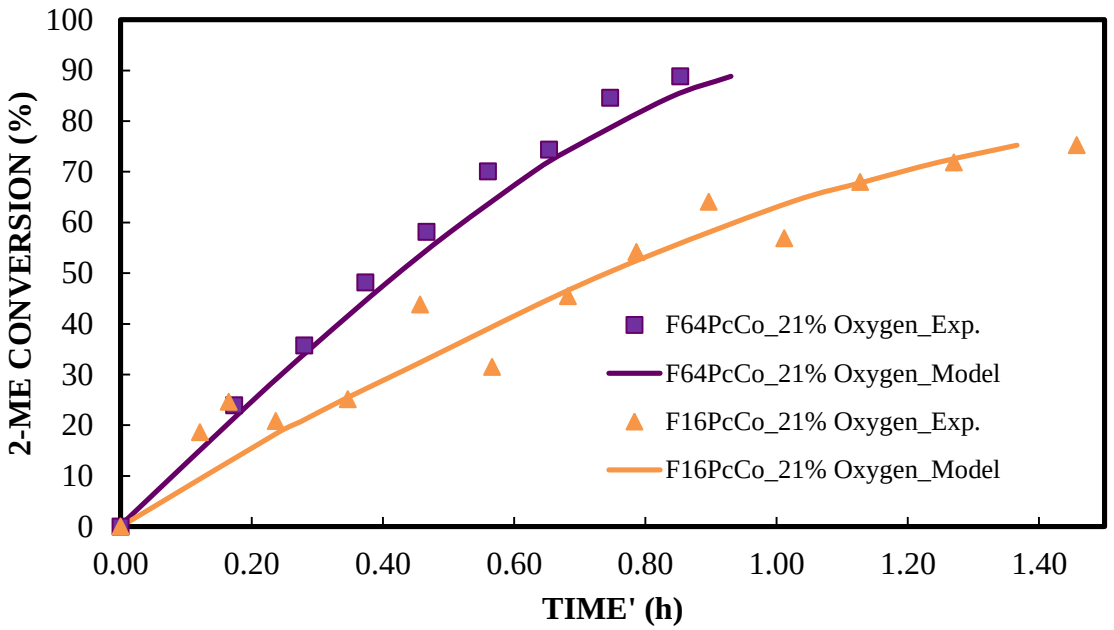

Figure 4.17 Experimental data and model fits for $F_{16}PcCo$ and $F_{64}PcCo$ catalyzed oxidation of 2-ME under air, in the presence of 2.58 mmol/L NaOH at 22 °C, 1 atm.

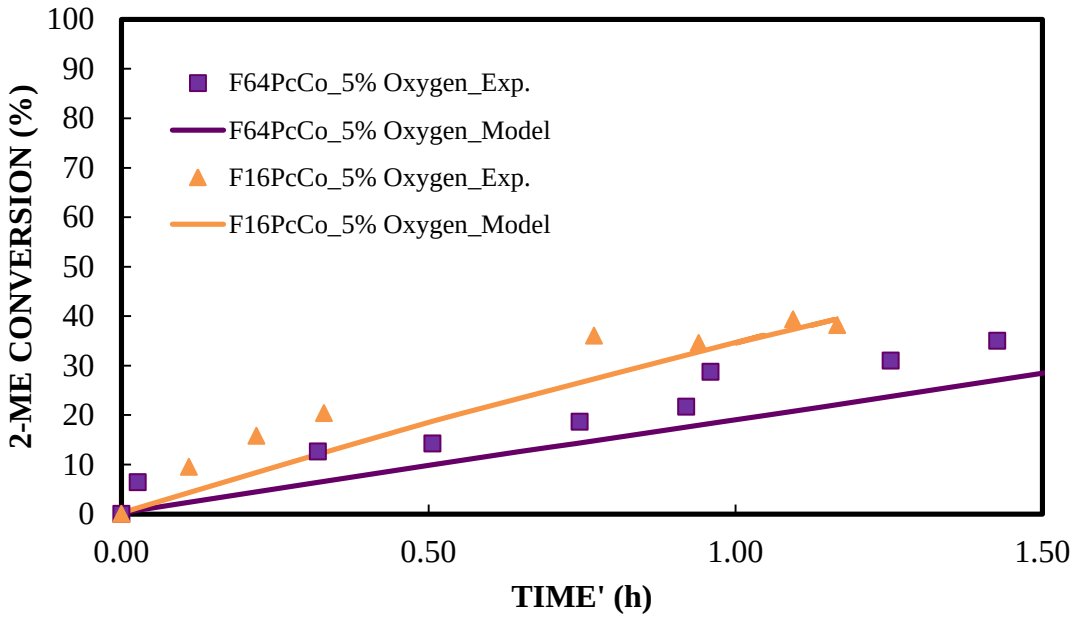

Figure 4.18 Experimental data and model fits for $F_{16}PcCo$ and $F_{64}PcCo$ catalyzed oxidation of 2-ME under diluted O_2 (5% O_2, balance N_2), in the presence of 2.58 mmol/L NaOH at 22 °C, 1 atm.

4.3.7 Correlation of Kinetic Parameters to Phthalocyanine Structure

Table 4.5 shows the values K_2, K_3 and k_4, as they relate to the F_{16}PcCo and F_{64}PcCo catalysts. Lewis acidity increases mainly due to the number and positioning of fluorine and fluoroalkylated groups. F_{16}PcCo has a larger number of aromatic fluorine groups that cause the structure to have more electron withdrawing capabilities. However, the aromatic fluorine groups also exhibit π-back bonding, where a small amount of electrons are simultaneously donated into the metal center.[46,47] On the other hand, aliphatic fluorine groups, which surround the F_{64}PcCo molecule, do not exhibit this phenomenon. With that said, Lewis acidity increases as we progress for H_{16}PcCo to F_{16}PcCo to F_{64}PcCo.

According to Tables 4.2-4.4 and Figure 4.9, model I accurately describes H_{16}PcCo catalyzed oxidations of 2-ME. The least Lewis acidic molecule of the studied catalysts had substrate binding as the slow step, indicating H_{16}PcCo is a relatively weak oxidizer.

According to Table 4.5, Lewis acidity directly affects K_2 (substrate binding) and K_3 (electron transfer from metal center to coordinated oxygen). As Lewis acidity increases (F_{16}PcCo $\rightarrow$ F_{64}PcCo), the phthalocyanine becomes a stronger oxidizer and increases the value of K_2. Lewis acidity is directly proportional to the electron deficiency of the metal center, decreasing its willingness to "give-up" an electron. This is shown in the decrease in the value of K_3 as Lewis acidity increases (F_{16}PcCo $\rightarrow$ F_{64}PcCo).

The metal center of the phthalocyanine becomes more sterically bulky as we evolve from H_{16}PcCo to F_{16}PcCo to F_{64}PcCo, due to the size and number of fluorine and fluoro-alkyl groups. This steric bulkiness causes faster acceleration of product, formed in the catalyst cavity. This phenomenon is consistent with the increase in the value of k_4

(expulsion of thiyl radical) as steric bulkiness increases (F_{16}PcCo $\rightarrow$ F_{64}PcCo).

4.4 Conclusions

In the absence of Pc, but with NaOH, the RSH was consumed by direct reaction with dissolved O_2. The non-Pc oxidation (i.e. non-Pc) of thiol was slow when compared to Pc catalytic reactions, but was still considered in the kinetic analyses. Purely peroxide-induced oxidations with no O_2 present and stoichiometric initial concentrations of 2-ME and H_2O_2 showed the peroxide (H_2O_2) reaction was fast relative to oxygen-induced reactions. Non-Pc oxidation of 2-mercaptoethanol was described by a reaction rate that is first order in thiol concentration and first order in dissolved O_2 as typical for acid/base catalysis. The rate-determining step is the coupling of RS^- to O_2, while the rate constant was calculated as $k_2=1.93x10^{-6}$ liter/mmol-h.

Phthalocyanine catalysts subject to dimerization present a reduced effective catalyst concentration that can significantly impact the perceived rate of aerobic thiol oxidations. Experimental thiol conversion data were corrected for such aggregation. This calculation led to a more accurate, and fairer, subsequent kinetic analyses and Conversion vs "Corrected Time" data.

A trial-and-error procedure that incorporates the mass transfer resistance effects, and using initial rates, provided a means to estimate kinetic parameters. These estimated kinetic parameters, from initial rate data, also generated fit to the entire range of 2-ME conversion vs. time data. An important result was that mass transfer resistances were not present for 2-ME oxidations under the conditions of this study.

The rates of substrate binding and electron transfer are directly related to the Lewis acidity of catalyst molecules. Substrate binding is directly related to Lewis

acidity. Substrate binding is found to be the slow step for the insufficiently Lewis acidic H_{16}PcCo. The additional fluorine groups adequately changes the structure of the phthalocyanine catalyst, in that the rate-determining step for catalyzed 2-ME oxidations is also changed. The more Lewis acidic F_{64}PcCo has the greatest K_2 value, followed by F_{16}PcCo. Similar observations are made for the electron transfer from metal center to coordinated O_2 (K_3). The more Lewis acidic molecule exhibits lower K_3 values.

Thiyl expulsion (k_4) has a direct correlation to steric hindrance. The less sterically hindered catalyst molecule F_{16}PcCo has a lower k_4 value and slowest reaction rate. While, the most sterically hindered, F_{64}PcCo, has the largest k_4 value and fastest reaction rate. The rate-determining step for aerobic 2-mercaptoethanol oxidations, catalyzed by F_{16}PcCo and F_{64}PcCo, is this expulsion of the thiyl radical from the catalyst molecule.

CHAPTER 5

BENCH SCALE OXIDATION OF 4-FLUOROBENZENTHIOL

5.1 Introduction

Experiments and kinetic analyses were conducted to elucidate the mechanism of action for 4-fluorobenzenthiol (4-FBT) oxidations via fluorinated, metal-centered, phthalocyanine catalysts, H_{16}PcCo, F_{16}PcCo, and F_{64}PcCo. Experiments were done under similar conditions to those carried out with 2-mercaptoethanol (2-ME). 4-Fluorobenzenethiol was chosen as an alternate thiol to observe the effects of a larger and less basic reagent that is believed to be more reactive (see Figure 1.1). Investigation and comparison of the two structurally different thiols provided better understanding of the significance of steric bulkiness and Lewis acidity in the design of novel catalysts. Kinetic analysis sought to quantitatively observe these effects by understanding the rate-determining step and kinetic parameter trends based on structure.

It is hypothesized that in the oxidation of 4-FBT, catalyzed by H_{16}PcCo, F_{16}PcCo, and F_{64}PcCo, the expulsion of the thiol radical from the catalyst is the rate-determining step, with the disulfide (RSSR) product formed outside of the catalyst cavity. However, this expulsion will be accelerated by the size of the 4-FBT thiyl radical.

The discussion below provides quantitative data and analysis, which further revealed correlations between not only catalyst but also thiol structure with kinetics of thiol oxidations.

5.2 Special Experimental Considerations

Oxidations of 4-fluorobenzenethiol (142 mmol/L) in the presence of 0.25 wt.% aq. NaOH (2.58 mmol/L) were conducted at various gas phase oxygen compositions (5%, 21% and 100%) at 22 ^{0}C and 1 atm. Oxidations were catalyzed by 0.0105mmol/L of commercial phthalocyanines (H_{16}PcCo, F_{16}PcCo), as well as a novel phthalocyanine (F_{64}PcCo). Experiments were conducted in a small (50 ml), bench-scale reactor. The only product formed is 4-fluorophenyl disulfide.[14]

Unfortunately, 4-fluorobenzenethiol was found to be highly reactive in air.[50] Due to this sensitivity, 4-fluorobenzenethiol solutions were prepared and handled in an Atmosbag (Sigma-Aldrich), purged and filled with Nitrogen. Solutions containing 4-fluorobenzenethiol were also stored in a reinforced box, which was evacuated, then filled with Nitrogen.

5.3 Hydroxide-Catalyzed Oxidation of 4-Fluorobenzenthiol

A mechanism describing 4-Fluorobenzenthiol conversion in the absence of Pc-catalyst should first be understood. This "non-Pc" RSH oxidation pathway begins with the fast acid-base equilibrium to produce thiolate ion (RS^-), which is the active reagent.[35] The rate-determining step was assumed to be the coupling of RS^- to O_2, with the other steps were in a fast equilibria. Appendix A presents this mechanism, inspired by Wallace and Schriesheim,[36] while Appendices B and C provide detailed derivations of proposed non-Pc models, which are Equations 5.1 and 5.2, respectively. Both possible rate forms are tested against experimental data.

$$-\frac{d[RSH]}{dt} = -4k_{app}[O_2][RSH] \qquad \text{First Order} \qquad (5.1)$$

where $k_{app} = \dfrac{k_2 K_1 [OH^-]}{[H_2O]}$

$$-\frac{d[RSH]}{dt} = -4k_{app}[O_2][RSH]^2 \qquad \text{Second Order} \qquad (5.2)$$

where $k_{app} = \dfrac{k_3 K_2 K_1^2 [OH^-]^2}{[H_2O]^2}$

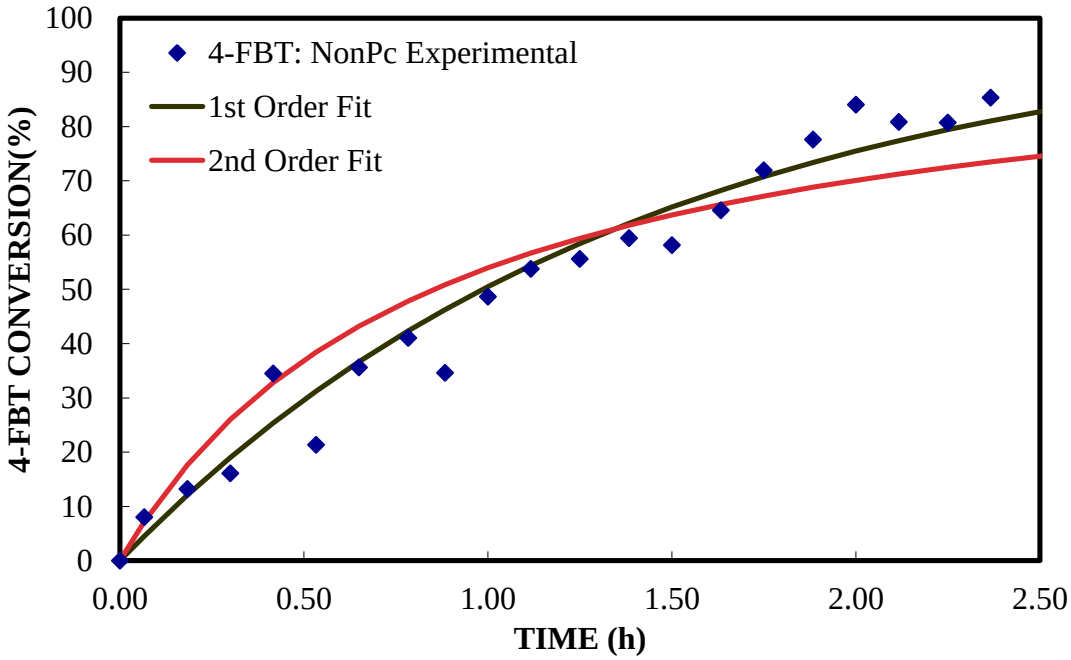

Figure 5.1 1st order and 2nd order fits of hydroxide-catalyzed oxidation of 4-FBT under pure O_2, in the presence of 2.58 mmol/L NaOH at 1 atm and 22 °C.

Table 5.1 Numerical Value and Statistics of Rate parameter, k_{app}, for 1st and 2nd order Hydroxide-Catalyzed Rate Models for 4-FBT and 2-ME (for comparison) Oxidations Under Pure O_2, in the Presence of 2.58 mmol/L NaOH at 22 °C and 1 atm *(k_{app} has the units of L/mmol/h for 1st order model and (L/mmol/h)^2 for 2nd order model; values for 2-ME are taken from Table 4.1)*

Thiol	Model	k_{app}	r^2
2-ME	1st Order	6.50E-03	0.966
	2nd Order	7.00E-05	0.942
4-FBT	1st Order	2.24E-02	0.965
	2nd Order	2.00E-04	0.890

The first order regression for 4-FBT is statistically preferred, as shown in Table 5.1. The data fitted to the first order model yields k_{app} = 0.022 L/mmol-h at 22 °C. Other concentrations were estimated: $[OH^-]$ = 2.58 mmol/L and $[H_2O]$ = 1072 mmol/L. Knowing the pK_a of 4-FBT (pKa = 6.54) and H_2O (pKa = 15.7) for the initial acid/base reaction involving 4-FBT and OH^-, K_1 was estimated as $K_1=10^{-6.54}/10^{-15.7}$ = 1.45E+09. The dissolved $[O_2]$ = 8.10 mmol/L, based on the constant O_2 gas pressure and Henry's Law constant = 99.54 atm-L/mol at 22 °C.[43, 44] The rate constant k_2 = 2.45E-04 h^{-1} at 22 °C was calculated for the rate determining step involving the 4-FBT thiolate coupling with O_2 in solution. The above follows a general acid/base chemistry, where there is an equilibrium involving the addition of a base to the substrate followed by a slow reaction of the complex.[38]

Figure 5.2 presents experimental data for both 2-ME and 4-FBT thiol conversion with time under pure O_2 with NaOH serving as the sole "catalyst." Immediately, there was an observed difference in rates of oxidation between the two thiols. The 4-FBT has a smaller pKa value (6.54) compared to 2-ME (9.64), indicating it is more acidic. The larger, less basic, 4-FBT molecule reacts at a far greater rate. As a more acidic molecule, 4-FBT has a larger K_1 value than 2-ME ($K_{1,4\text{-FBT}}$=1.45E+09 >> $K_{1,2\text{-ME}}$=1.14E+06), which means more 4-FBT thiolate is being produced at a faster rate. With a higher

concentration of active reagent, one would expect an overall faster reaction rate. Thereby, the basicity of the thiol molecule is directly related to the reaction rate of the oxidation, in which it is involved. Also, pure liquid 4-FBT is very sensitive to air, and might break down to its thiolate even in the presence of O_2, even in the absence of NaOH. This would result in an even faster increase in concentration of the active thiolate reagent concentration.

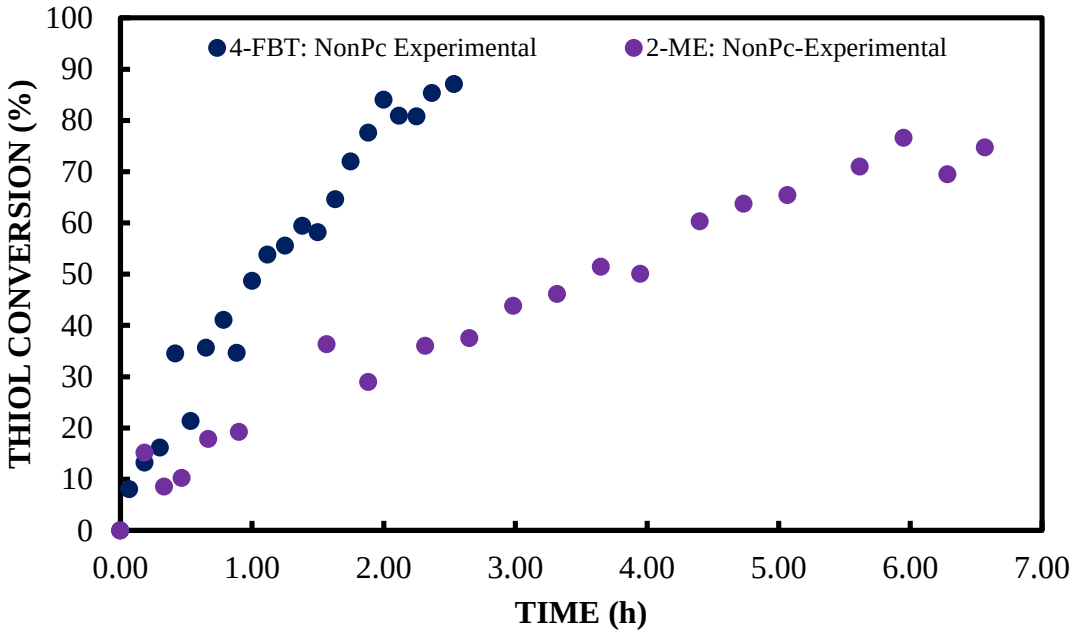

Figure 5.2 Non-Pc oxidation of 4-FBT and non-Pc oxidation of 2-ME under pure O_2, in the presence of 2.58 mmol/L NaOH at 1 atm and 22 °C.

Hydrogen peroxide has been shown to play a significant role in the oxidation of thiols.[23-28] It has been observed that the oxidation of 2-ME occurs significantly faster via H_2O_2 when compared to non-Pc (Figure 4.2) or any of the studied catalysts (Figure 4.4). One can assume from the above observations that the reaction of intermediate H_2O_2 with 4-FBT is similarly faster than the oxidation by O_2 via the phthalocyanine catalysts. As

with the 2-ME kinetic modeling, the result is that any derived rate of 4-FBT Pc-catalyzed oxidation by O_2 was doubled to account for the H_2O_2 contribution.

5.4 Pc-Catalyzed Oxidation of 4-Flourobenzenethiol

5.4.1 Experimental Data

As with the 2-ME work in Chapter 4, the above "non-Pc" analysis was taken into consideration when studying Pc-Catalyzed oxidations of 4-FBT. While GC analysis provides the means to calculate total 4-FBT conversion with time, analysis from Section 5.3 allows one to solve for 4-FBT conversion via the non-Pc pathway at time, t. The total observed conversion minus conversion due to the non-Pc pathway gives conversion due to the Pc-catalytic mechanism. In addition to this correction, all 4-FBT conversion vs t data have also been corrected for dimerization effects, as described in Chapter 4, calculated by Loas[14], where the effective percentage of monomer present is assumed to be 85%, 35% and 80% for H_{16}PcCo, F_{16}PcCo and F_{64}PcCo, respectively. The figures which follow describing Pc-catalyzed 4-FBT oxidation were so corrected.

5.4.2 Qualitative Observations of Unsubstituted Cobalt(II) Phthalocyanine – (H_{16}PcCo)

Figure 5.3 presents H_{16}PcCo oxidations of 2-ME and 4-FBT oxidations. As discussed in Chapter 4, 2-ME oxidation via H_{16}PcCo appears to be zero order in dissolved [O_2]. However, 4-FBT oxidations in the presence of H_{16}PcCo appeared to be dependent on dissolved [O_2]. In fact, the more dissolved [O_2] present in solution, the *lower* the extent of reaction for 4-FBT oxidations catalyzed by H_{16}PcCo. Recall that Chapter 1 addressed the inspiration for fluorinated phthalocyanine catalysts – that the C-H bonds surrounding the H_{16}PcCo scaffold are susceptible to various forms of chemical attack. The 4-FBT

thiolate (RS^-) is a much stronger electrophile and might attack the C-H bonds of $H_{16}PcCo$ more readily than its 2-ME counterpart.

Recalling Section 5.2, pure 4-FBT is very reactive in air. In the absence of solvent, a potential reaction mechanism begins with attachment and removal of protons from RSH by O_2 on the surface and dissolved in the pure liquid 4-FBT. The resulting RS^- then reacts with other O_2 as the oxidation proceeds unassisted. Now, in the presence of higher O_2 concentrations, assisted by hydroxide, the thiolate RS^- may be formed at rates and concentrations that the insufficiently Lewis acidic $H_{16}PcCo$ catalyst cannot handle. This leads to an abundance of the electrophilic 4-FBT thiolate in solution, which might in turn attack the C-H bonds surrounding $H_{16}PcCo$. The result is a loss of catalytic activity because of a loss of active catalyst.

Due to the above, kinetic analysis of $H_{16}PcCo$ catalyzed oxidations of 4-FBT would provide inconclusive results. However, these observations reflect the importance of protecting the phthalocyanine catalyst from degrading agents, such as electrophiles, nucleophiles, and radicals. Such is the inspiration for the fluorinated Pc's wherein the C-F bonds of $F_{16}PcCo$ and $F_{64}PcCo$ are more survivable in the presence of a reactive thiolate.

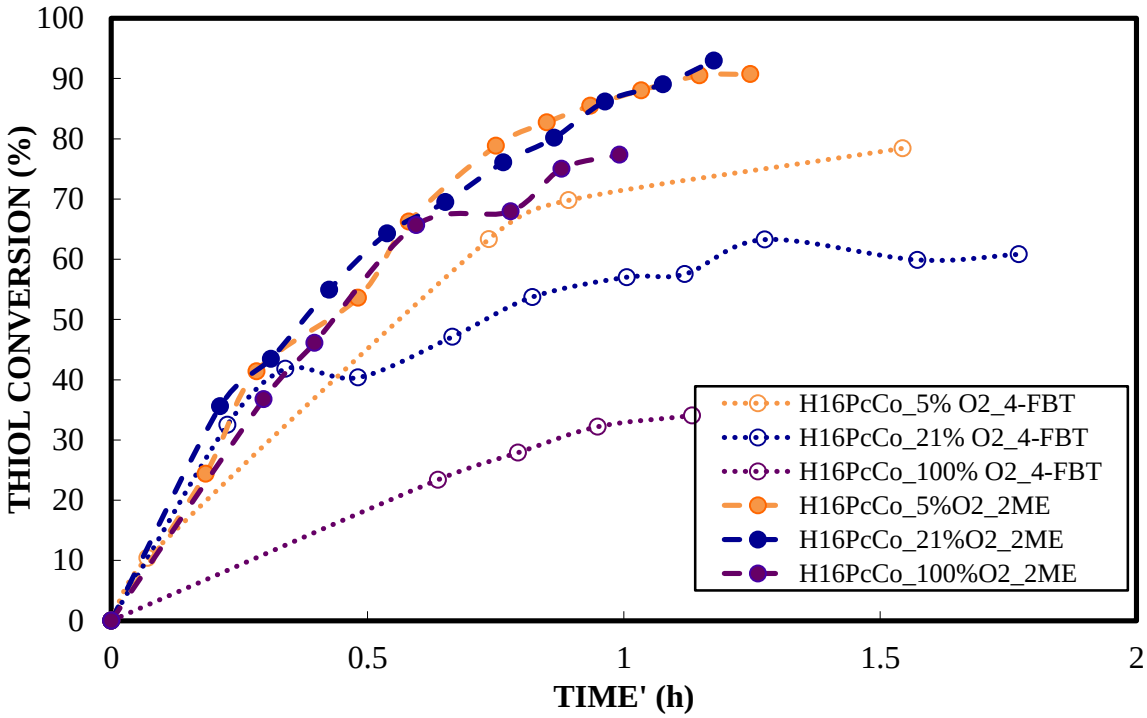

Figure 5.3 $H_{16}PcCo$ Catalyzed oxidation of 2-ME and 4-FBT under pure O_2, air, and diluted O_2 (5% O_2, balance N_2), in the presence of 2.58 mmol/L NaOH at 22° C and 1 atm.

5.4.3 Qualitative Observations of Fluorinated Cobalt(II) Phthalocyanines – ($F_{16}PcCo$ & $F_{64}PcCo$)

Most 4-Flourobenzenethiol oxidations involving $F_{16}PcCo$ and $F_{64}PcCo$ exhibited faster reaction rates than that of 2-ME under the same conditions, such as O_2 partial pressure, as shown by Figures 5.4 and 5.5. The larger 4-FBT molecule may facilitate the expulsion of its thiyl ($RS^{\bullet}$) radical more readily than 2-ME, assuming this remains the slow step in the Pc-catalyzed pathway. In 100% gaseous O_2, in the presence of $F_{64}PcCo$ catalyst, 2-ME and 4-FBT exhibited comparable reaction rates. This is likely due to counteracting effects of the steric bulk of the thiols. For example, substrate binding is facilitated by the smaller size of 2-ME, while radical expulsion is accelerated by the larger 4-FBT. Either way, the true mechanism and effects were quantitatively explained by determining the slow step and estimating kinetic parameters.

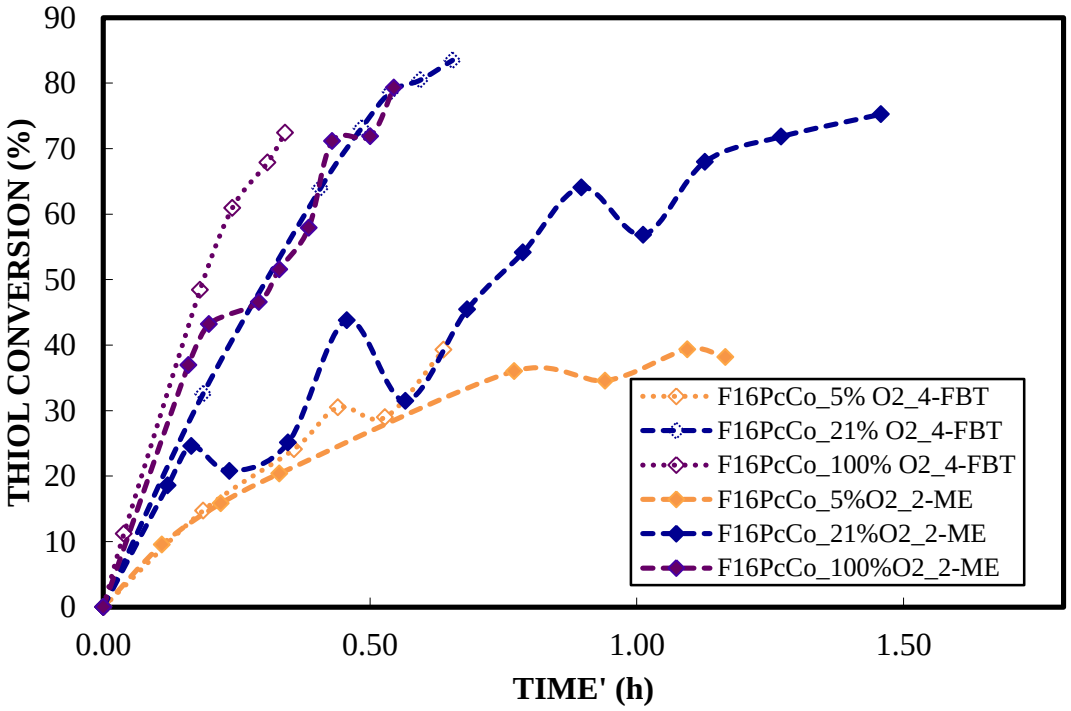

Figure 5.4 $F_{16}PcCo$ Catalyzed oxidation of 2-ME and 4-FBT under pure O_2, air, and diluted O_2 (5% O_2, balance N_2), in the presence of 2.58 mmol/L NaOH at 22° C and 1 atm.

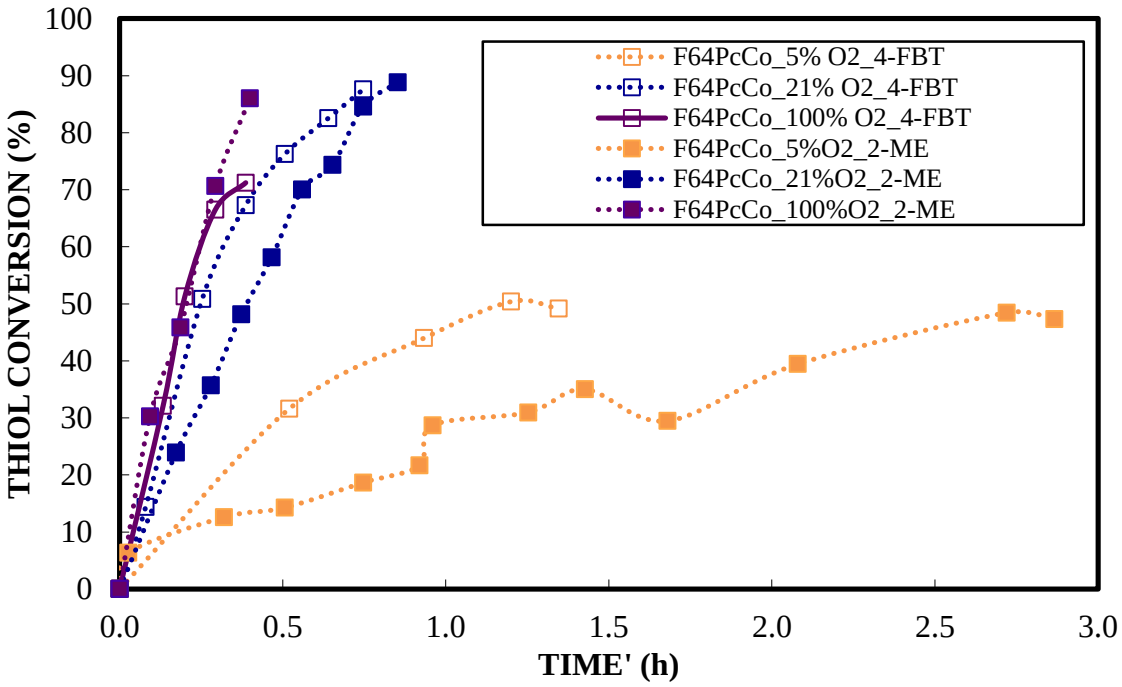

Figure 5.5 F_{64}PcCo Catalyzed oxidation of 2-ME and 4-FBT under pure O_2, air, and diluted O_2 (5% O_2, balance N_2), in the presence of 2.58 mmol/L NaOH at 22° C and 1 atm.

5.4.4 Identification of Preferred Rate Model for Fluorinated Cobalt(II) Phthalocyanines – (F_{16}PcCo & F_{64}PcCo)

Models I-VIII were previously derived in Appendices D thru K. Models were fitted to experimental data by nonlinear regression. Criteria for choosing the correct model include: positive rate constants; relatively large r^2 values; small 95% confidence values, relative to corresponding parameter; models and constants which are chemically and physically logical; and models and constants which are consistent with literature, when such comparisons are possible. Tables 5.2 thru 5.4 provide kinetic parameters of derived models (Figure 2.1) fitted to 4-FBT data at various O_2 partial pressures for F_{16}PcCo and F_{64}PcCo catalysis.

Models I, II, and III provided the best fits for 4-FBT oxidation via F_{16}PcCo and F_{64}PcCo catalysts. Once again, a further look into models I, II, and III was required for discernment between the models. Equations 4.3, 4.4, and 4.5 are expanded forms of models I, II and III, respectively, based on Figure 2.1**.** These models were derived in Appendices D, E, and F.

$$-r_I \approx 4(k_2 K_1 [OH^-]/[Cat]_T /[H_2O])[RSH] \tag{4.3}$$

Where $k_2 K_1 [OH^-]/[Cat]_T /[H_2O] \equiv \alpha_I$

$$-r_{II} \approx \frac{4k_3 K_2 K_1 ([OH^-]/[H_2O])[O_2][Cat]_T [RSH]}{1+K_2 K_1 ([OH^-]/[H_2O])[RSH]} \tag{4.4}$$

Where $k_3 K_2 K_1 ([OH^-]/[H_2O])[O_2][Cat]_T \equiv \alpha_{II}$, $K_2 K_1 ([OH^-]/[H_2O]) \equiv \beta_{II}$

$$-r_{III} \approx \frac{4k_4 K_3 K_2 K_1 ([OH^-]/[H_2O])[O_2][Cat]_T [RSH]}{1+K_2 K_1 ([OH^-]/[H_2O])(1+K_3[O_2])[RSH]} \tag{4.5}$$

Where $k_4 K_3 K_2 K_1 ([OH^-]/[H_2O])[O_2][Cat]_T \equiv \alpha_{III}$,

$$K_2 K_1([OH^-]/[H_2O])(1+K_3[O_2]) \equiv \beta_{III}$$

Conversion from RSH to RS^- is represented by the equilibrium constant K_1. Substrate RS^- binding to Co(II), and reduction of Co(II) to Co(I), is represented by either K_2 (an equilibrium constant) or k_2 (a rate constant), and is directly related to the Lewis acidity of the metal center. The attachment of dissolved O_2, and electron transfer from the metal center to coordinated O_2, is represented by either K_3 (an equilibrium constant) or k_3 (a rate constant). The rate constant k_4 represents the rate constant for the expulsion of $RS^{\bullet}$ thiyl radical from the metal center.

Equation 4.3 (Model I) was immediately eliminated as a possibility for F_{16}PcCo and F_{64}PcCo catalysis of 4-FBT. Figures 5.4 and 5.5 show a definite dependence of reaction rate on dissolved [O_2]. Rate Model I has no such dependence. Quantitative analysis was then performed, focusing on models II and III, to better choose the correct rate-model and understand the dependence of kinetic parameters on phthalocyanine structure. Figures 5.6 and 5.7 are graphical representations of model II/III fitted F_{16}PcCo and F_{64}PcCo catalyzed oxidations 4-FBT at various dissolved [O_2], respectively.

Table 5.2 Numerical Values for Lumped KineticParameters (Models I-VIII of Table 2.1) for Catalytic (F_{16}PcCo and F_{64}PcCo) Oxidations of 4-FBT Under 5% Gas Phase O_2 Composition, in the Presence of 2.58 mmol/L NaOH at 22 °C and 1 atm. * Represents Relatively Large 95% Confidence Value

F_{16}PcCO Oxidation of 2-ME at 5% O_2 Concentration					
Model	I	II/III	IV/V	VI	VII/VIII
α	0.82	0.22	0.003		
β	-	0.0013	-22.6	**DOES NOT CONVERGE**	**DOES NOT CONVERGE**
γ	-	-	-0.0018		
r^2	0.972	0.972	0.977		
F_{64}PcCO Oxidation of 2-ME at 5% O_2 Concentration					
Model	I	II/III	IV/V	VI	VII/VIII
α	0.0698	0.16	8.78	4.00E-04	1.75E-04
β	-	0.0008	12320	-0.015	-0.036
γ	-	-	-0.62	-	6.41E-05
r^2	0.833	0.943	0.946	0.947	0.959

Table 5.3 Numerical Values for Lumped Kinetic Parameters (Models I-VIII of Table 2.1) for Catalytic (F_{16}PcCo and F_{64}PcCo) Oxidations of 4-FBT Under 21% Gas Phase O_2 Composition, in the Presence of 2.58 mmol/L NaOH at 22 °C and 1 atm. *Represents Relatively Large 95% Confidence Value

F_{16}PcCO Oxidation of 2-ME at 21% O_2 Concentration					
Model	I	II/III	IV/V	VI	VII/VIII
α	0.29	1.05			0.018
β	-	0.0074	**DOES NOT CONVERGE**	**DOES NOT CONVERGE**	-0.044
γ	-	-			4.00E-04
r^2	0.987	0.998			0.997
F_{64}PcCO Oxidation of 2-ME at 21% O_2 Concentration					
Model	I	II/III	IV/V	VI	VII/VIII
α	0.31	0.73	0.33*		0.66*
β	-	0.012	0.49*	**DOES NOT CONVERGE**	2.04*
γ	-	-	3.00E-04*		6.00E-04*
r^2	0.998	0.998	0.998		0.998

Table 5.4 Numerical Values for Lumped Kinetic Parameters (Models I-VIII of Table 2.1) for Catalytic (F_{16}PcCo and F_{64}PcCo) Oxidations of 4-FBT Under 100% Gas Phase O_2 Composition, in the Presence of 2.58 mmol/L NaOH at 22 °C and 1 atm. * Represents Relatively Large 95% Confidence Value

F_{16}PcCO Oxidation of 2-ME at 100% O_2 Concentration					
Model	I	II/III	IV/V	VI	VII/VIII
α	0.41	0.986			0.012
β	-	0.0006	**DOES NOT CONVERGE**	**DOES NOT CONVERGE**	-0.038
γ	-	-			1.89E-04
r^2	0.997	0.997			0.998
F_{64}PcCO Oxidation of 2-ME at 100% O_2 Concentration					
Model	I	II/III	IV/V	VI	VII/VIII
α	0.39	0.54			0.0034
β	-	0.0018	**DOES NOT CONVERGE**	**DOES NOT CONVERGE**	-0.052
γ	-	-			1.55E-04
r^2	0.997	0.999			0.996

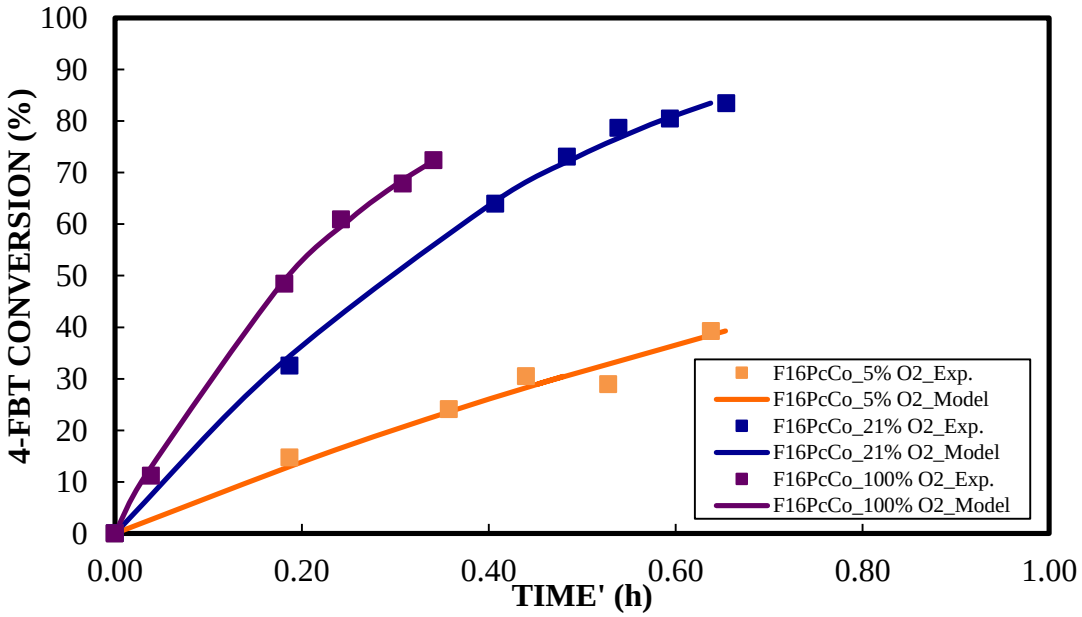

Figure 5.6 Experimental data and model fits, based on model II/II for F_{16}PcCo catalyzed oxidation of 4-FBT under O_2, air and diluted O_2 (5% O_2, balance N_2), in the presence of 2.58 mmol/L NaOH at 22 °C, 1 atm.

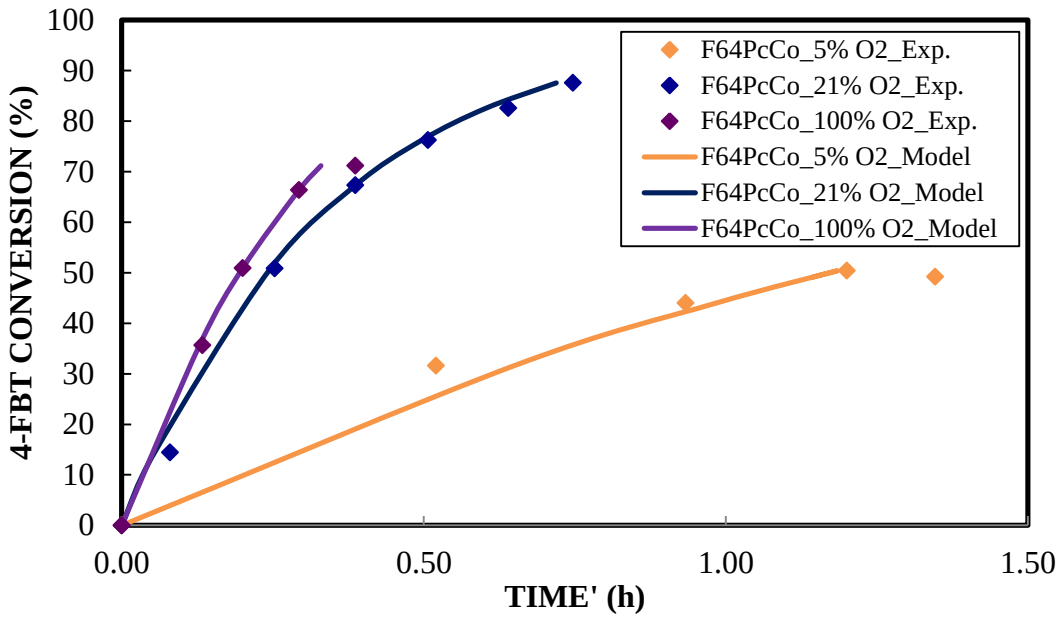

Figure 5.7 Experimental data and model fits, based on models II/III. for F_{64}PcCo catalyzed oxidation of 2-ME under O_2, air and diluted O_2 (5% O_2, balance N_2), in the presence of 2.58 mmol/L NaOH at 22 °C, 1 atm.

5.4.5 Quantitative Estimation of Kinetic Rate and Equilibrium Constants for Fluorinated Cobalt(II) Phthalocyanines (F_{16}PcCo & F_{64}PcCo)

Similarly to kinetic analysis of 2-ME oxidations found in Section 4.3.5, initial rates were examined in order to decide on the correct rate model. Recalling that Equations 4.4 and 4.5 can be reduced to initial rates, where the thiol concentration is large.

$$-r_{II_0} \approx 4k_3[O_2]_0[Cat]_T \tag{4.6}$$

$$-r_{III_0} \approx \frac{4k_4K_3[O_2]_0[Cat]_T}{1+1+K_3[O_2]_0} \tag{4.7}$$

Figure 5.8 provided initial rate data as a function of dissolved oxygen concentration as estimated by Henry's law[43,44] at 1 atm and 22 °C. Equation 4.6 suggest initial rate is linear with dissolved oxygen concentration with a y-intercept of zero. Figure 5.8 implies that Equation 4.6, or rate model II, does not represent the correct rate-determining step for 4-FBT oxidations via F_{16}PcCo or F_{64}PcCo catalysts.

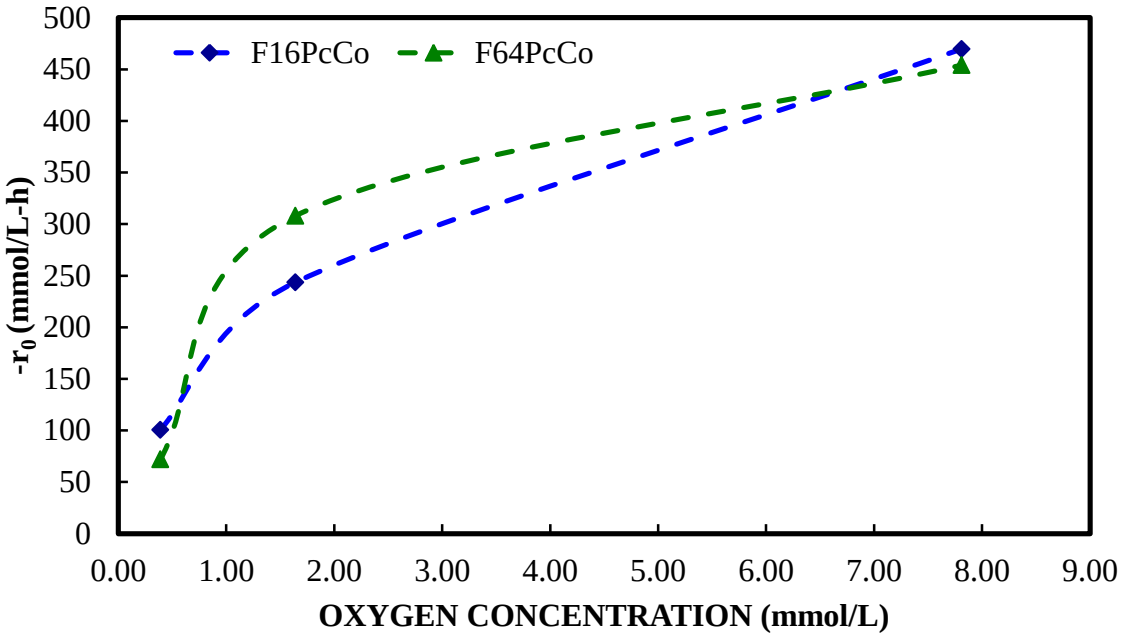

Figure 5.8 Initial rates of F_{16}PcCo and F_{64}PcCo catalyzed oxidations as a function of liquid oxygen concentration, estimated by Henry's constant[43,44] in the presence of 2.58 mmol/L NaOH at 22° C and 1 atm.

Figure 4.13 presented initial rate vs. catalyst amount data, in which a mass transfer resistance begins to occur for oxidations occurring faster than ~2300 mmol/L-h. It can be argued that this threshold rate for a mass transfer resistance is characteristic of the reactor used in this study. Initial rates of studied 4-FBT oxidations, found in Figure 5.8, are below the mass transfer resistance threshold, suggesting all data studied are not limited by mass transfer effects.

Similarly to the trial-and-error procedure used in Section 4.3.5, the reciprocal of Equation 4.7 was applied to inverse reaction rate vs. inverse dissolved [O_2] data for 4-FBT oxidations catalyzed by F_{16}PcCo and F_{64}PcCo. The Matlab™ program used for this calculation can be found in Appendices N and O for F_{16}PcCo and F_{64}PcCo, respectively. The consequence of claiming negligible mass transfer resistance is that the dissolved [O_2] was estimated from Henry's Law, based on O_2 partial pressure and reactor temperature.

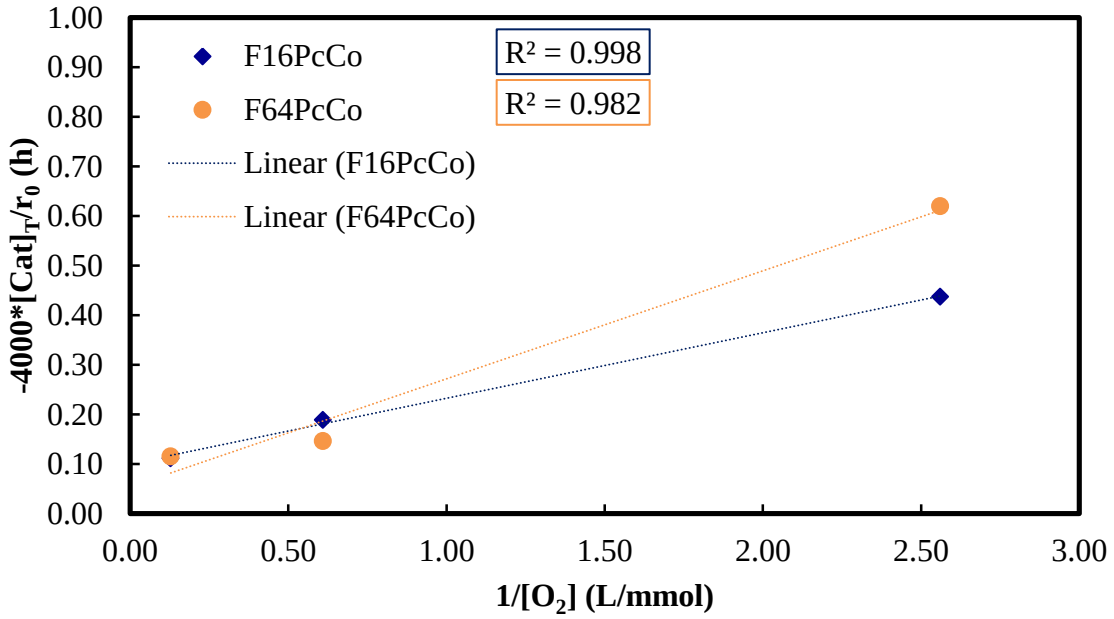

Figure 5.9 Inverse initial rate of F_{16}PcCo and F_{64}PcCo catalyzed oxidations of 4-FBT as a function of inverse dissolved oxygen concentration, in the presence of 2.58 mmol/L NaOH at 22 ^{o}C and O_2 partial pressure = 1 atm.

Table 4.5 shows values for K_3 and k_4, and concentrations of dissolved O_2 based on Henry's Law for F_{16}PcCo and F_{64}PcCo catalyzed 2-ME oxidations. Knowing the pK_a of 4-FBT (pKa = 6.54) and H_2O (pKa = 15.7) for the initial acid/base reaction involving 2-ME and OH^-, K_1 was estimated as $K_1=10^{-6.54}/10^{-15.7} = 1.45x10^9$. The kinetic parameter describing substrate binding, K_2, was determined by fitting to complete data sets after values of K_1, K_3, and k_4 for F_{16}PcCo and F_{64}PcCo 4-FBT oxidations were known.

Table 5.5 Kinetic Parameters and Dissolved [O_2] for F_{16}PcCo and F_{64}PcCo Catalyzed Oxidations of 4-Fluorobenzenethiol, Derived from Model III Initial Rates of F_{16}PcCo, F_{64}PcCo, Oxidations of 4-FBT Under Various Gas Phase O_2 Initial Concentrations, in the Presence of 2.58 mmol/L NaOH at 22 °C, 1 atm.,where $y=-4000*[Cat]_T/r_0$ (h)

Cat_T (mmol/L)	km (mmol/L-h-atm)	H (L-atm/mmol)	H_2O (mmol/L)	OH^- (mmol/L)	K_1	
0.01	5000	0.10	1.10E+03	2.58	1.45E+09	
F_{16}PcCo	fm	0.33				
$-r_0$ (mmol/L-h)	y (h)	$[O_2]$ (mmol/L)	$[1/O_2]$ (L/mmol)	k_4 (1/h)	K_3 (L/mmol)	K_2 (L/mmol)
96.0	0.44	0.40	2.50	9.93E+03	0.76	8.63E-10
222	0.19	1.70	0.58			
376	0.11	8.02	0.12			
F_{64}PcCo	fm	0.80				
$-r_0$ (mmol/L-h)	y (h)	$[O_2]$ (mmol/L)	$[1/O_2]$ (L/mmol)	k_4 (1/h)	K_3 (L/mmol)	K_2 (L/mmol)
67.7	0.62	0.40	2.50	1.83E+04	0.29	6.95E-10
287	0.15	1.70	0.58			
364	0.12	8.02	0.12			

5.5 Catalytic Factors Affecting Thiol Oxidation Kinetics

5.5.1 Correlation of Kinetic Parameters to Thiol and Catalyst Structure

Two effects are in play when transitioning from the F_{16}PcCo to the bulky fluorinated F_{64}PcCo molecule. These effects include steric hindrance and Lewis acidity. Choice of thiol may also result in some unexpected kinetic conclusions. Studying trends of quantitative data provided by Table 5.6 should elucidate the true effects of both catalyst and thiol structure.

Table 5.6 Kinetic Parameters of 2-ME and 4-FBT Oxidations Catalyzed by F_{16}PcCo and F_{64}PcCo Catalysts

Catalyst/Thiol	**K_2 (L/mmol)**	**K_3 (L/mmol)**	**k_4 (1/h)**
F_{16}PcCo/2-ME	8.00E-07	1.19	8.00E+03
F_{64}PcCo/2-ME	3.46E-06	0.19	1.73E+04
F_{16}PcCo/4-FBT	8.63E-10	0.76	9.93E+03
F_{64}PcCo/4-FBT	6.95E-10	0.29	1.83E+04

5.5.2 Catalyst Stability

The transition from 2-mercaptoethanol to 4-fluorobenzenethiol has various kinetic consequences. It is imperative to understand possible outcomes in changing thiols regarding steric bulkiness and Lewis acidity, as mentioned previously. The catalyst stability in the presence of a more aggressive thiolate is also important.

Section 5.4.2 discusses the likely degradation of H_{16}PcCo as a result of electrophilic substitution. The 4-FBT thiol rapidly converts into its active thiolate, particularly in oxygen rich solutions. The electronegative fluorine and aromatic resonance afforded by the benzene ring add to the electrophilicity of the thiolate, which increases its likelihood of replacing a perimeter H surrounding the H_{16}PcCo molecule. Unfortunately, kinetic analysis of 4-FBT oxidation data involving H_{16}PcCo was not possible due to the perceived lack of catalyst stability. In future work, independent verification by an analytical method such as ultraviolet/visible (uv/vis) spectroscopy might be used to quantify the remaining H_{16}PcCo.

Returning to the inspiration of fluorinated phthalocyanine catalysts, the above mechanism of deactivation does not occur for F_{16}PcCo and F_{64}PcCo catalyzed oxidations of 4-FBT. The C-F bonds on the perimeters of these molecules appear to be immune to the more aggressive electrophilic 4-FBT thiolate than the 2-ME thiolate.

5.5.3 Steric Bulkiness & Lewis Acidity

Steric bulkiness typically increases as the number of fluorine atoms increase from F_{16}PcCo to F_{64}PcCo catalysts. The rate of substrate binding may decrease with increasing steric bulkiness because of difficulty to reach the metal center, and may be reflected in the K_2 values.

The effects Lewis acidity of the catalyst molecule may be observed in both substrate binding (K_2) and electron transfer from catalyst center to coordinated O_2 (K_3). Greater Lewis acidity causes a catalyst to be a better "oxidizer," increasing the rate of substrate binding. Meanwhile, an increased Lewis acidic molecule holds on to electrons more tightly, decreasing the rate of which it gives up an electron.

Thiyl radical expulsion may increase as steric bulkiness increases because the additional fluorine atoms might quicken the ejection of these radicals once formed. On the other hand, the bulky fluorinated groups may hinder the same expulsion in which it accelerates. Rate of thiyl product expulsion may be affected in various ways due to the size of 4-FBT. These effects can be revealed by studying values of k_4.

5.5.3.1 Substrate Binding and Electron Transfer to Metal Center (K_2). The parameter describing substrate binding (K_2) increases as we change from F_{16}PcCo to F_{64}PcCo for the smaller 2-ME thiolate, consistent with the greater electronegativity of 64 F atoms. The K_2 for the larger 4-FBT thiolate slightly decreases. Although F_{64}PcCo is a better "oxidizer" than the F_{16}PcCo molecule, the bulkiness of the F_{64}PcCo molecule may hinder the binding of the larger 4-FBT substrate. F_{16}PcCo has a more open structure allowing for facilitated substrate binding.

Substrate binding and electron transfer to the metal center, as described by K_2, reflects how readily the PcCo(II) oxidizes the chosen thiolate. The values of K_2 are considerably lower for 4-FBT oxidation when compared to 2-ME as seen by the comparison in Table 5.6. The Lewis acidic, fluorinated phthalocyanines, oxidized the more basic 2-ME thiol faster than 4-FBT. The aromatic resonance of the benzene ring

and attached F of 4-FBT strongly holds on to its electrons, and the attachment and electron transfer from thiol to metal center is less favorable.

5.5.3.2 Lewis Acidity (K_3). Lewis acidity is important when studying the rate of electron transfer from the metal center to the coordinated O_2, defined by K_3. There is an increase in electron deficiency from F_{16}PcCo to F_{64}PcCo. F_{64}PcCo yields lower K_3 values, indicating the slowest rate of electron transfer, confirming that F_{64}PcCo is the more Lewis acidic catalyst.

Similar observations were made earlier for 2-ME cases (Section 4.3.6). There is no significant correlation when comparing K_3 values of 2-ME with that of 4-FBT. This is likely because electron transfer from metal center to coordinated O_2 is just that, an issue dealing with the metal center of catalyst and coordinated O_2. This is an internal matter, in which choice of thiol has little relevance.

5.5.4 Expulsion of Thiyl Radical from Catalyst Cavity (k_4)

As established in the 2-ME studies, the thiyl radical wants to escape the catalyst cavity. The greater amount of inherent cavity bulkiness, the faster the rate of radical expulsion due to steric hindrance. This continues to hold true for 4-FBT oxidation as shown by Table 5.6, $k_{4\text{-F16PcCo}} << k_{4\text{-F64PcCo}}$.

When comparing kinetic parameters of 2-ME and 4-FBT oxidations, k_4 is accelerated for all cases. Although K_2 values for 4-FBT oxidations are four orders of magnitude lower than that of 2-ME, Figures 5.4 and 5.5 show conversion of 4-FBT are generally faster than 2-ME. This compliments the large effect k_4 has on thiol oxidations via fluorinated catalysts, further suggesting thiyl radical expulsion is rate-determining.

5.6 Conclusions

Substrate binding increases with the readiness of the thiolate to give up an electron. Higher basicity results in more rapid substrate binding. In the case of a larger thiol (4-FBT), the rate of substrate binding is slowed down by a sterically bulky catalyst (F_{64}PcCo). Lewis acidity continues to be reflected in the rate of electron transfer from metal center to the coordinated oxygen. In addition, this electron transfer was found to be an internal issue and is not significantly affected by the chosen thiol.

As with 2-mercaptoethanol, the rate-determining step for 4-fluorobenzenethiol oxidations was shown to be the expulsion of thiyl radical from the catalyst cavity. The expulsion of the 4-FBT thiyl radical increases as steric bulkiness of the catalyst increases.

Using 4-fluorobenzenethiol affects the kinetics due to its increased acidity and size, as well as stability of the particular catalysts. The H_{16}PcCo catalyst is not adequately protected against the highly reactive 4-FBT molecule. Meanwhile, the fluorine atoms surrounding F_{16}PcCo and F_{64}PcCo not only provide improved kinetics, but also shield the catalyst molecule from hostile deactivation agents.

CHAPTER 6

SUPPLEMENTARY CATALYTIC THIOL OXIDATION EXPERIMENTS

6.1 Effects of Initial Hydroxide Concentration on Catalytic Oxidations

Sodium hydroxide (NaOH) is added as a necessary precursor in all phthalocyanine (Pc) catalyzed oxidations of thiols. Section 4.2 discussed the "nonPc" oxidation of 2-ME, catalyzed solely by NaOH. Theoretical analysis, supported by experimental data, showed that the rate of hydroxide-catalyzed (non-Pc) oxidation of 2-ME by O_2 has a linear dependence with NaOH. These observations were not shared with Pc-catalyzed oxidations. This may be explained through studying and understanding kinetic rate models and further scrutiny of possible stability issues.

Figures 6.1 thru 6.3 present experimental 2-ME conversion data, corrected for the non-Pc contribution to total conversion, at varying concentrations of NaOH, catalyzed by H_{16}PcCo, F_{16}PcCo, and F_{64}PcCo, respectively. There were negligible differences in these catalytic oxidations as the initial NaOH concentration changes. A relative uncertainty RSD = +/- 7% were added to figures in this chapter when claiming statistically insignificant variation in data.

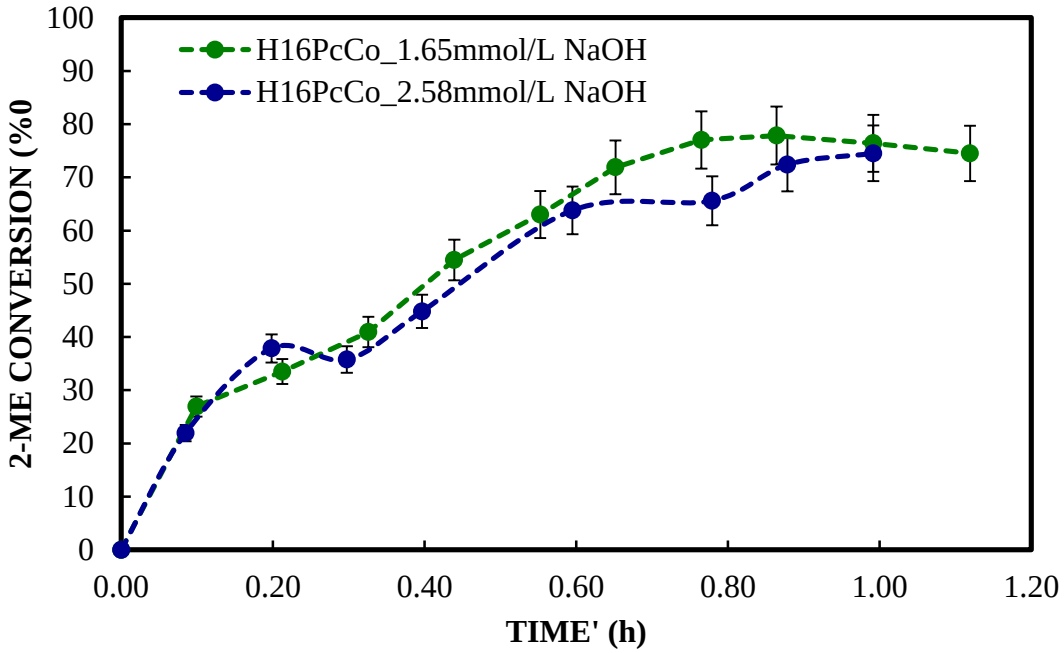

Figure 6.1 $H_{16}PcCo$ catalyzed oxidation of 2-ME in 1.65 and 2.58 mmol/L NaOH under pure O_2 at 1 atm and 22 °C. RSD=+/- 7%.

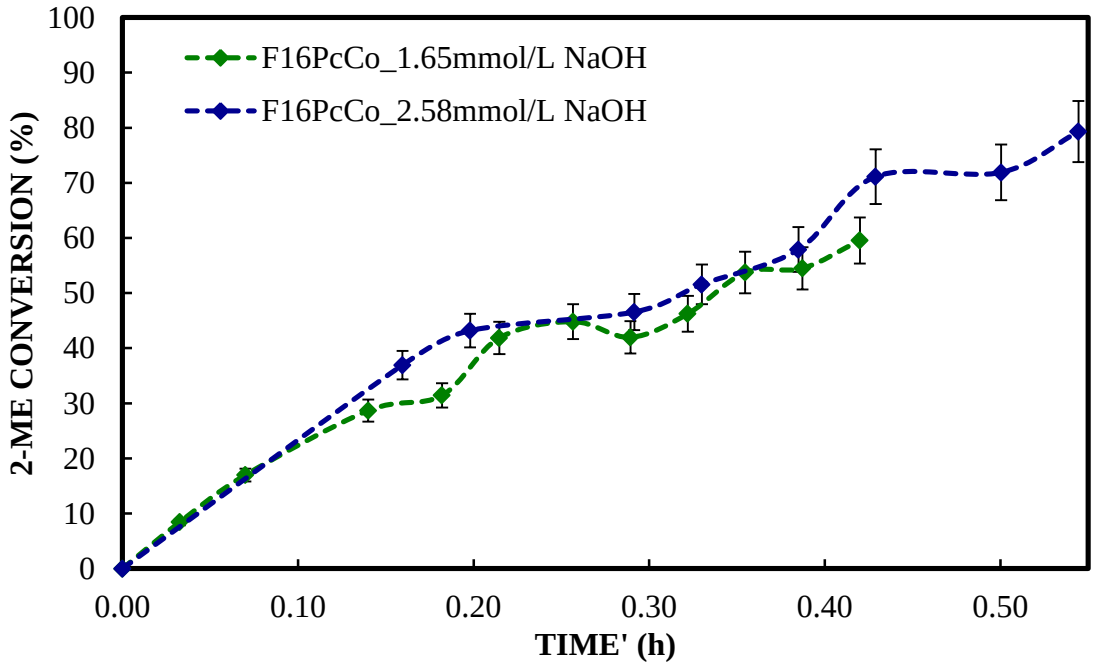

Figure 6.2 $F_{16}PcCo$ catalyzed oxidation of 2-ME in 1.65 and 2.58 mmol/L NaOH under pure O_2 at 1 atm and 22 °C. RSD=+/- 7%

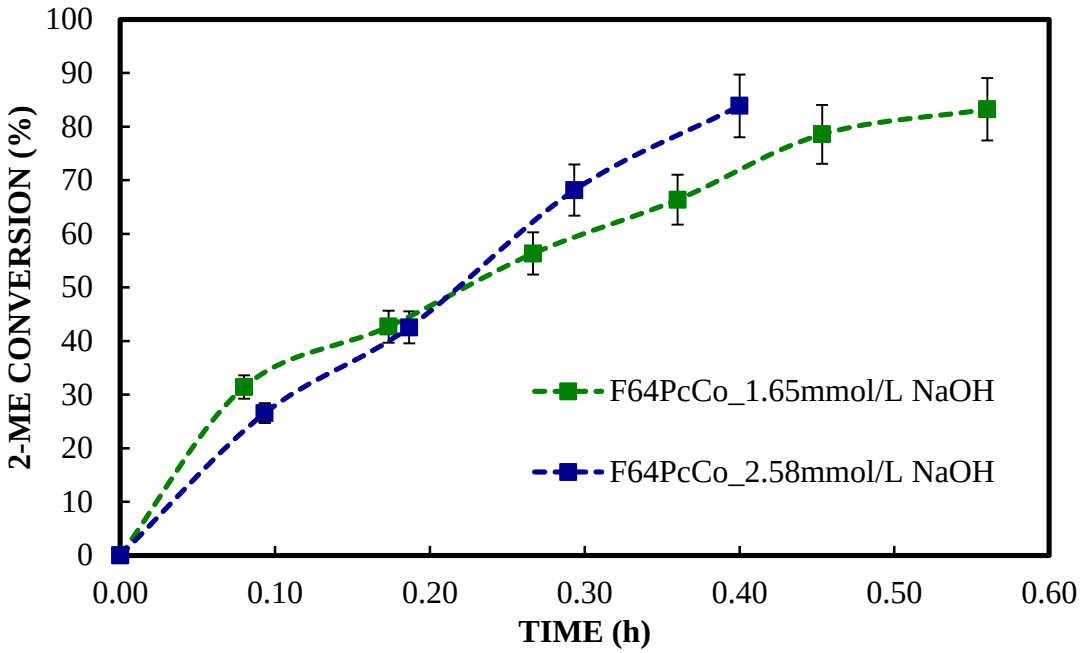

Figure 6.3 F_{64}PcCo catalyzed oxidation of 2-ME in 1.65 and 2.58 mmol/L NaOH under pure O_2 at 1 atm and 22 °C. RSD=+/- 7%

Recall that NaOH was added to the initial solution to convert thiol (RSH) to thiolate (RS^-), which is the active reagent. Although NaOH is consumed in the preliminary step, it is regenerated in both O_2-induced and H_2O_2-induced non-elementary reactions, as shown by Equations 2.2 and 2.3, respectively. The NaOH concentration in the reaction solution is essentially constant. This process occurs via a catalytic cycle (Figure 2.3), which contains the rate-determining step for catalytic oxidations of thiols. This rate-determining step dominates the rate of thiol consumption as well as the rate of hydroxide regeneration.

Although to a lesser extent than 4-FBT cases, a stability study performed by Loas[14] showed H_{16}PcCo stability decreases with time for 2-ME oxidations. This issue of stability may be exacerbated with an increase in NaOH concentration. As more NaOH is added, there is an increase in $[RS^-]$ due to the K_1 acid/base reaction. As mentioned in Chapter 4, an increase in $[RS^-]$ may also increase the likelihood of electrophilic

substitution in which the thiolate may attack the C-H bonds surrounding the H_{16}PcCo catalyst. Loas also mentioned possible mechanisms of deactivation include nucleophilic (OH^-) and radical (H_2O_2) degradation pathways.[14] These factors may all cause a minimal change in observed reaction rates when altering NaOH concentration. In others words, increasing NaOH accelerates the reaction rate according to the model invokes deactivation causing a decrease in effective catalyst concentration and subsequent reduction in reaction rate according to the model.

On the other hand, the rate model describing F_{16}PcCo and F_{64}PcCo thiol oxidations contains the variable [OH^-] in both the numerator and denominator. The dependence on [OH^-] essentially cancels out as shown by the weak impact of NaOH in Figure 6.2 (F_{16}PcCo) and Figure 6.3 (F_{64}PcCo). The apparent nullification of [OH^-] supports earlier assumptions in analysis using initial rate data which suggested $\beta >> 1$ early in thiol oxidations.

$$-r_{III} \approx \frac{4k_4K_3K_2K_1([OH^-]/[H_2O])[O_2][Cat]_T[RSH]}{1+K_2K_1([OH^-]/[H_2O])(1+K_3[O_2])[RSH]} \tag{4.5}$$

Where $k_4K_3K_2K_1([OH^-]/[H_2O])[O_2][Cat]_T \equiv \alpha_{III}$,

$K_2K_1([OH^-]/[H_2O])(1+K_3[O_2]) \equiv \beta_{III}$

Sensitivity tests were conducted for F_{16}PcCo and F_{64}PcCo catalyzed oxidations of 2-ME at arbitrary [OH^-] values based on the above model. Figures 6.4 and 6.5 are the calculated rates vs thiol concentration based on equation 4.5 and kinetic parameters found in Table 4.6. Even if the NaOH concentration is increased by 500%, there is only an increase of ~33% in rate of thiol consumption. The insignificant impact of changing NaOH seen in Figures 6.2 and 6.3 and the quantitative observations of Figures 6.4 and

6.5 supported rate model III as the correct form for thiol oxidations catalyzed by F_{16}PcCo and F_{64}PcCo.

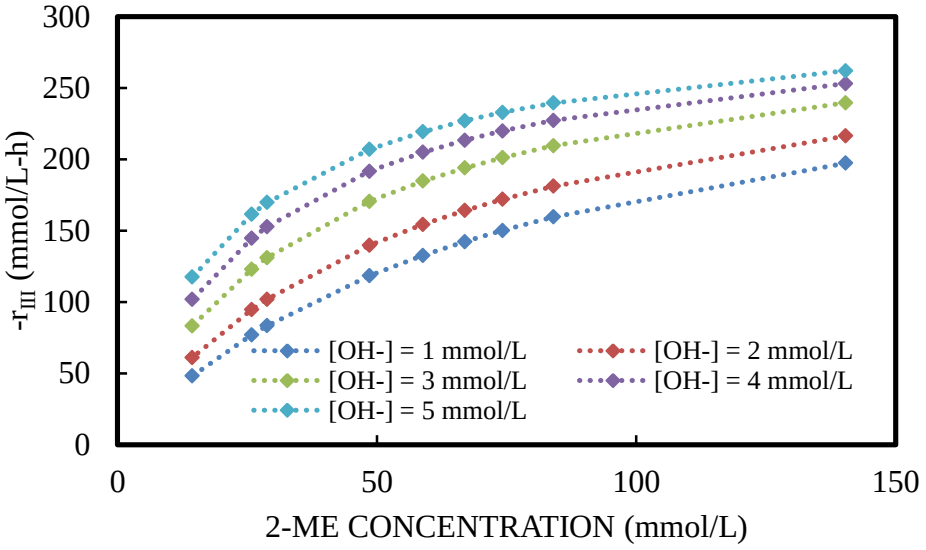

Figure 6.4 Rate vs 2-ME concentration under pure O_2 at 1 atm and 22 °C based on rate model III and F_{16}PcCo kinetic parameters at hypothetical values of NaOH concentration.

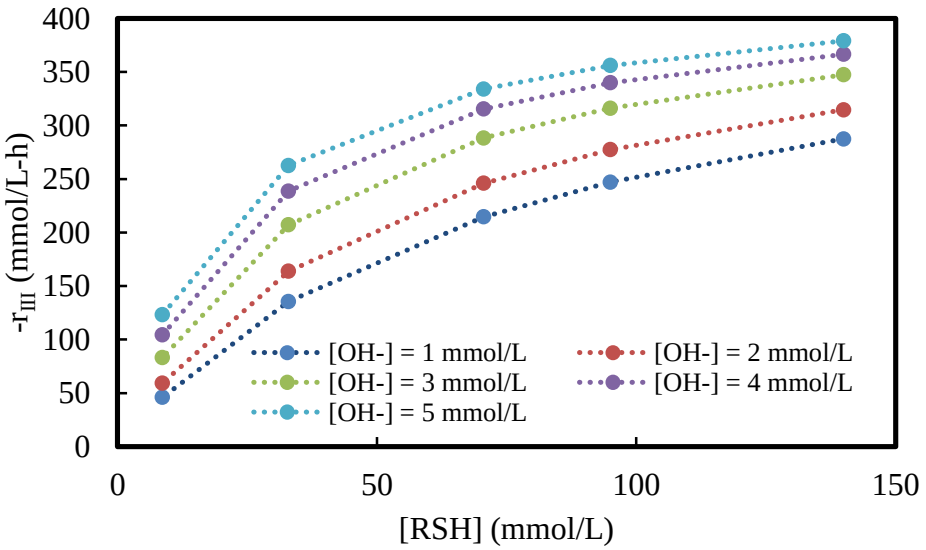

Figure 6.5 Rate vs 2-ME concentration under pure O_2 at 1 atm and 22 °C based on rate model III and F_{64}PcCo kinetic parameters at hypothetical values of NaOH concentration.

6.2 Stability of Fluorinated Phthalocyanine Catalyst

Supplementary experiments were conducted on the unsubstituted (H_{16}PcCo) and perfluoroalkylated (F_{64}PcCo) phthalocyanine to observe their stability. After the completion of the baseline catalytic run loaded with 140mmol/L 2-ME, 0.0105mmol/L catalyst and 2.58mmol/L NaOH in 50ml of THF, an additional 7.2 mmol of 2-ME (original amount added to solution) was reloaded to the reaction solution. Completion of catalytic oxidation was detected when 2-ME concentration went to nearly zero. This final concentration was noted in order to calculate the total concentration of 2-ME initially present after 7.2 mmol of 2-ME was added. Conversions are based on the calculated initial concentrations of baseline or reloaded experiments. Liquid samples were extracted as usual after 2-ME was reloaded. Less stable catalysts were expected to have a decreased conversion for the reloaded case.

Figures 6.6 and 6.7 present 2-ME conversion data, corrected for the non-Pc contribution, showing the baseline and "reloaded" experiments. The "reloaded" conversion was based on the initial 2-ME concentration of the reloaded solution. The 2-ME oxidation involving H_{16}PcCo plateaus quickly at a conversion of ~45% in the "reloaded" experiment. F_{64}PcCo-catalyzed experiments also level off at ~55% when limited thiol is reloaded.

Turnover number (TON)[51] is defined as the maximum number of molecules of substrate that a catalyst can convert to product per catalytic site. The turnover frequency (TOF) is the maximum number of substrate molecules converted to product per site per second. TON and TOF were calculated by observing the total amount of 2-ME converted in original and reloaded experiments as well as the total time in Figures 6.6 and 6.7. The TON and TOF are accepted indicators of catalyst productivity and stability.

In the current cases, the TON was estimated as 14600 mmol-RSH/mmol-Pc and 17850 mmol-RSH/mmol-Pc for H_{16}PcCo and F_{64}PcCo, respectively. The corresponding TOF for H_{16}PcCo and F_{64}PcCo oxidations of 2-ME are 2.93 mmol-RSH/mmol-Pc/s and 5.51 mmol-RSH/mmol-Pc/s. This suggests that F_{64}PcCo is a superior catalyst in its ability to convert more thiol per amount of catalyst and a faster rate. The above observation coincides with Loas[14] where F_{64}PcCo is shown to be far more stable than the H_{16}PcCo catalyst.

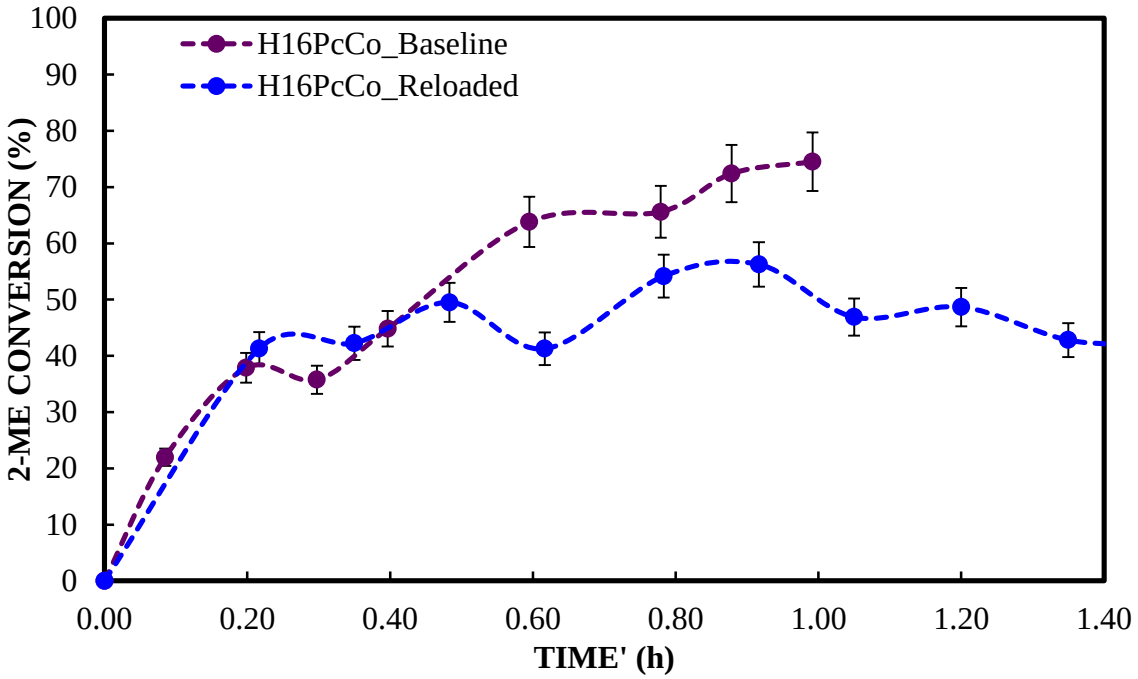

Figure 6.6 Baseline H_{16}PcCo catalyzed oxidation of 140 mmol/L 2-ME in 2.58 mmol/L NaOH under pure O_2 at 1 atm and 22 °C. Reaction is reloaded with 7 mmol/L of 2-ME added to initial reaction solution after baseline experiment reaches near 100% 2-ME conversion. RSD=+/- 7%.

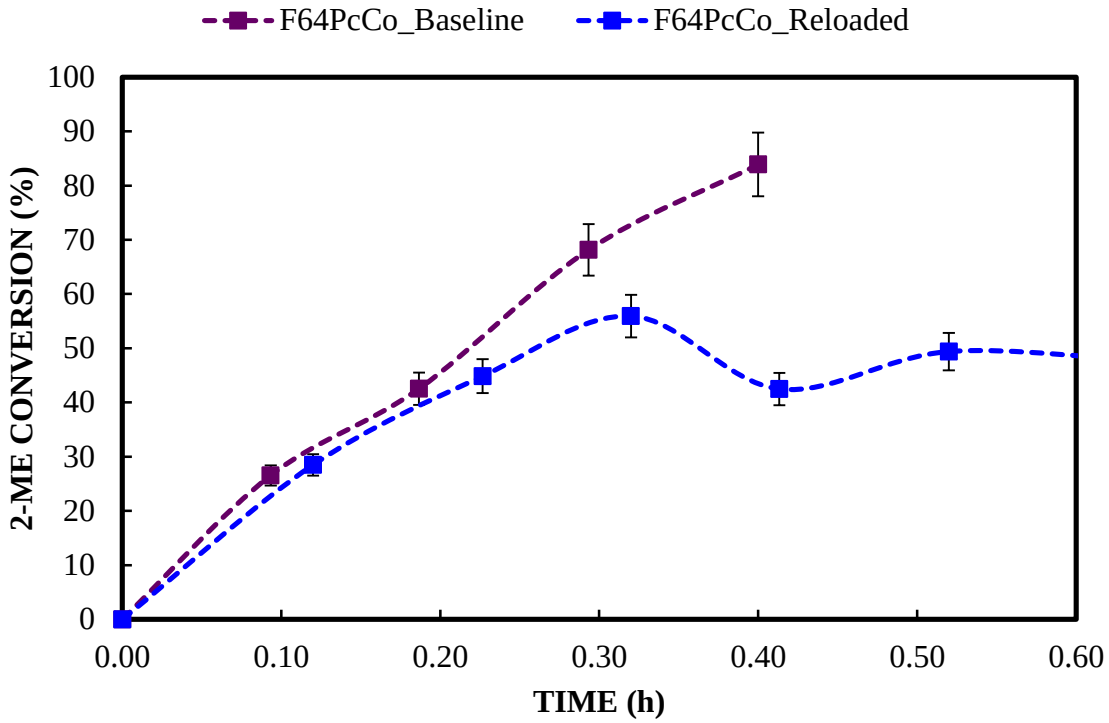

Figure 6.7 Baseline F_{64}PcCo catalyzed oxidation of 140 mmol/L 2-ME in 2.58 mmol/L NaOH under pure O_2 at 1 atm and 22 °C. Reaction is reloaded with 7 mmol/L of 2-ME added to initial reaction solution after baseline experiment reaches near 100% 2-ME conversion. RSD=+/- 7%

6.3 Inhibitory Effects Caused by Production of Disulfide in Catalytic Oxidations

A set of experiments was conducted to test if the generation of disulfide product would inhibit the reaction rate of catalyzed thiol oxidations. Recall that the overall oxidation reaction is $4RSH + O_2 \rightarrow 2RSSR + 2H_2O$. Approximately 80mmol/L of 2-hydroxyethyl disulfide was added to the initial reaction solution for 2-ME oxidations individually catalyzed by H_{16}PcCo, F_{16}PcCo, and F_{64}PcCo.

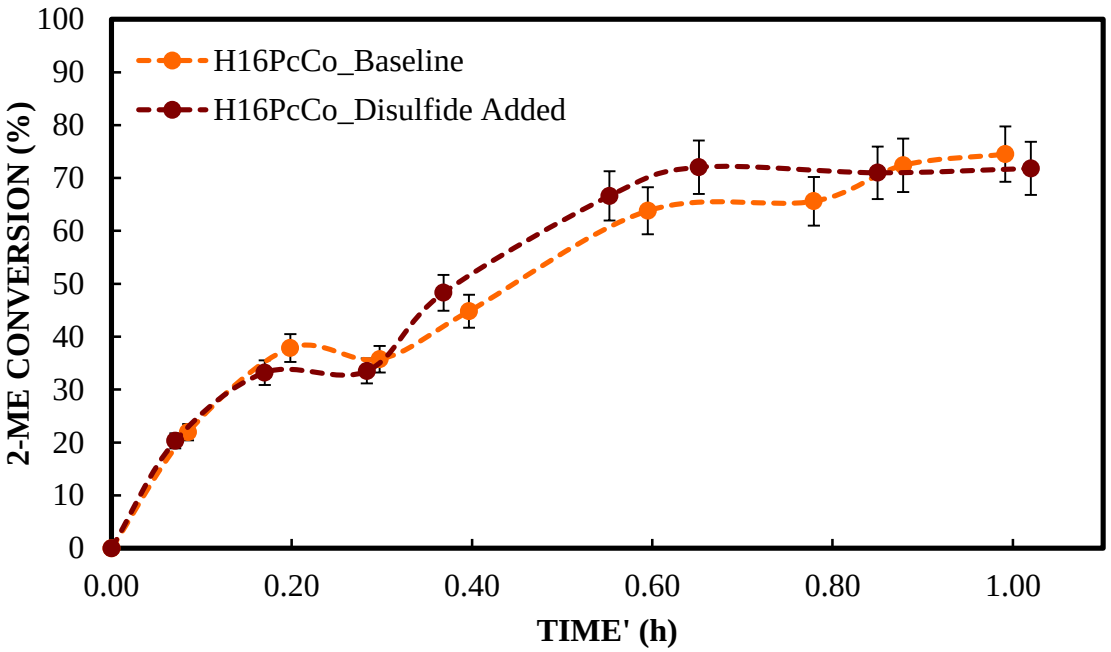

Figure 6.8 Baseline H_{16}PcCo catalyzed oxidation of 140 mmol/L 2-ME in 2.58 mmol/L NaOH under pure O_2 at 1 atm and 22 °C. Reaction is repeated with 80mmol/L of 2-Hydroexyethyl Disulfide added to initial reaction solution. RSD=+/- 7%.

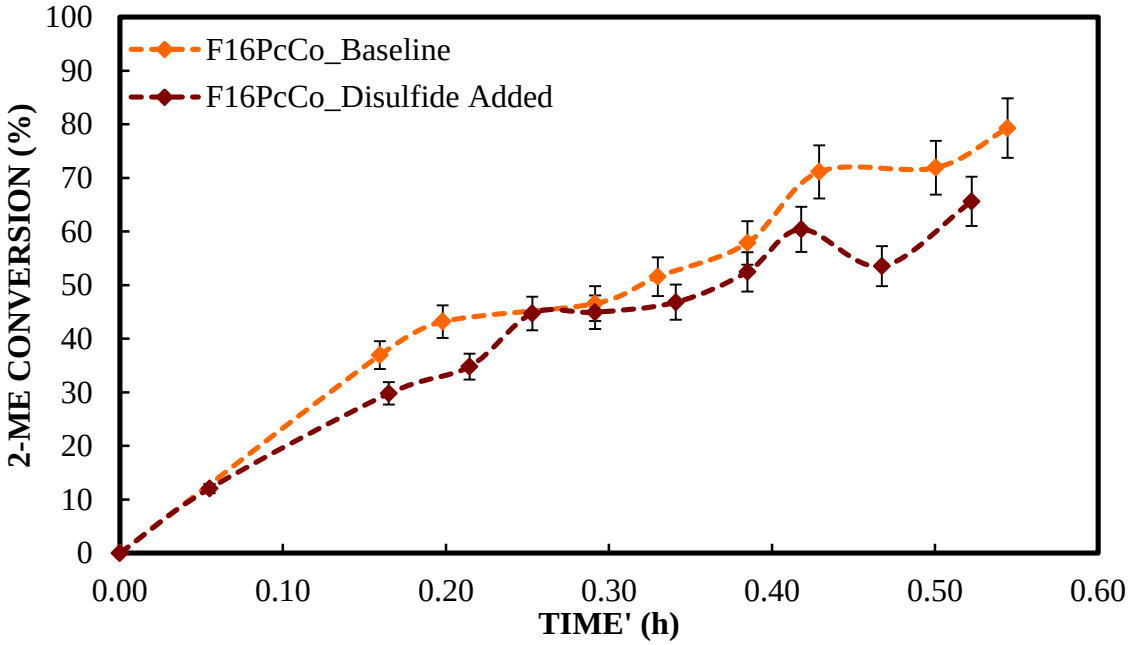

Figure 6.9 Baseline F_{16}PcCo catalyzed oxidation of 140 mmol/L 2-ME in 2.58 mmol/L NaOH under pure O_2 at 1 atm and 22 °C. Reaction is repeated with 80mmol/L of 2-Hydroexyethyl Disulfide added to initial reaction solution. RSD=+/- 7%.

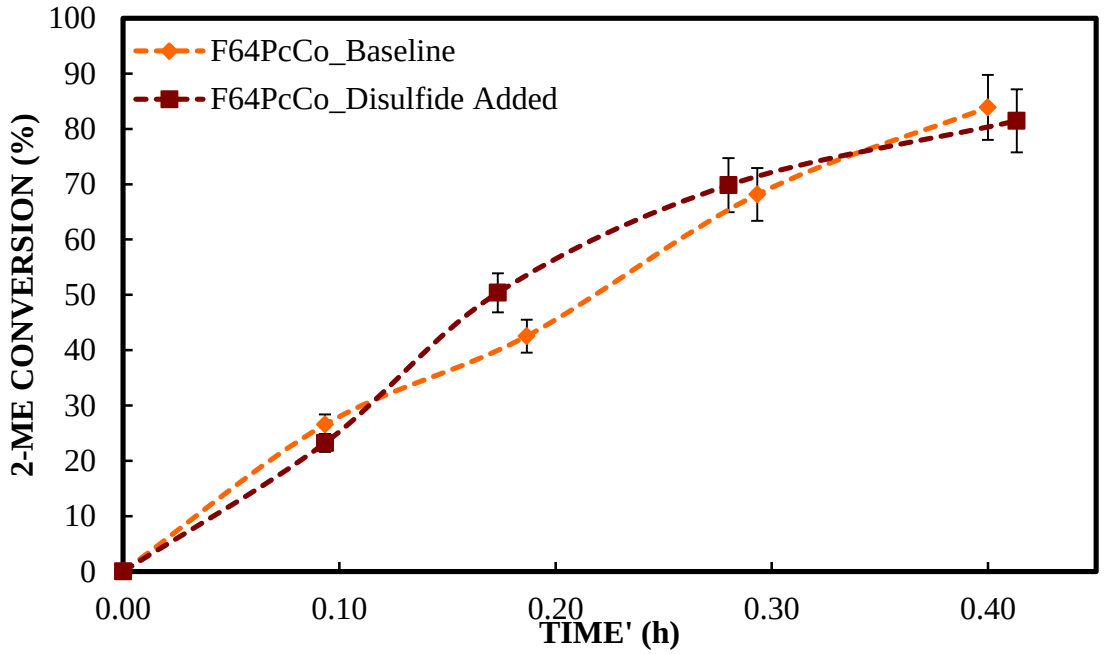

Figure 6.10 Baseline F_{64}PcCo catalyzed oxidation of 140 mmol/L 2-ME in 2.58 mmol/L NaOH under pure O_2 at 1 atm and 22 °C. Reaction is repeated with 80mmol/L of 2-Hydroexyethyl Disulfide added to initial reaction solution. RSD=+/- 7%.

Figures 6.8-6.10 show that the addition of disulfide to the initial reaction mixture has no appreciable effect on the rates of thiol oxidation. Chapter 2 shows that only Mechanism B (assumes disulfide is formed in the catalyst cavity) models include the disulfide product [RSSR] in the rate form. Figures 6.8-6.10 further supports the rejection of Mechanism B models. The above also strengthened the claims made in Chapters 4 and 5 that Models I (H_{16}PcCo catalyzed oxidations) and III (F_{16}PcCo & F_{64}PcCo catalyzed oxidations) of Mechanism A, neither of which are a function of [RSSR], describe Pc-catalyzed oxidations of thiols.

6.4 Temperature-Dependent Phthalocyanine Catalyzed Oxidation of 2-ME

Temperature experiments were conducted on phthalocyanine catalyzed oxidations of 2-mercaptoethanol (2-ME) to elucidate the effects of change in temperature on kinetic parameters. 2-ME was oxidized catalytically via H_{16}PcCo and F_{16}PcCo under various oxygen concentrations and temperatures. At this point in this study, no F_{64}PcCo remained for additional experiments.

Experimental conditions were similar to those used in prior experiments where pressure is held constant at 1 atm; initial thiol, NaOH and catalyst concentrations are 140 mmol/L, 2.58 mmol/L and 0.0105 mmol/L, respectively. Temperatures were held constant at 10 ºC, 15.5 ºC and 21 ºC using a "cold finger" in the circulating water bath. Temperatures in the reactor are held at +/- 2 ºC of the desired T.

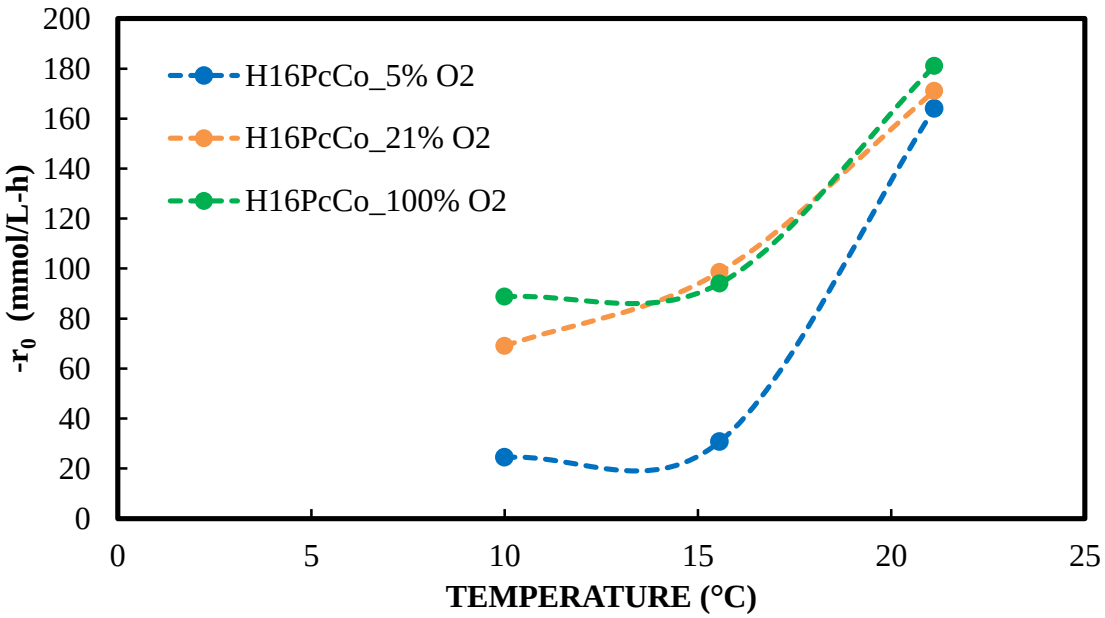

Figure 6.11 Initial rates of H_{16}PcCo catalyzed oxidation of 140 mmol/L 2-ME in 2.58 mmol/L NaOH under various gaseous O_2 compositions held at1 atm and various constant reaction temperatures.

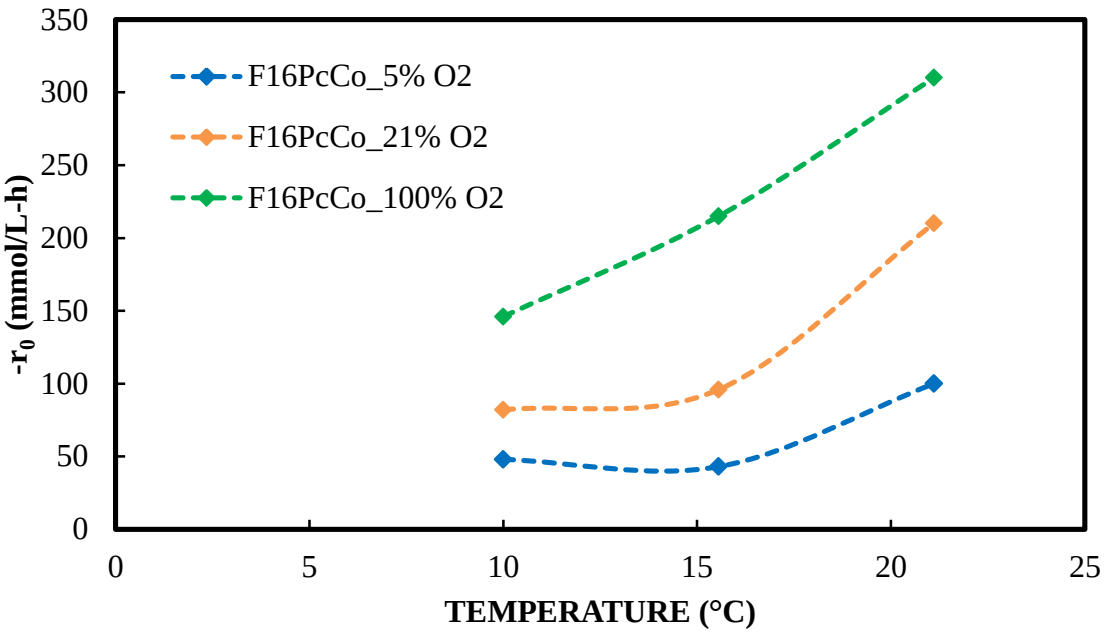

Figure 6.12 Initial rates of F_{16}PcCo catalyzed oxidation of 140 mmol/L 2-ME in 2.58 mmol/L NaOH under various gaseous O_2 compositions held at1 atm and various constant reaction temperatures.

Figures 6.11 and 6.12 present observed initial rates as functions of temperature. Some important points can be made. First, for both catalysts, the initial rates generally rose sharply with increasing temperature. Typically, in interfacial systems like the current study, reaction rates increase rapidly with increasing temperature until mass transfer resistance begins to dominate. At this point, the observed reaction rates usually increase more slowly. The data suggest that both catalyzed systems are reaction-limited at these temperatures.

Section 6.1 discussed the possible degradation of H_{16}PcCo, even in the presence of 2-ME. Figure 6.11 show slower reaction rates as temperature and gaseous O_2 content decrease. As a result of lower temperature, H_{16}PcCo catalyzed reactions become slower and more susceptible to deactivation, as illustrated by Loas[14] where H_{16}PcCo catalyst stability decreases with time.

Table 6.1 shows kinetic parameters K_2, K_3 and k_4, for F_{16}PcCo oxidations at various temperatures calculated similarly to the trial-and-error procedure found in Section 4.3.5. Matlab codes for the above calculations can be found in Appendices L, P and Q. Substrate binding (K_2) occurs at a faster rate as temperature increases. The rise in temperature causes an increase in random diffusion and particle movement in the solution. Substrate binding is thereby facilitated by an increase in temperature. Similar observations are made for thiyl expulsion (k_4). However, electron transfer (K_3) does not seem to be affected by temperature.

Table 6.1 Kinetic Parameters as a Function of Reaction Temperature

F_{16}PcCo	$-r_0$(mmol/L-hr) 5% O_2	$-r_0$(mmol/L-hr) 21% O_2	r_0(mmol/L-hr) 100% O_2	K_2 (L/mmol)	K_3 (L/mmol)	k_4 (L/mmol)
10 ^oC	48.2	82.3	146	4.83E-08	1.37	3221
15.5 ^oC	43.4	66.9	215	6.50E-08	1.06	3410
21 ^oC	100	209	310	8.00E-07	1.19	8018

6.5 Conclusions

The above experiments provide supplemental information to the kinetic studies of thiol oxidations catalyzed by H_{16}PcCo, F_{16}PcCo, and F_{64}PcCo up to this point. The observations were interpreted in view of the preferred kinetic models supported in Chapters 4 for thiol 2-ME. First, although a NaOH concentration term appears in all catalytic rate models for 2-ME oxidation, the data here show little, if any, dependence on NaOH for the catalytic reactions. The rate-determining step, found in the catalytic cycle, controls other essential non-catalytic mechanisms in the range of studied NaOH concentrations. These mechanisms include the consumption and regeneration of hydroxide as well as H_2O_2 production. There are likely stability issues involving

H_{16}PcCo catalyzed thiol oxidations. However, the weak dependence of NaOH on F_{16}PcCo and F_{64}PcCo catalyzed thiol oxidation supports the choice of rate model III and the conclusion that the rate-determining step is the expulsion of the thiyl radical from the catalyst cavity

Second, the catalyzed oxidation rates are effectively independent of disulfide [RSSR], which is consistent with the preferred model from Chapter 4. There are no inhibitory effects caused by the production of the disulfide product.

The F_{64}PcCo catalyst is the superior catalyst when compared to H_{16}PcCo and F_{16}PcCo. Not only does F_{64}PcCo exhibit lower dimerization than F_{16}PcCo, but its Turnover Number and Turnover Frequency were shown to be greater than those for H_{16}PcCo.

Finally, catalyzed initial rates rise rapidly with temperature. This suggests a reaction-limited kinetic regime. Catalytic steps dependent on motion of involved reactants (K_2) and products (k_4) are directly related to temperature of reaction, while the internal step (K_3) simply depends on Lewis acidity of the catalyst molecule.

CHAPTER 7

SUMMARY & SUGGESTIONS

The study quantitatively presented correlations of kinetic parameters in the absence and presence of phthalocyanine catalysts.

In the absence of Pc, but with NaOH, both 2-ME and 4-FBT consumption is described by a 1^{st} order model. NonPc oxidation of 2-ME is linear with NaOH as the model suggests. Further studies would call for similar experiments to test the linearity of 4-FBT with NaOH concentration. Results should be similar to that of 2-ME oxidations. 4-FBT reacts at a greater rate than 2-ME in the absence of Pc catalysts, likely due to the greater tendency 4-FBT to give up a proton. Even in pure liquid, exposed to air, O_2 reacts at the surface, leaving RS^- or RS. The more sensitive thiol is believed to break down into its thiolate form, even in the absence of NaOH. NMR tests should be able to identify the state of thiol with time under various conditions. During nonPc oxidations, assisted by NaOH, concentration of thiolate is greater for 4-FBT oxidations, accelerating the rate of oxidation. The rate constant for nonPc oxidations are $k_2=1.93x10^{-6}$ liter/mmol-h and k_2 = 2.45E-04 for 2-ME and 4-FBT oxidations, respectively.

An investigation of H_2O_2-induced oxidation of 2-ME was also performed. Purely H_2O_2-induced oxidations were found to be sufficiently faster than both nonPc and Pc catalyzed oxidations. Although assumed to follow a similar trend, further studies can be conducted to experimentally test H_2O_2-induced oxidation of 4-FBT and other complex thiols.

The rates of substrate binding and electron transfer are directly related to the Lewis acidity of catalyst molecules. Substrate binding is found to be the slow step for the insufficiently Lewis acidic $H_{16}PcCo$ when studying 2-ME oxidations. Some stability issues appeared in the presence pure O_2. On the other hand, in the presence of 4-FBT, $H_{16}PcCo$ had trouble with stability for all gaseous O_2 compositions. The $H_{16}PcCo$ catalyst is not adequately protected against the highly reactive 4-FBT molecule. Meanwhile, the fluorine atoms surrounding $F_{16}PcCo$ and $F_{64}PcCo$ not only provide improved kinetics, but also shield the catalyst molecule from hostile deactivation agents.

Further studies would suggest to quantitatively observe the chemical resistance of $H_{16}PcCo$, $F_{16}PcCo$ $F_{64}PcCo$ and identify likely degradation pathways. Past stability studies[14] may not have sufficiently accounted for mass transfer effects of their reaction system. In terms of stability, the time scale for degradation may have been inaccurate because less O_2 than what was predicted to be present in reaction solution. However, in a mass transfer resistance free system, the presence of degrading species are higher (due to larger dissolved O_2 concentration), leaving catalysts more susceptible to such attack.

The Lewis acidity of a catalyst can be increased to the point in which its rate determining step is altered, as seen with fluorinated phthalocyanine catalysts. The rate-determining step for $F_{16}PcCo$ and $F_{64}PcCo$ oxidations of 2-ME and 4-FBT is the radical expulsion of thiyl from the catalyst cavity. There is a direct correlation between substrate binding (K_2) and Lewis acidity; electron transfer from metal center to coordinated O_2 (K_3) and Lewis acidity; and expulsion of thiyl radical (k_4) and steric bulkiness. These relationships hold true despite thiol chosen. However, substrate binding is decelerated, while radical expulsion is accelerated in the presence of larger thiols due to steric

hindrance. The use of other phthalocyanine derivatives and complex thiols, in terms of size and acidity, may serve to strengthen the claims made by this dissertation.

Catalytic steps dependent on reactants (K_2) and products (k_4) are directly related to temperature of reaction, while the internal step (K_3) might simply depend on Lewis acidity of the catalyst molecule. Similar experiments may be conducted in the presence of less volatile solvent, i.e. water. Although H_2O will not supply as much solubility as THF, using water as a solvent would be advantageous in comparing kinetic parameters to more realistic industrial systems and provide better control temperature dependent experiments.

In conclusion, the consequences of manipulating chemical properties of industrial phthalocyanine molecules are better understood and can now be applied to the development of novel catalysts, which can be used in a variety of applications.

APPENDIX A

REACTION MECHANISMS

Appendix A shows literature and proposed mechanisms for non-catalytic, phthalocyanine catalyzed, and hydrogen peroxide induced oxidation of thiols. This section also provides key equations to be used in derivation of reaction models.

Total Thiol Oxidation

Overall Stoichiometry: $4RSH + O_2 \rightarrow 2H_2O + 2RSSR$

a. $2RSH + O_2 \rightarrow H_2O_2 + RSSR$ (via O_2) *multi-step*

b. $2RSH + H_2O_2 \rightarrow 2H_2O + RSSR$ (via H_2O_2) *multi-step*

Thiol consumption occurs via the above set of complex (parallel and consecutive) reactions:

$$-\frac{d[RSH]}{dt} = r_a + r_b \tag{A.1}$$

where r_a and r_b represent the rates of multi-step reactions a and b above, which will be written in terms of RSH consumption via $O_2$and H_2O_2, respectively. In this study, consumption of RSH via O_2 occurs via both a non-catalytic path (minor) and a catalytic (phthalocyanine) path (dominant). Each pathway consumes two of the four RSH noted in the overall stoichiometry. Each pathways produces H_2O_2 as a reactive intermediate that consumes the remaining two RSH of the overall four. Both paths require OH^- to generate the thiolate (RS^-) from thiol (RSH).

Proposed Non-Catalytic Mechanism

1. $RSH + OH^- \Leftrightarrow RS^- + H_2O$ times 2
2. $RS^- + O_2 \Leftrightarrow RSO_2^-$
3. $RS^- + RSO_2^- \Leftrightarrow RSSR + O_2^{2-}$
4. $O_2^{2-} + 2H_2O \Leftrightarrow H_2O_2 + 2OH^-$

The above pathway is kinetically analyzed in Appendix B.

Proposed Catalytic Mechanism A

Coupling of thiyl ($RS^\bullet$) radicals occurs in solution, outside of the catalyst cavity.

1. $RSH + OH^- \Leftrightarrow RS^- + H_2O$ times 2
2. $RS^- + PcCo(II) \Leftrightarrow RS^\bullet \ldots PcCo(I)$
3. $O_2 + RS^\bullet \ldots PcCo(I) \Leftrightarrow RS^\bullet \ldots PcCo(II) \ldots O_2^-$
4. $RS^\bullet \ldots PcCo(II) \ldots O_2^- \Leftrightarrow RS^\bullet + PcCo(II) \ldots O_2^-$
5. $RS^\bullet + RS^\bullet \Leftrightarrow RSSR$

For simplification purposes in derivations of mechanism A models, let $A=RS^-$, $B=O_2$, $S=PcCo(II)=PcCo(II) \ldots O_2^-$, $DS_1=RS^\bullet \ldots PcCo(I)$, $DS_2=RS^\bullet \ldots PcCo(II) \ldots O_2^-$, $D=RS^\bullet$

1. $RSH + OH^- \Leftrightarrow RS^- + H_2O$ times 2
2. $A + S \Leftrightarrow DS_1$
3. $B + DS_1 \Leftrightarrow DS_2$
4. $DS_2 \Leftrightarrow D + S$
5. $D + D \Leftrightarrow RSSR$

Proposed Catalytic Mechanism B

Coupling of thiyl ($RS^{\bullet}$) radicals occurs inside of the catalyst cavity.

1. $RSH + OH^- \Leftrightarrow RS^- + H_2O$ times 2
2. $RS^- + PcCo(II) \Leftrightarrow RS^{\bullet}\ldots PcCo(I)$
3. $O_2 + RS^{\bullet}\ldots PcCo(I) \Leftrightarrow RS^{\bullet}\ldots PcCo(II)\ldots O_2^-$
4. $RS^- + RS^{\bullet}\ldots PcCo(II)\ldots O_2^- \Leftrightarrow RS^{\bullet}RS^{\bullet}\ldots PcCo(I)\ldots O_2^-$
5. $RS^{\bullet}RS^{\bullet}\ldots PcCo(I)\ldots O_2^- \Leftrightarrow RSSR\ldots PcCo(II)\ldots O_2^{2-}$
6. $RSSR\ldots PcCo(II)\ldots O_2^{2-} \Leftrightarrow RSSR + PcCo(II) + O_2^{2-}$

For simplification purposes in the derivation of mechanism B models, let $A=RS^-$, $B=O_2$, $C=O_2^{2-}$, D=RSSR, S=PcCo(II), $DS_1=RS^{\bullet}\ldots PcCo(I)$, $DS_2=RS^{\bullet}\ldots PcCo(II)\ldots O_2^-$, $DS_3=RSSR\ldots PcCo(I)\ldots O_2^-$, $DS_4=RSSR\ldots PcCo(II)\ldots O_2^{2-}$

1. $RSH + OH^- \Leftrightarrow RS^- + H_2O$ times 2
2. $A + S \Leftrightarrow DS_1$
3. $B + DS_1 \Leftrightarrow DS_2$
4. $A + DS_2 \Leftrightarrow DS_3$
5. $DS_3 \Leftrightarrow DS_4$
6. $DS_4 \Leftrightarrow D + C + S$

Initial Acid/Base Reaction

The initial reaction, which transforms the thiol into thiolate, is in fast equilibrium and can be used to solve for thiolate concentration:

$$r_1 = k_1[RSH][OH^-] - k_{-1}[RS^-][H_2O] \quad \text{(A.2)}$$

$$[RS^-] \approx \frac{K_1[RSH][OH^-]}{[H_2O]} \quad \text{(A.3)}$$

where $K_1 = k_1/k_{-1}$ and $r_1/k_1 \approx 0$ since k_1 assumed large due to "fast equilibrium' for this step.

Hydrogen Peroxide Induced Reaction Mechanism

The kinetics for the consumption of RSH by intermediate H_2O_2 (denoted as reaction b) are found in the literature[23] where the reaction via H_2O_2 has a set of elementary equations:

1. $RSH + OH^- \Leftrightarrow RS^- + H_2O$ times 2
2. $RS^- + H_2O_2 \rightarrow RSOH + OH^-$ *(slow)*
3. $RS^- + RSOH \Leftrightarrow RSSR + OH^-$

Net: $2RSH + H_2O_2 \rightarrow RSSR + 2H_2O$

Step 2 is shown to be the rate-determining step and a model is provided:

$$-\left(\frac{d[H_2O_2)}{dt}\right)_b = k_{H_2O_2}[RS^-][H_2O_2] \qquad \text{(A.4)}$$

Substituting the Equation A.3 result into A.4 yields:

$$-\left(\frac{d[H_2O_2)}{dt}\right)_b = \frac{k_{H_2O_2}K_1[OH^-]}{[H_2O]}[RSH][H_2O_2] \qquad \text{(A.5)}$$

By the net stoichiometry noted above, the thiol consumption rate for this stage is:

$$-r_b = \frac{2k_{H_2O_2}K_1[OH^-]}{[H_2O]}[RSH][H_2O_2] \qquad \text{(A.6)}$$

The amount of hydrogen peroxide available at a given time is a function of its rate of production by the oxygen-induced reaction pathways (catalytic and non-catalytic) and its rate of consumption in the secondary thiol reaction pathway just shown. Utilizing the pseudo-steady state hypothesis, $[H_2O_2]$ can be estimate through the following sequence:

$$\frac{d[H_2O_2]}{dt} \approx 0 \qquad \text{(PSSH)} \qquad \text{(A.7)}$$

$$\frac{d[H_2O_2]}{dt} = r_a - r_b \approx 0 \qquad \text{(A.7a)}$$

$$r_a \approx r_b \qquad \text{(A.8)}$$

$$r_a \approx k_{H_2O_2}[RSH][H_2O_2] \qquad \text{(A.9)}$$

$$[H_2O_2] \approx \frac{r_a}{k_{H_2O_2}[RSH]} \qquad \text{(A.10)}$$

Equation A.10 can be used to estimate the concentration of hydrogen peroxide specific to r_a, which depends on the choice of the non-catalytic or catalytic rate-determining pathway for the reaction of RSH with O_2.

APPENDIX B

NON-CATALYTIC MODEL I

1. $RSH + OH^- \Leftrightarrow RS^- + H_2O$ times 2
2. $RS^- + O_2 \rightarrow RSO_2^-$ *slow*
3. $RS^- + RSO_2^- \Leftrightarrow RSSR + O_2^{2-}$
4. $O_2^{2-} + 2H_2O \Leftrightarrow H_2O_2 + 2OH^-$

Net: $2RSH + O_2 \rightarrow RSSR + 2H_2O$

Appendix B derives kinetics for the non-catalytic oxidation of RS^- by dissolved O_2, called *nonPc Model I*, which assumes that step 2 (thiolate reacting with oxygen to form sulfoxide intermediate) in the non-catalytic mechanism is the rate-determining step.

Assuming step 2 is the rate-determining step and only the forward reaction is considered, the non-catalytic oxidation of thiol as a function of thiolate and oxygen concentrations via oxygen-induced reaction can be written:

$$-\frac{d[O_2]}{dt} = k_2[RS^-][O_2] \tag{B.1}$$

Plugging in the value of thiolate, equation A.3, the thiol consumption in terms of thiol concentration, can be found:

$$-\frac{d[O_2]}{dt} = k_{app}[RSH][O_2] \tag{B.2}$$

where . $k_{app} = \dfrac{k_2 K_1 [OH^-]}{[H_2O]}$

Considering the net stoichiometry for this stage, the rate of thiol consumption is:

$$-r_a = 2k_{app}[RSH][O_2] \tag{B.3}$$

From equation A.8,

$$-r_a \approx -r_b = 2k_{app}[RSH][O_2] \quad \text{(B.4)}$$

Combining equation B.4 with equation A.1, the thiol consumption in terms of the total rate of thiol consumption, can be found:

$$-\frac{d[RSH]}{dt} = 4k_{app}[RSH][O_2] \quad \text{(B.5)}$$

Using Equation B.3, the concentration of hydrogen peroxide, is estimated from A.10:

$$[H_2O_2] = \frac{k_{app}[O_2]}{k_{H_2O_2}} \quad \text{(B.6)}$$

Equation B.5 can be used to estimate the concentration of hydrogen peroxide specific for the non-catalytic reaction of RS^- with dissolved O_2.

APPENDIX C

NON-CATALYTIC MODEL II

1. $RSH + OH^- \Leftrightarrow RS^- + H_2O$ times 2
2. $RS^- + O_2 \Leftrightarrow RSO_2^-$
3. $RS^- + RSO_2^- \rightarrow RSSR + O_2^{2-}$ *slow*
4. $O_2^{2-} + 2H_2O \Leftrightarrow H_2O_2 + 2OH^-$
5. Net: $2RSH + O_2 \rightarrow RSSR + 2H_2O$

Appendix C, derives *nonPc Model II*, which assumes step 3 above (thiolate reacting with sulfoxide intermediate to form disulfide product and superoxide) in the non-catalytic mechanism is the rate-determining step.

Assuming step 3 is the rate-determining step and only the forward reaction is considered:

$$-\frac{d[O_2]}{dt} = r_3 = k_3[RS^-][RSO_2^-] \tag{C.1}$$

For $[RSO_2^-]$, assume step 2 is in fast equilibrium:

$$r_2 = k_2[RS^-][O_2] - k_{-2}[RSO_2^-] \tag{C.2}$$

$$[RSO_2^-] \approx K_2[RS^-][O_2] \tag{C.3}$$

where $K_2 = k_2 / k_{-2}$ and $r_2 / k_2 \approx 0$

Substituting Equation C.3 into C.1 yields the non-catalytic oxidation of thiol as a function of thiolate and oxygen concentrations via oxygen-induced reaction can be written:

$$-\frac{d[O_2]}{dt} = k_3K_2[O_2][RS^-]^2 \tag{C.4}$$

Using Equation A.3 for thiolate, the rate of thiol consumption for this stage is:

$$-\frac{d[O_2]}{dt} = k_{app}[O_2][RSH]^2 \quad \text{(C.5)}$$

where $k_{app} = \frac{k_3 K_2 K_1^2 [OH^-]^2}{[H_2O]^2}$

Considering the net stoichiometry for this stage, the rate of thiol consumption is:

$$-r_a = 2k_{app}[O_2][RSH]^2 \quad \text{(C.6)}$$

From equation A.8:

$$-r_a \approx -r_b = 2k_{app}[O_2][RSH]^2 \quad \text{(C.7)}$$

Combining equation C.7 with equation A.1, the thiol consumption in terms of the total rate of thiol consumption, can be found:

$$-\frac{d[RSH]}{dt} = -4k_{app}[O_2][RSH]^2 \quad \text{(C.8)}$$

The concentration of hydrogen peroxide is estimated using equations A.10 and C.6:

$$[H_2O_2] = \frac{k_{app}[O_2][RSH]}{k_{H_2O_2}} \quad \text{(C.9)}$$

APPENDIX D

CATALYTIC MODEL I

1. $RSH + OH^- \Leftrightarrow RS^- + H_2O$ times 2
2. $A + S \rightarrow DS_1$ *slow*
3. $B + DS_1 \Leftrightarrow DS_2$
4. $DS_2 \Leftrightarrow D + S$

   Net: $RS^- + O_2 \rightarrow RS^{\bullet} + O_2^-$ (see *Note* below)
5. $D + D \Leftrightarrow RSSR$

The above mechanism is consistent with Figure 2.3 within Chapter 2. For mechanism A models, the following abbreviations are used: $A=RS^-$, $B=O_2$, $S=PcCo(II)=PcCo(II)\ldots O_2^-$, $DS_1=RS^{\bullet}\ldots PcCo(I)$, $DS_2=RS^{\bullet}\ldots PcCo(II)\ldots O_2^-$, $D=RS^{\bullet}$

Note: It was stated in Section 2.2.2 that attachment of a second RS^- to the catalyst site $PcCo(II)\ldots O_2^-$ is probably equally likely as attachment of the first RS^- to site PcCo(II). Therefore, the derived rate expression based on the above simplified mechanism should be doubled. This doubling will be done when the derivation is complete later in this section.

Appendix D derives Pc Model I, which assumes step 2 (thiolate binding and transferring an electron to metal center of phthalocyanine) in the proposed catalytic mechanism A, where radical-radical coupling to form disulfide occurs in solution outside of the Pc catalyst molecule, is the rate-determining step.

Assuming step 2 is the rate-determining step and only the forward reaction is considered:

$$-\frac{d[O_2]}{dt} = r_2 = k_2[A][S] \qquad (D.1)$$

Must do a catalyst balance to find [S], the "concentration" of vacant catalyst sites:

$[S]_T = [S] + [DS_1] + [DS_2]$

where $[S]_T$ = concentration of total sites. For $[DS_2]$, assume step 4 is in fast equilibrium:

$$r_4 = k_4[DS_2] - k_{-4}[D][S] \tag{D.2}$$

$$[DS_2] = \frac{[D][S]}{K_4} \tag{D.3}$$

where $K_4 = k_4 / k_{-4}$ and $r_4 / k_4 \approx 0$

For $[DS_1]$, assume step 3 is in fast equilibrium:

$$r_3 = k_3[B][DS_1] - k_{-3}[DS_2] = 0 \tag{D.4}$$

$$[DS_1] = \frac{[DS_2]}{K_3[B]} = \frac{[D][S]}{K_4 K_3[B]} \tag{D.5}$$

where $K_3 = k_3 / k_{-3}$

Plugging the above back into the catalyst balance, [S] can be found:

$$[S]_T = [S] + \frac{[D][S]}{K_4 K_3[B]} + \frac{[D][S]}{K_4} \tag{D.6}$$

$$[S] = \frac{[S]_T}{1 + \frac{[D]}{K_4}\left(\frac{1}{K_3[B]} + 1\right)} \tag{D.7}$$

Catalytic oxidation of thiol as a function of thiolate, oxygen and catalyst concentrations via oxygen-induced reaction can be written:

$$-\frac{d[O_2]}{dt} = \frac{k_2[A][S]_T}{1 + \frac{[D]}{K_4}\left(1 + 1/K_3[B]\right)} \tag{D.8}$$

This rate now should be doubled to account for the second RS^- as discussed in the *Note* earlier in this section; i.e. the RS^- attaching to the site $PcCo(II)\ldots O_2^-$.

$$r_a \approx \frac{2k_2[A][S]_T}{1+\frac{[D]}{K_4}\left(1+ {}^{1}\!/\!_{K_3[B]}\right)} \tag{D.9}$$

From equation A.8:

$$r_a = r_b \approx \frac{2k_2[A][S]_T}{1+\frac{[D]}{K_4}\left(1+ {}^{1}\!/\!_{K_3[B]}\right)} \tag{D.10}$$

Finally, the two RS^- consumed by the intermediate H_2O_2 must be accounted for. The total thiol consumption can now be found by combining equations A.1 and D.10:

$$-\frac{d[RSH]}{dt} = \frac{4k_2[A][S]_T}{1+\frac{[D]}{K_4}\left(1+ {}^{1}\!/\!_{K_3[B]}\right)} \text{ or } -\frac{d[RSH]}{dt} = \frac{4k_2[RS^-][Cat]_T}{1+\frac{[RS^\bullet]}{K_4}\left(1+ {}^{1}\!/\!_{K_3[O_2]}\right)} \tag{D.11}$$

Assuming $RS^\bullet$ is rapidly consumed (step 5 above) with a very favorable equilibrium, it concentration is small and thereby, short-lived in solution $[RS^\bullet] \rightarrow 0$. This gives:

$$-\frac{d[RSH]}{dt} = 4k_2[RS^-][Cat]_T \tag{D.12}$$

Plugging in the value of thiolate from Equation A.3, can be found:

$$-\frac{d[RSH]}{dt} = 4\alpha[RSH] \tag{D.13}$$

where $\alpha \equiv \frac{k_2K_1[OH^-][Cat]_T}{[H_2O]}$

Concentration of hydrogen peroxide, is calculated from equations A.10 and D.9:

$$H_2O_2 \approx \frac{k_2[A][S]_T}{k_{H_2O_2}[RSH]\left(1+\frac{[D]}{K_4}\left(1+ {}^{1}\!/\!_{K_3[B]}\right)\right)} \tag{D.14}$$

Using the assumption $[RS^\bullet] \rightarrow 0$ as above and plugging in appropriate values Equation D.13 simplifies to:

$$H_2O_2 \approx \frac{\alpha}{k_{H_2O_2}} \qquad \text{(D.15)}$$

APPENDIX E

CATALYTIC MODEL II

1. $RSH + OH^- \Leftrightarrow RS^- + H_2O$ times 2
2. $A + S \Leftrightarrow DS_1$
3. $B + DS_1 \rightarrow DS_2$ *slow*
4. $DS_2 \Leftrightarrow D + S$

   Net: $RS^- + O_2 \rightarrow RS^{\bullet} + O_2^-$
5. $D + D \Leftrightarrow RSSR$

Note: The nomenclature here is consistent with that used for Catalytic Model I.

Appendix E derives Pc Model II, which assumes step 3 (oxygen attachment and the transferring of an electron to the oxygen from the metal center of phthalocyanine) in the proposed catalytic mechanism A, where radical-radical coupling to form disulfide occurs in solution away from the catalyst molecule, is the rate-determining step.

Assuming step 3 is the rate-determining step and only the forward reaction is considered:

$$-\frac{d[O_2]}{dt} = r_3 = k_3[B][DS_1] \tag{E.1}$$

For $[DS_1]$, assume step 2 is in fast equilibrium:

$$r_2 = k_2[A][S] - k_{-2}[DS_1] \tag{E.2}$$

$$[DS_1] = K_2[A][S] \tag{E.3}$$

where $K_2 = k_2 / k_{-2}$ and $r_2 / k_2 \approx 0$

$$r_a = k_3 K_2[B][A][S] \tag{E.4}$$

Must do a catalyst balance to find [S]: $[S]_T = [S] + [DS_1] + [DS_2]$

For $[DS_2]$, assume step 4 is in fast equilibrium:

$$r_4 = k_4[DS_2] - k_{-4}[D][S] \tag{E.5}$$

$$[DS_2] = \frac{[D][S]}{K_4} \tag{E.6}$$

where $K_4 = {k_4}/{k_{-4}}$ and ${r_4}/{k_4} \approx 0$

Plugging the above back into the catalyst balance, [S] can be found:

$$[S]_T = [S] + K_2[A][S] + \frac{[D][S]}{K_4} \tag{E.7}$$

$$[S] = \frac{[S]_T}{1 + K_2[A] + \frac{[D]}{K_4}} \tag{E.8}$$

Catalytic oxidation of thiol as a function of thiolate, oxygen and catalyst concentrations via oxygen-induced reaction can be written:

$$-\frac{d[O_2]}{dt} = \frac{k_3 K_2[A][B][S]_T}{1 + K_2[A] + \frac{[D]}{K_4}} \tag{E.9}$$

This rate now should be doubled to account for the second RS^- as discussed in the *Note* earlier in Appendix D earlier; i.e. the RS^- attaching to the site $PcCo(II)\ldots O_2^-$.

$$r_a \approx \frac{2k_3 K_2[A][B][S]_T}{1 + K_2[A] + \frac{[D]}{K_4}} \tag{E.10}$$

From equation A.8:

$$r_a = r_b \approx \frac{2k_3 K_2[A][B][S]_T}{1 + K_2[A] + \frac{[D]}{K_4}} \tag{E.11}$$

Finally, the two RS- consumed by the intermediate H_2O_2 must be accounted for. The total thiol consumption can now be found by combining equations A.1 and E.11:

$$-\frac{d[RSH]}{dt} = \frac{4k_3K_2[A][B][S]_T}{1+K_2[A]+\dfrac{[D]}{K_4}} \text{ or } -\frac{d[RSH]}{dt} = \frac{4k_3K_2[RS^-][O_2][Cat]_T}{1+K_2[RS^-]+\dfrac{[RS^\bullet]}{K_4}} \quad \text{(E.12)}$$

Assuming $RS^\bullet$ is rapidly consumed (step 5 above) with a very favorable equilibrium, it concentration is small and thereby, short-lived in solution $[RS^\bullet] \rightarrow 0$. This gives:

$$-\frac{d[RSH]}{dt} = \frac{4k_3K_2[RS^-][O_2][Cat]_T}{1+K_2[RS^-]} \quad \text{(E.13)}$$

Plugging in the value of thiolate, A.3, the total thiol consumption in terms of thiol concentration, can be found:

$$-\frac{d[RSH]}{dt} = \frac{4\alpha[RSH]}{1+\beta[RSH]} \quad \text{(E.14)}$$

where $\alpha = \dfrac{k_3K_2K_1[OH^-][O_2][Cat]_T}{[H_2O]}$, and $\beta = \dfrac{K_2K_1[OH^-]}{[H_2O]}$

Concentration of hydrogen peroxide is estimated from equations A.10 and E.10:

$$H_2O_2 \approx \frac{k_3K_2[A][B][S]_T}{k_{H_2O_2}[RSH]\left(1+K_2[A]+\dfrac{[D]}{K_4}\right)} \quad \text{(E.14)}$$

Using the assumption $[RS^\bullet] \rightarrow 0$ as above and plugging in appropriate values, Equation E.14 simplifies to:

$$H_2O_2 \approx \frac{\alpha}{k_{H_2O_2}(1+\beta[RSH])} \quad \text{(E.15)}$$

APPENDIX F

CATALYTIC MODEL III

1. $RSH + OH^- \Leftrightarrow RS^- + H_2O$ times 2
2. $A + S \Leftrightarrow DS_1$
3. $B + DS_1 \Leftrightarrow DS_2$
4. $DS_2 \rightarrow D + S$ *slow*

   Net: $RS^- + O_2 \rightarrow RS^{\bullet} + O_2^-$
5. $D + D \Leftrightarrow RSSR$

Note: The nomenclature here is consistent with that used for Catalytic Model I.

Appendix F, derives Pc Model III, which assumes step 4 (expulsion of $RS^{\bullet}$ radical from the metal center of phthalocyanine) in the proposed catalytic mechanism A, where radical-radical coupling to form disulfide occurs in solution, is the rate-determining step.

Assuming step 4 is the rate-determining step and only the forward reaction is considered:

$$-\frac{d[O_2]}{dt} = r_4 = k_4[DS_2] \tag{F.1}$$

For $[DS_2]$, assume step 3 is in fast equilibrium:

$$r_3 = k_3[B][DS_1] - k_{-3}[DS_2] \tag{F.2}$$

$$[DS_2] = K_3[B][DS_1] \tag{F.3}$$

where $K_3 = k_3 / k_{-3}$ and $r_3 / k_3 \approx 0$

For $[DS_1]$, assume step 2 is in fast equilibrium:

$$r_2 = k_2[A][S] - k_{-2}[DS_1] \tag{F.4}$$

where $K_2 = k_2 / k_{-2}$ and $r_2 / k_2 \approx 0$

$$[DS_1] = K_2[A][S] \tag{F.5}$$

Combing equations F.1, F.3 and F.5:

$$-\frac{d[O_2]}{dt} = k_4 K_3 K_2 [B][A][S] \tag{F.6}$$

Must do a catalyst balance to find [S]:

$[S]_T = [S] + [DS_1] + [DS_2]$

Plugging the above back into the catalyst balance, [S] can be found:

$$[S]_T = [S] + K_2[A][S] + K_3 K_2 [A][B][S] \tag{F.7}$$

$$[S] = \frac{[S]_T}{1 + K_2[A] + K_3 K_2 [B][A]} \tag{F.8}$$

Catalytic oxidation of thiol as a function of thiolate, oxygen and catalyst concentrations via oxygen-induced reaction can be written:

$$-\frac{d[O_2]}{dt} = \frac{k_4 K_3 K_2 [B][A][S]_T}{1 + K_2[A](1 + K_3 K_2 [B])} \tag{F.9}$$

This rate now should be doubled to account for the second RS^- as discussed in the *Note* in Appendix D earlier; i.e. the RS^- attaching to the site $PcCo(II)\ldots O_2^-$.

$$r_a = \frac{2k_4 K_3 K_2 [B][A][S]_T}{1 + K_2[A](1 + K_3 K_2 [B])} \tag{F.10}$$

From equation A.8:

$$r_a = r_b \approx \frac{2k_4 K_3 K_2 [B][A][S]_T}{1 + K_2[A](1 + K_3 K_2 [B])} \tag{F.11}$$

Finally, the two RS^- consumed by the intermediate H_2O_2 must be accounted for. The total thiol consumption can now be found by combining equations A.1 and F.11:

$$-\frac{d[RSH]}{dt} = \frac{4k_4 K_3 K_2 [B][A][S]_T}{1 + K_2[A](1 + K_3[B])} \text{ or } -\frac{d[RSH]}{dt} = \frac{4k_4 K_3 K_2 [O_2][RS^-][Cat]_T}{1 + K_2[RS^-](1 + K_3[O_2])} \tag{F.12}$$

Plugging in the value of thiolate, A.3, the total thiol consumption in terms of thiol concentration, can be found:

$$-\frac{d[RSH]}{dt} = \frac{4\alpha[RSH]}{1+\beta[RSH]} \tag{F.13}$$

where $\alpha = \frac{k_4 K_3 K_2 K_1 [OH^-][O_2][Cat]_T}{[H_2O]}$, and $\beta = \frac{K_2 K_1 [OH^-](1+K_3[O_2])}{[H_2O]}$

Concentration of hydrogen peroxide, is calculated from equation A.10 and F.10:

$$[H_2O_2] = \frac{k_4 K_3 K_2 [B][A][S]_T}{k_{H_2O_2}[RSH](1+K_2[A](1+K_3 K_2[B]))} \tag{F.14}$$

plugging in appropriate values which can also be written as:

$$[H_2O_2] = \frac{\alpha}{k_{H_2O_2}(1+\beta[RSH])} \tag{F.15}$$

APPENDIX G

CATALYTIC MODEL IV

1. $RSH + OH^- \Leftrightarrow RS^- + H_2O$ times 2
2. $A + S \rightarrow DS_1$ *slow*
3. $B + DS_1 \Leftrightarrow DS_2$
4. $A + DS_2 \Leftrightarrow DS_3$
5. $DS_3 \Leftrightarrow DS_4$
6. $DS_4 \Leftrightarrow D + C + S$

Net: $2RS^- + O_2 \rightarrow RSSR + O_2^{2-}$

The above mechanism is consistent with Figure 2.4 within Chapter 2. For simplification purposes in the derivation of mechanism B models, let $A=RS^-$, $B=O_2$, $C=O_2^{2-}$, D=RSSR, S=PcCo(II), $DS_1=RS^{\bullet}\ldots PcCo(I)$, $DS_2=RS^{\bullet}\ldots PcCo(II)\ldots O_2^-$, $DS_3=RSSR\ldots PcCo(I)\ldots O_2^-$, $DS_4=RSSR\ldots PcCo(II)\ldots O_2^{2-}$

Appendix G derives Pc Model IV, which assumes step 2 (thiolate binding and transferring an electron to metal center of phthalocyanine) in the proposed catalytic mechanism B, where radical-radical coupling to form disulfide occurs within the catalyst cavity, is the rate-determining step.

For simplification purposes, from A.3, let $[RS^-]=[A]=k^*[X]$, where [X]=[RSH] and

$$k^* = \frac{K_1[OH^-]}{[H_2O]}$$

Assuming step 2 is the rate-determining step and only the forward reaction is considered:

$$-\frac{d[O_2]}{dt} = r_2 = k_2[A][S] \qquad \text{(G.1)}$$

Must do a catalyst balance to find [S]: $[S]_T = [S] + [DS_1] + [DS_2] + [DS_3] + [DS_4]$

For $[DS_4]$, assume step 6 is in fast equilibrium:

$$r_6 = k_6[DS_4] - k_{-6}[D][C][S] \tag{G.2}$$

$$[DS_4] = \frac{[D][C][S]}{K_6} \tag{G.3}$$

where $K_6 = {}^{k_6}\!/_{k_{-6}}$ and ${}^{r_6}\!/_{k_6} \approx 0$

For $[DS_3]$, assume step 5 is in fast equilibrium:

$$r_5 = k_5[DS_3] - k_{-5}[DS_4] \tag{G.4}$$

$$[DS_3] = \frac{[DS_4]}{K_5} = \frac{[D][C][S]}{K_6 K_5} \tag{G.5}$$

where $K_5 = {}^{k_5}\!/_{k_{-5}}$ and ${}^{r_5}\!/_{k_5} \approx 0$

For $[DS_2]$, assume step 4 is in fast equilibrium:

$$r_4 = k_4[A][DS_2] - k_{-4}[DS_3] \tag{G.6}$$

$$[DS_2] = \frac{[DS_3]}{K_4[A]} = \frac{[D][C][S]}{K_6 K_5 K_4 k^*[X]} \tag{G.7}$$

where $K_4 = {}^{k_4}\!/_{k_{-4}}$ and ${}^{r_4}\!/_{k_4} \approx 0$

For $[DS_1]$, assume step 3 is in fast equilibrium:

$$r_3 = k_3[B][DS_1] - k_{-3}[DS_2] = 0 \tag{G.8}$$

$$[DS_2] = \frac{[DS_2]}{K_3[B]} = \frac{[D][C][S]}{K_6 K_5 K_4 K_3 k^*[B][X]} \tag{G.9}$$

where $K_3 = {}^{k_3}\!/_{k_{-3}}$ and ${}^{r_3}\!/_{k_3} \approx 0$

Plugging the above back into the catalyst balance, [S] can be found:

$$[S]_T = [S]\left\{1+\frac{[D][C]}{K_6}\left(1+\frac{1}{K_5}+\frac{1}{K_5K_4k^*[X]}+\frac{1}{K_5K_4K_3k^*[B][X]}\right)\right\} \quad \text{(G.10)}$$

$$[S] = \frac{[S]_T}{\left\{1+\frac{[D][C]}{K_6}\left(1+\frac{1}{K_5}+\frac{1}{K_5K_4k^*[X]}+\frac{1}{K_5K_4K_3k^*[B][X]}\right)\right\}} \quad \text{(G.11)}$$

From total thiol oxidation stoichiometry:

$$[RSSR] = \frac{RSH_0 - RSH}{2} \text{ or } [D] = \frac{[X_0]-[X]}{2}$$

$$[S] = \frac{[S]_T}{\left\{1+\frac{[X_0][C](1+1/K_5)}{2K_6}+\frac{[X_0][C](1+1/K_3[B])}{2K_6K_5K_4k^*[X]}-\frac{[X][C](1+1/K_5)}{2K_6}-\frac{[C](1+1/K_3[B])}{2K_6K_5K_4k^*}\right\}} \quad \text{(G.12)}$$

Catalytic oxidation of thiol as a function of thiolate, oxygen and catalyst concentrations via oxygen-induced reaction can be written from G.1 using G.12:

$$-\frac{d[O_2]}{dt} = \frac{k_2[A][S]_T}{\left\{k'+\frac{[X_0][C](1+1/K_3[B])}{2K_6K_5K_4k^*[X]}-\frac{[X][C](1+1/K_5)}{2K_6}\right\}} \quad \text{(G.13)}$$

$$-\frac{d[O_2]}{dt} = \frac{(k_2/k')k^*[X][S]_T}{\left\{1+\frac{[X_0][C](1+1/K_3[B])}{2K_6K_5K_4k'k^*[X]}-\frac{[X][C](1+1/K_5)}{2K_6k'}\right\}} \quad \text{(G.14)}$$

where

$$k' = 1+\frac{[X_0][C](1+1/K_5)}{2K_6}-\frac{[C](1+1/K_3[B])}{2K_6K_5K_4k^*} = 1+\frac{[RSH_0][O_2^{2-}](1+1/K_5)}{2K_6}-\frac{[O_2^{2-}](1+1/K_3[O_2])}{2K_6K_5K_4k^*}$$

This rate was written based on the consumption of one dissolved O_2. As the net stoichiometry above shows, two RS^- are consumed.

$$r_a = \frac{2(k_2/k')k^*[X][S]_T}{\left\{1+\frac{[X_0][C](1+1/K_3[B])}{2K_6K_5K_4k'k^*[X]}-\frac{[X][C](1+1/K_5)}{2K_6k'}\right\}} \quad \text{(G.15)}$$

From equation A.8:

$$r_a = r_b \approx \frac{2(k_2/k')k^*[X][S]_T}{\left\{1+\frac{[X_0][C](1+1/K_3[B])}{2K_6K_5K_4k'k^*[X]}-\frac{[X][C](1+1/K_5)}{2K_6k'}\right\}} \quad \text{(G.16)}$$

Finally, the two RS- consumed by the intermediate H_2O_2 must be accounted for. The total thiol consumption can now be found by combining equations A.1 and G.16:

$$-\frac{d[RSH]}{dt} = \frac{4(k_2/k')k^*[X][S]_T}{\left\{1+\frac{[X_0][C](1+1/K_3[B])}{2K_6K_5K_4k'k^*[X]}-\frac{[X][C](1+1/K_5)}{2K_6k'}\right\}} \quad \text{(G.17)}$$

$$-\frac{d[RSH]}{dt} = \frac{4\alpha[RSH]}{1+\frac{\beta}{[RSH]}-\gamma[RSH]} \quad \text{(G.18)}$$

where $\alpha = (k_2/k')k^*[Cat]_T$, and $\beta = \frac{[RSH_0][O_2^{2-}](1+1/K_3[O_2])}{2K_6K_5K_4k'k^*}$ and $\gamma = \frac{[O_2^{2-}](1+1/K_5)}{2K_6k'}$

Concentration of hydrogen peroxide, is calculated from equation A.10 and G.14:

$$[H_2O_2] \approx \frac{r_a}{2k_{H_2O_2}[RSH]} = \frac{(k_2/k')k^*[X][S]_T}{k_{H_2O_2}[RSH]\left\{1+\frac{[X_0][C](1+1/K_3[B])}{2K_6K_5K_4k'k^*[X]}-\frac{[X][C](1+1/K_5)}{2K_6k'}\right\}}$$

$$[H_2O_2] \approx \frac{\alpha}{k_{H_2O_2}\left\{1+\frac{\beta}{[RSH]}-\gamma[RSH]\right\}} \quad \text{(G.19)}$$

APPENDIX H

CATALYTIC MODEL V

1. $RSH + OH^- \Leftrightarrow RS^- + H_2O$ times 2
2. $A + S \rightarrow DS_1$ *slow*
3. $B + DS_1 \Leftrightarrow DS_2$
4. $A + DS_2 \Leftrightarrow DS_3$
5. $DS_3 \Leftrightarrow DS_4$
6. $DS_4 \Leftrightarrow D + C + S$

Net: $2RS^- + O_2 \rightarrow RSSR + O_2^{2-}$

The above mechanism is consistent with Figure 2.4 within Chapter 2. For simplification purposes in the derivation of mechanism B models, let $A=RS^-$, $B=O_2$, $C=O_2^{2-}$, D=RSSR, S=PcCo(II), $DS_1=RS^{\bullet}\ldots$PcCo(I), $DS_2=RS^{\bullet}\ldots$PcCo(II)$\ldots O_2^-$, $DS_3=$RSSR…PcCo(I)$\ldots O_2^-$, $DS_4=$RSSR…PcCo(II)$\ldots O_2^{2-}$

Appendix H, derives Pc Model V, which assumes step 3 (oxygen attachment and the transferring of an electron to the oxygen from the metal center of phthalocyanine) in the proposed catalytic mechanism B, where radical-radical coupling to form disulfide occurs within the catalyst cavity, is the rate-determining step.

For simplification purposes, from A.9, let $[RS^-]=[A]=k^*[X]$, where [X]=[RSH] and

$$k^* = \frac{\sqrt{K_1}[OH^-]}{[H_2O]}$$

Assuming step 3 is the rate-determining step and only the forward reaction is considered:

$$-\frac{d[O_2]}{dt} = r_3 = k_3[B][DS_1] \qquad \text{(H.1)}$$

For [DS_1], assume step 2 is in fast equilibrium:

$$r_2 = k_2[A][S] - k_{-2}[DS_1] \tag{H.2}$$

$$[DS_1] = K_2[A][S] \tag{H.3}$$

where $K_2 = {}^{k_2}\!/_{k_{-2}}$ and ${}^{r_2}\!/_{k_2} \approx 0$

$$-\frac{d[O_2]}{dt} = k_3 K_2[B][A][S] \tag{H.4}$$

Must do a catalyst balance to find [S]:

$[S]_T = [S] + [DS_1] + [DS_2] + [DS_3] + [DS_4]$

For [DS_4], assume step 6 is in fast equilibrium:

$$r_6 = k_6[B][DS_4] - k_{-6}[D][C][S] \tag{H.5}$$

$$[DS_4] = \frac{[D][C][S]}{K_6} \tag{H.6}$$

where $K_6 = {}^{k_6}\!/_{k_{-6}}$ and ${}^{r_6}\!/_{k_6} \approx 0$

For [DS_3], assume step 5 is in fast equilibrium:

$$r_5 = k_5[DS_3] - k_{-5}[DS_4] \tag{H.7}$$

$$[DS_3] = \frac{[DS_4]}{K_5} = \frac{[D][C][S]}{K_6 K_5} \tag{H.8}$$

where $K_5 = {}^{k_5}\!/_{k_{-5}}$ and ${}^{r_5}\!/_{k_5} \approx 0$

For [DS_2], assume step 4 is in fast equilibrium:

$$r_4 = k_4[A][DS_2] - k_{-4}[DS_3] \tag{H.9}$$

$$[DS_2] = \frac{[DS_3]}{K_4[A]} = \frac{[D][C][S]}{K_6 K_5 K_4 k^*[X]} \tag{H.10}$$

where $K_4 = {}^{k_4}\!/_{k_{-4}}$ and ${}^{r_4}\!/_{k_4} \approx 0$

Plugging the above back into the catalyst balance, [S] can be found:

$$[S]_T = [S]\left\{1 + K_2[A] + \frac{[D][C]}{K_6}\left(1 + \frac{1}{K_5} + \frac{1}{K_5 K_4 k^*[X]}\right)\right\} \tag{H.11}$$

$$[S] = \frac{[S]_T}{\left\{1 + K_2 k^*[X] + \frac{[D][C]}{K_6}\left(1 + \frac{1}{K_5} + \frac{1}{K_5 K_4 k^*[X]}\right)\right\}} \tag{H.12}$$

From total thiol oxidation stoichiometry:

$$[RSSR] = \frac{RSH_0 - RSH}{2} \text{ or } [D] = \frac{[X_0] - [X]}{2}$$

$$[S] = \frac{[S]_T}{\left\{1 + K_2 k^*[X] + \frac{[X_0][C](1+1/K_5)}{2K_6} + \frac{[X_0][C]}{2K_6 K_5 K_4 k^*[X]} - \frac{[C]}{2K_6 K_5 K_4 k^*} - \frac{[X][C](1+1/K_5)}{2K_6}\right\}} \tag{H.13}$$

Catalytic oxidation of thiol as a function of thiolate, oxygen and catalyst concentrations via oxygen-induced reaction can be written from H.4:

$$-\frac{d[O_2]}{dt} = \frac{k_3 K_2 [B][A][S]_T}{\left\{k' + K_2 k^*[X] + \frac{[X_0][C]}{2K_6 K_5 K_4 k^*[X]} - \frac{[X][C](1+1/K_5)}{2K_6}\right\}} \tag{H.14}$$

$$-\frac{d[O_2]}{dt} = \frac{\left(k_3 K_2 / k'\right) k^*[B][X][S]_T}{\left\{1 + \frac{[X_0][C]}{2K_6 K_5 K_4 k^* k'[X]} + \left(\frac{K_2 k^*}{k'} - \frac{[C](1+1/K_5)}{2K_6 k'}\right)[X]\right\}} \tag{H.15}$$

where $k' = 1 + \frac{[X_0][C](1+1/K_5)}{2K_6} - \frac{[C]}{2K_6 K_5 K_4 k^*} = 1 + \frac{[RSH_0][O_2^{2-}](1+1/K_5)}{2K_6} - \frac{[O_2^{2-}]}{2K_6 K_5 K_4 k^*}$

This rate was written based on the consumption of one dissolved O_2. As the net stoichiometry above shows, two RS^- are consumed.

$$r_a \approx \frac{2\left(k_3 K_2 / k'\right) k^*[B][X][S]_T}{\left\{1 + \frac{[X_0][C]}{2K_6 K_5 K_4 k^*[X]} + \left(\frac{K_2 k^*}{k'} - \frac{[C](1+1/K_5)}{2K_6 k'}\right)[X]\right\}} \tag{H.16}$$

From equation A.8:

$$r_a = r_b \approx \frac{2\left(k_3K_2/k'\right)k^*[B][X][S]_T}{\left\{1+\frac{[X_0][C]}{2K_6K_5K_4k^*k'[X]}+\left(\frac{K_2k^*}{k'}-\frac{[C](1+1/K_5)}{2K_6k'}\right)[X]\right\}} \tag{H.17}$$

Finally, the two RS^- consumed by the intermediate H_2O_2 must be accounted for. The total thiol consumption can now be found by combining equations A.1 and H.17:

$$-\frac{d[RSH]}{dt} = \frac{4\left(k_3K_2/k'\right)k^*[B][X][S]_T}{\left\{1+\frac{[X_0][C]}{2K_6K_5K_4k^*k'[X]}+\left(\frac{K_2k^*}{k'}-\frac{[C](1+1/K_5)}{2K_6k'}\right)[X]\right\}} \tag{H.18}$$

$$-\frac{d[RSH]}{dt} = \frac{4\alpha[RSH]}{1+\frac{\beta}{[RSH]}-\gamma[RSH]} \tag{H.19}$$

where $\alpha = \left(k_3K_2/k'\right)k^*[O_2][Cat]_T$, $\beta = \frac{[RSH_0][O_2^{2-}]}{2K_6K_5K_4k^*k'}$ and $\gamma = \frac{K_2k^*}{k'} - \frac{[O_2^{2-}](1+1/K_5)}{2K_6k'}$

Concentration of hydrogen peroxide, is calculated from equation A.10 and H.16:

$$[H_2O_2] \approx \frac{r_a}{2k_{H_2O_2}[RSH]} = \frac{\left(k_3K_2/k'\right)k^*[B][X][S]_T}{k_{H_2O_2}[RSH]\left\{1+\frac{[X_0][C]}{2K_6K_5K_4k^*k'[X]}+\left(\frac{K_2k^*}{k'}-\frac{[C](1+1/K_5)}{2K_6k'}\right)[X]\right\}}$$

$$[H_2O_2] \approx \frac{\alpha}{k_{H_2O_2}\left\{1+\frac{\beta}{[RSH]}+\gamma[RSH]\right\}} \tag{H.20}$$

APPENDIX I

CATALYTIC MODEL VI

1. $RSH + OH^- \Leftrightarrow RS^- + H_2O$ times 2
2. $A + S \rightarrow DS_1$ *slow*
3. $B + DS_1 \Leftrightarrow DS_2$
4. $A + DS_2 \Leftrightarrow DS_3$
5. $DS_3 \Leftrightarrow DS_4$
6. $DS_4 \Leftrightarrow D + C + S$

Net: $2RS^- + O_2 \rightarrow RSSR + O_2^{2-}$

The above mechanism is consistent with Figure 2.4 within Chapter 2. For simplification purposes in the derivation of mechanism B models, let $A=RS^-$, $B=O_2$, $C=O_2^{2-}$, D=RSSR, S=PcCo(II), $DS_1=RS^{\bullet}\ldots PcCo(I)$, $DS_2=RS^{\bullet}\ldots PcCo(II)\ldots O_2^-$, $DS_3=RSSR\ldots PcCo(I)\ldots O_2^-$, $DS_4=RSSR\ldots PcCo(II)\ldots O_2^{2-}$

Appendix I, derives Pc Model VI, which assumes step 4 (2^{nd} thiolate binding and transferring an electron to metal center of phthalocyanine) in the proposed catalytic mechanism B, where radical-radical coupling to form disulfide occurs within the catalyst cavity, is the rate-determining step.

For simplification purposes, from A.9, let $[RS^-]=[A]=k^*[X]$, where [X]=[RSH] and

$$k^* = \frac{\sqrt{K_1}[OH^-]}{[H_2O]}$$

Assuming step 4 is the rate-determining step and only the forward reaction is considered:

$$-\frac{d[O_2]}{dt} = r_4 = k_4[A][DS_2] \qquad \text{(I.1)}$$

For $[DS_2]$, assume step 3 is in fast equilibrium:

$$r_3 = k_3[B][DS_1] - k_{-3}[DS_2] = 0 \quad \text{(I.2)}$$

$$[DS_2] = K_3[B][DS_1] \quad \text{(I.3)}$$

where $K_3 = k_3 / k_{-3}$

For [DS_1], assume step 2 is in fast equilibrium:

$$r_2 = k_2[A][S] - k_{-2}[DS_1] \quad \text{(I.4)}$$

$$[DS_1] = K_2[A][S] \quad \text{(I.5)}$$

where $K_2 = k_2 / k_{-2}$ and $r_2 / k_2 \approx 0$

Combing equations I.1, I.3 and I.5:

$$-\frac{d[O_2]}{dt} = k_4 K_3 K_2 [B][A]^2[S] \quad \text{(I.6)}$$

Must do a catalyst balance to find [S]:

$[S]_T = [S] + [DS_1] + [DS_2] + [DS_3] + [DS_4]$

For [DS_4], assume step 6 is in fast equilibrium:

$$r_6 = k_6[B][DS_4] - k_{-6}[D][C][S] \quad \text{(I.7)}$$

$$[DS_4] = \frac{[D][C][S]}{K_6} \quad \text{(I.8)}$$

where $K_6 = k_6 / k_{-6}$ and $r_6 / k_6 \approx 0$

For [DS_3], assume step 5 is in fast equilibrium:

$$r_5 = k_5[DS_3] - k_{-5}[DS_4] \quad \text{(I.9)}$$

$$[DS_3] = \frac{[DS_4]}{K_5} = \frac{[D][C][S]}{K_6 K_5} \quad \text{(I.10)}$$

where $K_5 = k_5 / k_{-5}$ and $r_5 / k_5 \approx 0$

Plugging the above back into the catalyst balance, [S] can be found:

$$[S]_T = [S]\left\{1 + K_2[A] + K_3K_2[B][A] + \frac{[D][C]}{K_6}\left(1 + \frac{1}{K_5}\right)\right\} \tag{I.11}$$

$$[S] = \frac{[S]_T}{\left\{1 + K_2k^*\left(1 + K_3[B]\right)[X] + \frac{[D][C]}{K_6}\left(1 + \frac{1}{K_5}\right)\right\}} \tag{I.12}$$

From total thiol oxidation stoichiometry:

$$[RSSR] = \frac{RSH_0 - RSH}{2} \text{ or } [D] = \frac{[X_0] - [X]}{2}$$

$$[S] = \frac{[S]_T}{\left\{1 + K_2k^*\left(1 + K_3[B]\right)[X] + \frac{[X_0][C]}{2K_6}\left(1 + \frac{1}{K_5}\right) - \frac{[X][C]}{2K_6}\left(1 + \frac{1}{K_5}\right)\right\}} \tag{I.13}$$

Catalytic oxidation of thiol as a function of thiolate, oxygen and catalyst concentrations via oxygen-induced reaction can be written from I.6:

$$-\frac{d[O_2]}{dt} = \frac{k_4K_3K_2[B][A]^2[S]_T}{\left\{1 + K_2k^*\left(1 + K_3[B]\right)[X] + \frac{[X_0][C]}{2K_6}\left(1 + \frac{1}{K_5}\right) - \frac{[X][C]}{2K_6}\left(1 + \frac{1}{K_5}\right)\right\}} \tag{I.14}$$

$$-\frac{d[O_2]}{dt} = \frac{k_4K_3K_2k^{*2}[B][X]^2[S]_T}{\left\{k' + K_2k^*\left(1 + K_3[B]\right)[X] - \frac{[X][C]}{2K_6}\left(1 + \frac{1}{K_5}\right)\right\}} \tag{I.15}$$

where $k' = 1 + \frac{[X_0][C]}{2K_6}\left(1 + \frac{1}{K_5}\right) = 1 + \frac{[RSH_0][O_2^{2-}]}{2K_6}\left(1 + \frac{1}{K_5}\right)$

This rate was written based on the consumption of one dissolved O_2. As the net stoichiometry above shows, two RS^- are consumed.

$$r_a \approx \frac{2\left(k_4K_3K_2 \middle/ k'\right)k^{*2}[B][X]^2[S]_T}{\left\{1 + \left(\frac{K_2k^*\left(1 + K_3[B]\right)}{k'} - \frac{[C]}{2K_6k'}\left(1 + \frac{1}{K_5}\right)\right)[X]\right\}} \tag{I.16}$$

From equation A.8:

$$r_a = r_b \approx \frac{2\left(k_4 K_3 K_2 / k'\right) k^{*2} [B][X]^2 [S]_T}{\left\{1 + \left(\frac{K_2 k^* (1 + K_3[B])}{k'} - \frac{[C]}{2K_6 k'}\left(1 + \frac{1}{K_5}\right)\right)[X]\right\}} \tag{I.17}$$

Finally, the two RS- consumed by the intermediate H_2O_2 must be accounted for. The total thiol consumption can now be found by combining equations A.1 and I.17:

$$-\frac{d[RSH]}{dt} = \frac{4\left(k_4 K_3 K_2 / k'\right) k^{*2} [B][X]^2 [S]_T}{\left\{1 + \left(\frac{K_2 k^* (1 + K_3[B])}{k'} - \frac{[C]}{2K_6 k'}\left(1 + \frac{1}{K_5}\right)\right)[X]\right\}} \tag{I.18}$$

$$-\frac{d[RSH]}{dt} = \frac{4\alpha[RSH]^2}{1 + \beta[RSH]} \tag{I.19}$$

where $\alpha = \left(k_4 K_3 K_2 / k'\right) k^{*2} [O_2][Cat]_T$ and $\beta = \left(\frac{K_2 k^* (1 + K_3[O_2])}{k'} - \frac{[O_2^{2-}]}{2K_6 k'}\left(1 + \frac{1}{K_5}\right)\right)$

Concentration of hydrogen peroxide, is calculated from equation A.10 and I.16:

$$[H_2O_2] \approx \frac{r_a}{2k_{H_2O_2}[RSH]} = \frac{\left(k_4 K_3 K_2 / k'\right) k^{*2} [B][X]^2 [S]_T}{k_{H_2O_2}[RSH]\left\{1 + \left(\frac{K_2 k^* (1 + K_3[B])}{k'} - \frac{[C]}{2K_6 k'}\left(1 + \frac{1}{K_5}\right)\right)[X]\right\}}$$

$$[H_2O_2] \approx \frac{\alpha[RSH]}{k_{H_2O_2}\{1 + \beta[X]\}} \tag{I.20}$$

APPENDIX J

CATALYTIC MODEL VII

1. $RSH + OH^- \Leftrightarrow RS^- + H_2O$ times 2
2. $A + S \rightarrow DS_1$ *slow*
3. $B + DS_1 \Leftrightarrow DS_2$
4. $A + DS_2 \Leftrightarrow DS_3$
5. $DS_3 \Leftrightarrow DS_4$
6. $DS_4 \Leftrightarrow D + C + S$

Net: $2RS^- + O_2 \rightarrow RSSR + O_2^{2-}$

The above mechanism is consistent with Figure 2.4 within Chapter 2. For simplification purposes in the derivation of mechanism B models, let $A=RS^-$, $B=O_2$, $C=O_2^{2-}$, D=RSSR, S=PcCo(II), $DS_1=RS^{\bullet}\ldots PcCo(I)$, $DS_2=RS^{\bullet}\ldots PcCo(II)\ldots O_2^-$, $DS_3=RSSR\ldots PcCo(I)\ldots O_2^-$, $DS_4=RSSR\ldots PcCo(II)\ldots O_2^{2-}$.

Appendix J, derives Pc Model VII, which assumes step 5 (electron transfer from metal center of phthalocyanine center to attached peroxide) in the proposed catalytic mechanism B, where radical-radical coupling to form disulfide occurs within the catalyst cavity, is the rate-determining step.

For simplification purposes, from A.9, let $[RS^-]=[A]=k^*[X]$, where [X]=[RSH] and

$$k^* = \frac{\sqrt{K_1}[OH^-]}{[H_2O]}$$

Assuming step 5 is the rate-determining step and only the forward reaction is considered:

$$-\frac{d[O_2]}{dt} = r_5 = k_5[DS_3] \qquad \text{(J.1)}$$

For $[DS_3]$, assume step 4 is in fast equilibrium:

$$r_4 = k_4[A][DS_2] - k_{-4}[DS_3] \tag{J.2}$$

$$[DS_3] = K_4[A][DS_2] \tag{J.3}$$

where $K_4 = k_4 / k_{-4}$ and $r_4 / k_4 \approx 0$

For $[DS_2]$, assume step 3 is in fast equilibrium:

$$r_3 = k_3[B][DS_1] - k_{-3}[DS_2] = 0 \tag{J.4}$$

$$[DS_2] = K_3[B][DS_1] \tag{J.5}$$

where $K_3 = k_3 / k_{-3}$

For $[DS_1]$, assume step 2 is in fast equilibrium:

$$r_2 = k_2[A][S] - k_{-2}[DS_1] \tag{J.6}$$

$$[DS_1] = K_2[A][S] \tag{J.7}$$

where $K_2 = k_2 / k_{-2}$ and $r_2 / k_2 \approx 0$

Combining equations J.1, J.3, J.5 and J.7:

$$-\frac{d[O_2]}{dt} = k_5 K_4 K_3 K_2 [B][A]^2[S] \tag{J.8}$$

Must do a catalyst balance to find [S]:

$[S]_T = [S] + [DS_1] + [DS_2] + [DS_3] + [DS_4]$

For $[DS_4]$, assume step 6 is in fast equilibrium:

$$r_6 = k_6[B][DS_4] - k_{-6}[D][C][S] \tag{J.9}$$

$$[DS_4] = \frac{[D][C][S]}{K_6} \tag{J.10}$$

where $K_6 = k_6 / k_{-6}$ and $r_6 / k_6 \approx 0$

Plugging the above back into the catalyst balance, [S] can be found:

$$[S]_T = [S]\left\{1+K_2[A]+K_3K_2[B][A]+K_4K_3K_2[B][A]^2+\frac{[D][C]}{K_6}\right\} \qquad \text{(J.11)}$$

$$[S] = \frac{[S]_T}{\left\{1+K_2(1+K_3[B])k^*[X]+K_4K_3K_2k^{*2}[B][X]^2+\frac{[D][C]}{K_6}\right\}} \qquad \text{(J.12)}$$

From total thiol oxidation stoichiometry:

$$[RSSR] = \frac{RSH_0 - RSH}{2} \text{ or } [D] = \frac{[X_0]-[X]}{2}$$

$$[S] = \frac{[S]_T}{\left\{1+K_2(1+K_3[B])k^*[X]+K_4K_3K_2k^{*2}[B][X]^2+\frac{[X_0][C]}{K_6}-\frac{[X][C]}{K_6}\right\}} \qquad \text{(J.13)}$$

Catalytic oxidation of thiol as a function of thiolate, oxygen and catalyst concentrations via oxygen-induced reaction can be written from J.6:

$$r_a = \frac{k_5K_4K_3K_2[B][A]^2[S]_T}{\left\{1+\frac{[X_0][C]}{K_6}+\left(K_2(1+K_3[B])-\frac{[C]}{K_6}\right)k^*[X]+K_4K_3K_2k^{*2}[B][X]^2\right\}} \qquad \text{(J.14)}$$

$$r_a = \frac{k_5K_4K_3K_2k^{*2}[B][X]^2[S]_T}{\left\{k'+\left(K_2(1+K_3[B])-\frac{[C]}{K_6}\right)k^*[X]+K_4K_3K_2k^{*2}[B][X]^2\right\}} \qquad \text{(J.15)}$$

where $k' = 1+\frac{[X_0][C]}{K_6} = 1+\frac{[RSH_0][O_2^{2-}]}{K_6}$

This rate was written based on the consumption of one dissolved O_2. As the net stoichiometry above shows, two RS^- are consumed.

$$r_a = \frac{2\left(k_5K_4K_3K_2/k'\right)k^{*2}[B][X]^2[S]_T}{\left\{1+\left(K_2(1+K_3[B])-\frac{[C]}{K_6}\right)\frac{k^*}{k'}[X]+\frac{K_4K_3K_2k^{*2}[B]}{k'}[X]^2\right\}} \qquad \text{(J.16)}$$

From equation A.8:

$$r_a = r_b \approx \frac{2\left(k_5 K_4 K_3 K_2 / k'\right) k^{*2} [B][X]^2 [S]_T}{\left\{1 + \left(K_2 (1 + K_3 [B]) - \frac{[C]}{K_6} \right) \frac{k^*}{k'} [X] + \frac{K_4 K_3 K_2 k^{*2} [B]}{k'} [X]^2 \right\}} \tag{J.17}$$

Finally, the two RS^- consumed by the intermediate H_2O_2 must be accounted for. The total thiol consumption can now be found by combining equations A.1 and J.17:

$$-\frac{d[RSH]}{dt} = \frac{4\left(k_5 K_4 K_3 K_2 / k'\right) k^{*2} [B][X]^2 [S]_T}{\left\{1 + \left(K_2 (1 + K_3 [B]) - \frac{[C]}{K_6} \right) \frac{k^*}{k'} [X] + \frac{K_4 K_3 K_2 k^{*2} [B]}{k'} [X]^2 \right\}} \tag{J.18}$$

$$-\frac{d[RSH]}{dt} = \frac{2\alpha [RSH]^2}{1 + \beta [RSH] + \gamma [RSH]^2} \tag{J.19}$$

where $\alpha = \left(k_5 K_4 K_3 K_2 / k'\right) k^{*2} [O_2][Cat]_T$, $\beta = \left(K_2 (1 + K_3 [O_2]) - \frac{[O_2^{2-}]}{K_6} \right) \frac{k^*}{k'}$ and

$\gamma = \frac{K_4 K_3 K_2 k^{*2} [O_2]}{k'}$

Concentration of hydrogen peroxide, is calculated from equation A.10 and J.16:

$$[H_2O_2] \approx \frac{r_a}{2k_{H_2O_2}[RSH]} = \frac{\left(k_5 K_4 K_3 K_2 / k'\right) k^{*2} [B][X]^2 [S]_T}{k_{H_2O_2}[RSH] \left\{1 + \left(K_2 (1 + K_3 [B]) - \frac{[C]}{K_6} \right) \frac{k^*}{k'} [X] + \frac{K_4 K_3 K_2 k^{*2} [B]}{k'} [X]^2 \right\}}$$

$$[H_2O_2] \approx \frac{\alpha [RSH]}{k_{H_2O_2} \left\{1 + \beta [RSH] + \gamma [RSH]^2 \right\}} \tag{J.20}$$

APPENDIX K

CATALYTIC MODEL VIII

1. $RSH + OH^- \Leftrightarrow RS^- + H_2O$ times 2
2. $A + S \rightarrow DS_1$ *slow*
3. $B + DS_1 \Leftrightarrow DS_2$
4. $A + DS_2 \Leftrightarrow DS_3$
5. $DS_3 \Leftrightarrow DS_4$
6. $DS_4 \Leftrightarrow D + C + S$

Net: $2RS^- + O_2 \rightarrow RSSR + O_2^{2-}$

The above mechanism is consistent with Figure 2.4 within Chapter 2. For simplification purposes in the derivation of mechanism B models, let $A=RS^-$, $B=O_2$, $C=O_2^{2-}$, D=RSSR, S=PcCo(II), $DS_1=RS^{\bullet}\ldots PcCo(I)$, $DS_2=RS^{\bullet}\ldots PcCo(II)\ldots O_2^-$, $DS_3=RSSR\ldots PcCo(I)\ldots O_2^-$, $DS_4=RSSR\ldots PcCo(II)\ldots O_2^{2-}$.

Appendix K, derives Pc Model VIII, which assumes step 6 (expulsion of $RS^{\bullet}$ radical from the metal center of phthalocyanine) in the proposed catalytic mechanism B, where radical-radical coupling to form disulfide occurs within the catalyst cavity, is the rate-determining step.

For simplification purposes, from A.9, let $[RS^-]=[A]=k^*[X]$, where [X]=[RSH] and

$$k^* = \frac{\sqrt{K_1}[OH^-]}{[H_2O]}$$

Assuming step 6 is the rate-determining step and only the forward reaction is considered:

$$-\frac{d[O_2]}{dt} = r_6 = k_6[DS_4] \qquad \text{(K.1)}$$

For $[DS_4]$, assume step 5 is in fast equilibrium:

$$r_5 = k_5[DS_3] - k_{-5}[DS_4] \tag{K.2}$$

$$[DS_4] = K_5[DS_3] \tag{K.3}$$

where $K_5 = k_5 / k_{-5}$ and $r_5 / k_5 \approx 0$

For $[DS_3]$, assume step 4 is in fast equilibrium:

$$r_4 = k_4[A][DS_2] - k_{-4}[DS_3] \tag{K.4}$$

$$[DS_3] = K_4[A][DS_2] \tag{K.5}$$

where $K_4 = k_4 / k_{-4}$ and $r_4 / k_4 \approx 0$

For $[DS_2]$, assume step 3 is in fast equilibrium:

$$r_3 = k_3[B][DS_1] - k_{-3}[DS_2] = 0 \tag{K.6}$$

$$[DS_2] = K_3[B][DS_1] \tag{K.7}$$

where $K_3 = k_3 / k_{-3}$

For $[DS_1]$, assume step 2 is in fast equilibrium:

$$r_2 = k_2[A][S] - k_{-2}[DS_1] \tag{K.8}$$

$$[DS_1] = K_2[A][S] \tag{K.9}$$

where $K_2 = k_2 / k_{-2}$ and $r_2 / k_2 \approx 0$

Combining equation K.1, K.3, K.5, K7 and K.9:

$$-\frac{d[O_2]}{dt} = k_6 K_5 K_4 K_3 K_2 [B][A]^2[S] \tag{K.10}$$

Must do a catalyst balance to find [S]:

$[S]_T = [S] + [DS_1] + [DS_2] + [DS_3] + [DS_4]$

Plugging the above back into the catalyst balance, [S] can be found:

$$[S]_T = [S]\left\{1 + K_2[A] + K_3K_2[B][A] + K_4K_3K_2[B][A]^2 + K_5K_4K_3K_2[B][A]^2\right\} \quad \text{(K.11)}$$

$$[S] = \frac{[S]_T}{\left\{1 + (1 + K_3[B])K_2k^*[X] + (1 + K_5)K_4K_3K_2[B]k^{*2}[X]^2\right\}} \quad \text{(K.12)}$$

Catalytic oxidation of thiol as a function of thiolate, oxygen and catalyst concentrations via oxygen-induced reaction can be written from K.6:

$$-\frac{d[O_2]}{dt} = \frac{k_6K_5K_4K_3K_2k^{*2}[B][X]^2[S]_T}{\left\{1 + (1 + K_3[B])K_2k^*[X] + (1 + K_5)K_4K_3K_2[B]k^{*2}[X]^2\right\}} \quad \text{(K.13)}$$

This rate was written based on the consumption of one dissolved O_2. As the net stoichiometry above shows, two RS^- are consumed.

$$r_a = \frac{2k_6K_5K_4K_3K_2k^{*2}[B][X]^2[S]_T}{\left\{1 + (1 + K_3[B])K_2k^*[X] + (1 + K_5)K_4K_3K_2[B]k^{*2}[X]^2\right\}} \quad \text{(K.14)}$$

From equation A.8:

$$r_a = r_b \approx \frac{2k_6K_5K_4K_3K_2k^{*2}[B][X]^2[S]_T}{\left\{1 + (1 + K_3[B])K_2k^*[X] + (1 + K_5)K_4K_3K_2[B]k^{*2}[X]^2\right\}} \quad \text{(K.15)}$$

Finally, the two RS^- consumed by the intermediate H_2O_2 must be accounted for. The total thiol consumption can now be found by combining equations A.1 and K.15:

$$-\frac{d[RSH]}{dt} = \frac{4k_6K_5K_4K_3K_2k^{*2}[B][X]^2[S]_T}{\left\{1 + (1 + K_3[B])K_2k^*[X] + (1 + K_5)K_4K_3K_2[B]k^{*2}[X]^2\right\}} \quad \text{(K.16)}$$

$$-\frac{d[RSH]}{dt} = \frac{4\alpha[RSH]^2}{1 + \beta[RSH] + \gamma[RSH]^2} \quad \text{(K.17)}$$

Concentration of hydrogen peroxide, is calculated from equation A.10 and K.14:

$$[H_2O_2] \approx \frac{r_a}{2k_{H_2O_2}[RSH]} = \frac{k_6K_5K_4K_3K_2k^{*2}[B][X]^2[S]_T}{k_{H_2O_2}[RSH]\left\{1 + (1 + K_3[B])K_2k^*[X] + (1 + K_5)K_4K_3K_2[B]k^{*2}[X]^2\right\}}$$

$$[H_2O_2] \approx \frac{\alpha[RSH]}{k_{H_2O_2}\left\{1 + \beta[RSH] + \gamma[X]^2\right\}} \quad \text{(K.18)}$$

APPENDIX L

KINETIC PARAMETERS FOR F_{16}PcCo CATALYZED OXIDATION OF 2-MERCAPTOETHANOL

The Matlab code below calculates quantitative values for K_3 and k_4 for F_{16}PcCo catalyzed oxidation of 2-mercaptoethanol from initial rate data under 5%, 21% and 100% O_2 mixtures. The code assumes model III defines catalytic thiol oxidations and uses alpha and beta values from the 100% O_2 case at 22 °C and 1atm.

```
Ccat=0.0105; H=0.0995; km=5000; COH=2.58; CH2O=1100; K1=1.14e+6; pO2=0.8;
r5=100; r21=210; r100=310;
dm=[1;0];
db=[0;1];
Co2guess100=8.02;
Co2guess21=0.21*Co2guess100; Co2guess5=0.05*Co2guess100;
x=[Co2guess5^-1, Co2guess21^-1, Co2guess100^-1];
y=4*Ccat*[r5^-1,r21^-1,r100^-1];
p=polyfit(x,y,1);
m=p*dm;
b=p*db;
k4=1/b
K3=1/(m*k4)
```

APPENDIX M

KINETIC PARAMETERS FOR F_{64}PcCo CATALYZED OXIDATION OF 2-MERCAPTOETHANOL

The Matlab code below calculates quantitative values for K_3 and k_4 for F_{64}PcCo catalyzed oxidation of 2-mercaptoethanol from initial rate data under 5%, 21% and 100% O_2 mixtures. The code assumes model III defines catalytic thiol oxidations and uses alpha and beta values from the 100% O_2 case at 22 °C and 1atm.

```
Ccat=0.0105; H=0.0995; km=5000; COH=2.58; CH2O=1100; K1=1.14e+6; pO2=0.8;
r5=44.5; r21=179; r100=326;
dm=[1;0];
db=[0;1];
Co2guess100=8.02;
Co2guess21=0.21*Co2guess100; Co2guess5=0.05*Co2guess100;
x=[Co2guess5^-1, Co2guess21^-1, Co2guess100^-1];
y=4*Ccat*[r5^-1,r21^-1,r100^-1];
p=polyfit(x,y,1);
m=p*dm;
b=p*db;
k4=1/b
K3=1/(m*k4)
```

APPENDIX N

KINETIC PARAMETERS FOR F_{16}PcCo CATALYZED OXIDATION OF 4-FLUOROBENZENTHIOL

The Matlab code below calculates quantitative values for K_3 and k_4 for F_{16}PcCo catalyzed oxidation of 4-fluorobenzenethiol from initial rate data under 5%, 21% and 100% O_2 mixtures. The code assumes model III defines catalytic thiol oxidations and uses alpha and beta values from the 100% O_2 case at 22 °C and 1atm.

```
Ccat=0.0105; H=0.0995; km=5000; COH=2.58; CH2O=1100; K1=1.45E+9;
pO2=0.8;
r5=96.0; r21=222; r100=376;
dm=[1;0];
db=[0;1];
Co2guess100=8.02;
Co2guess21=0.21*Co2guess100; Co2guess5=0.05*Co2guess100;
x=[Co2guess5^-1, Co2guess21^-1, Co2guess100^-1];
y=4*Ccat*[r5^-1,r21^-1,r100^-1];
p=polyfit(x,y,1);
m=p*dm;
b=p*db;
k4=1/b
K3=1/(m*k4)
A=K3*H; B=H+(4*k4*K3*Ccat/km)-pO2*K3; C=-pO2;
Co2New100P=(-B+((B^2)-4*A*C)^0.5)/(2*A)
Co2New100N=(-B-((B^2)-4*A*C)^0.5)/(2*A)
```

APPENDIX O

KINETIC PARAMETERS FOR F_{64}PcCo CATALYZED OXIDATION OF 4-FLUOROBENZENTHIOL

The Matlab code below calculates quantitative values for K_3 and k_4 for F_{64}PcCo catalyzed oxidation of 4-fluorobenzenethiol from initial rate data under 5%, 21% and 100% O_2 mixtures. The code assumes model III defines catalytic thiol oxidations and uses alpha and beta values from the 100% O_2 case at 22 °C and 1atm.

```
Ccat=0.0105; H=0.0995; km=5000; COH=2.58; CH2O=1100; K1=1.45E+9;
pO2=0.8;
r5=67.7; r21=287; r100=364;
dm=[1;0];
db=[0;1];
Co2guess100=8.02;
Co2guess21=0.21*Co2guess100; Co2guess5=0.05*Co2guess100;
x=[Co2guess5^-1, Co2guess21^-1, Co2guess100^-1];
y=4*Ccat*[r5^-1,r21^-1,r100^-1];
p=polyfit(x,y,1);
m=p*dm;
b=p*db;
k4=1/b
K3=1/(m*k4)
A=K3*H; B=H+(4*k4*K3*Ccat/km)-pO2*K3; C=-pO2;
Co2New100P=(-B+((B^2)-4*A*C)^0.5)/(2*A)
Co2New100N=(-B-((B^2)-4*A*C)^0.5)/(2*A)
```

APPENDIX P

KINETIC PARAMETERS FOR F_{16}PcCo CATALYZED OXIDATION OF 2-MERCAPTOETHANOL AT 10 °C.

The Matlab code below calculates quantitative values for K_3 and k_4 for F_{16}PcCo catalyzed oxidation of 2-mercaptoethanol from initial rate data under 5%, 21% and 100% O_2 mixtures. The code assumes model III defines catalytic thiol oxidations and uses alpha and beta values from the 100% O_2 case at 10 °C and 1atm.

```
Ccat=0.0105; H=0.0995; km=5000; COH=2.58; CH2O=1100; K1=1.14e+6; pO2=0.8;
r5=48.2; r21=82.3; r100=146;
dm=[1;0];
db=[0;1];
Co2guess100=8.02;
Co2guess21=0.21*Co2guess100; Co2guess5=0.05*Co2guess100;
x=[Co2guess5^-1, Co2guess21^-1, Co2guess100^-1];
y=4*Ccat*[r5^-1,r21^-1,r100^-1];
p=polyfit(x,y,1);
m=p*dm;
b=p*db;
k4=1/b
K3=1/(m*k4)
```

APPENDIX Q

KINETIC PARAMETERS FOR F_{16}PcCo CATALYZED OXIDATION OF 2-MERCAPTOETHANOL 15 °C.

The Matlab code below calculates quantitative values for K_3 and k_4 for F_{16}PcCo catalyzed oxidation of 2-mercaptoethanol from initial rate data under 5%, 21% and 100% O_2 mixtures. The code assumes model III defines catalytic thiol oxidations and uses alpha and beta values from the 100% O_2 case at 15 °C and 1atm.

```
Ccat=0.0105; H=0.0995; km=5000; COH=2.58; CH2O=1100; K1=1.14e+6; pO2=0.8;
r5=43.4; r21=66.9; r100=215;
dm=[1;0];
db=[0;1];
Co2guess100=8.02;
Co2guess21=0.21*Co2guess100; Co2guess5=0.05*Co2guess100;
x=[Co2guess5^-1, Co2guess21^-1, Co2guess100^-1];
y=4*Ccat*[r5^-1,r21^-1,r100^-1];
p=polyfit(x,y,1);
m=p*dm;
b=p*db;
k4=1/b
K3=1/(m*k4)
```

REFERENCES

1. Oleson, J.; Haynes, V.; Ramaker, B.; Slough, R.; Whalen, H.; Sciance, T.; Saft, M.; Jost, D.; Tamarelli, W.; Turner S.; Brooks, D.; Artemis, D.; Kellogg, D., (Ed.) *Technology Vision 2020: The US Chemicals Industry*, American Chemical Society, Washington, D.C. 1996.

2. Parton, R.F.; Vankelecom, I.F.J.; Casselman, M.J.A.; Bezoukhanova, C.P.; Uytterhoeven, J.B.; Jacobs, P.A., *Nature*, **1994**, 370, 541.

3. Bench, B.A.; Beveridge, A.; Sharman, W.M.; Diebold, G.J.; van Lier, J.E.; Gorun, S.M., *Angew. Chem. Int. Edit.*, **2002**, 41, 747.

4. Tarbell, D.S., in: N. Kharasch (Ed.), *Inorganic Sulphur Compounds*, vol. 1, Pergamon: London, England, 1961.

5. Oswald, A.A.; Wallace, T.J, in: N. Kharasch, C.Y. Meyers (Ed.), *The Chemistry of Organic Sulphur Compound*, vol. 2, Pergamon: London, England , 1966.

6. Nriagu, J.O., *Sulfur in the Environment*; Eiley-Interscience: New York, New York, 1978.

7. Basu, B.; Satapathy, S.; Bhatnagar, A.K., *Catal. Rev.*, **1993**, 35, 571.

8. Wallace, T.J.; Schriesheim, A.; Hurwitz, H.; Glaser, M.B., *Ind. Eng. Chem. Proc. D.D.*, **1964**, 3, 237.

9. Capozzi, G.; Modena, G., *The Chemistry of the Thiol Group: Part 2*. Wiley: New York, New York, 1974.

10. Cook, A.H., *J. Chem. Soc.*, **1938**, 1768.

11. Kadish, K.M.; Smith, K.M.; Guilard, R., *The Porphyrin Hand- book*, vol. 15-20, *Academic Press*: New York, New York, 2003.

12. Leznoff, C.C.; Sosa-Sanchez, J.L., *Chem. Commun*, **2004**, 338.

13. Yoon S.M.; Song, H.J.; Hwang, I.; Kim, K.S.; Choi, H.C., *Chem. Commun.*, **2010**, 46, 231.

14. Loas, A.I., Rational Design of Hydrogen-Free Catalytic Active Sites. Ph.D. Thesis, New Jersey Institute of Technology, Newark, New Jersey, 2012.

15. Moons, H.; Lapok, L.; Loas, A.; van Doorslaer, S.; Gorun, S.M., *Inorg. Chem.*, **2010**, 49, 8779.

16. Keil, C.; Tsaryova, O.; Lapok, L.; Himcinschi, C.; Wo'hrle, D.; Hild, O.R.; Zahn, D.R.T.; Gorun S.M.; Schlettwein, D., *Thin Solid Films,* **2009**, 517, 4379.

17. Gerdes, R.; Lapok, L.; Tsaryova, O.; Wo'hrle, D.; Gorun, S.M., *Dalton T.*, **2009**, 1098.

18. Xia, X.; Su, Y.; Qian, J., *Ind. Eng. Chem. Res.*, **1995**, 34, 2001.

19. Xia, X.; Su, Y.; Qian, J., *Ind. Eng. Chem. Res.*, **1999**, 38, 1291.

20. Xia, X.; Su, Y.; Qian, J., *Fuel Sci. Tech. Int.*, **1996**, 14, 1205.

21. Tyapochkin, E.M.; Kozliak, E.I., *J. Mol. Catal. A-Chem.*, **2005**, 242, 1.

22. Ganguly, S.K.; Das, G.; Mohanty, B.; Bhargava, R.; Dawra, S., *Petrol. Sci. Technol.*, **2010**, 1287.

23. Giles, W.W.; Cha, J.A.; Lim, P.K., *Chem. Eng. Sci.*, **1986**, 41(12), 3129.

24. Leung, P.S. K.; Betterton, E. A.; Hoffmann, M. R., *J. Phys. Chem.*, **1989**, 93, 430.

25. Van Welzen, J.; Van Herk, A.M.; Kramer, H.; German, A.L., *J. Mol. Catal.*, **1990**, 59(30), 291.

26. Zwart, J.; van der Weide, H. C.; Bröker, N.; Rummens, C.; Schuit, G. C. A. J. Mol. Catal. **1977**, 3, 151.

27. Surdhar, P. S.; Armstrong, D. A., *J. Phys. Chem*. **1986**, 90, 5915.

28. Buck, T.; Schulz-Ekloff, G.; Andreev, A.; Wöhrle, D., *J. Mol. Catal.*, **1991**, 70, 259.

29. Bonnett, R. *Chemical Aspects of Photodynamic Therapy*; Gordon and Breach Science Publishers: Amsterdam, The Netherlands, 2000.

30. Bench, B.A. Ph.D. Dissertation, Brown University, Providence, Rhode Island, May 2001.

31. Minnes, R.; Weitman, H.; Lee, H.J.; Gorun, S. M.; Ehrenberg, B., *Photochem. & Photobiol*., **2006**, 82, 593.

32. Lukyanets, E.A.; Nemykin, V.N. *J. Porphyrins Phthalocyanines,* **2010**, *14*, 1.

33. Elemans, J.A.A.W.; van Hameren, R.; Nolte, R. J.M.; Rowan, A.E. *Adv. Mater.* **2006**, *18*, 1251.

34. Chen, Y.; Hanack, M.; Blau, W.J.; Dini, D.; Liu, Y.; Lin, Y.; Bai, J., *J. Mat. Sci.* **2006**, *41*, 2169.

35. Carr, N.L.; Shah, Y.T., *Can. J. Chem. Eng.* **1979**, 57, 35.

36. Wallace, T.J.; Schriesheim, A., *J. Org. Chem.* **1962**, 27, 1514.

37. Loas, A.; Gerdes, R.; Zhang, Y.; Gorun, S.M., *Dalton T.*, **2011**, 40, 5162.

38. Moore, J.W.; Pearson, R.G., *Kinetics and Mechanism: A Study of Homogeneous Chemical Reactions, 3rd Edition*, Wiley: New York, New York, 1981.

39. Tsaryova, O.; Schnurpfeil, G.; Wo'hrle, D., *J. Photoch. Photobio. A*, **2006**, 184, 50.

40. Ganguly, S.K.; Das, G.; Kumar, S.; Sain, B.; Garg, M.O., *Catal. Today*, **2012**, 198, 1, 246.

41. Ganguly, S.K.; Das, G.; Sain, B, in: P.K. Bajpai, H. Bhunia (Eds.), *Advances in Chemical Engineering*, MacMillan: New Dehli, India, 2011.

42. Leitao, A.; Rodrigues, A., *Chem. Eng. Sci.* **1989,** 44, 5, 1245.

43. Battino, R. (Ed.), *IUPAC Solubility Data Series, Vol. 7, Oxygen and Ozone*, Pergamon Press: Oxford, England, 1981.

44. Golovanov, B., Russ. *J. Gen. Chem.* **2005,** 75, 11, 1795.

45. Bartholomew, C.H.; Farrauto, R.J. *Fundamentals of Industrial Catalytic Processes*, 2nd edition, Wiley: New York, New York, 2005.

46. Miessler, G.L.; Donald, A.T., *Inorganic Chemistry*. Prentice Hall: Upper Saddle River, New Jersey, 2011.

47. Cotton, F.A.; Geoffrey W.; Carlos A.M., *Advanced Inorganic Chemistry*, Wiley: New York, New York, 1999.

48. THF Solutions: http://www.intermediates.basf.com/chemicals/web/en/function/conversions:/publish/content/news-and-publications/brochures/download/BASF_THF_Brochure.pdf (Accessed: December, 2013)

49. Farrauto, R.J., *Industrial Catalysis: A Practical Guide*, Springer: New York, New York, 2007.

50. Martell, A.E.; Smith, R.M. *Critical Stability Constant*, vol. 3, Plenum Press: New York, New York, 1977.

51. Berger, L.; Slein, M.W.; Colowick S.P.; Cori, C.F., *J. Gen. Physiol.* **1946,** 29, 6, 379.

52. Yang, Y.C.; Ward, J.R.; Seiders, R.P., *Inorg. Chem.* **1985,** 24, 12, 1766